DUDLEY KNOX LIBRARY
NAVAL POSTGRADUATE SCHOOL
MONTEREY, CALIFORNIA 93943-5002

NAVAL POSTGRADUATE SCHOOL

Monterey, California

THESIS

ANALYSIS OF WATER COLUMN STABILITY USING SHIPBOARD AND SUBMARINE DENSITY AND SHEAR MEASUREMENTS

by

Edward G. Beale, Jr.

December 1986

Thesis Advisor	E.B. Thornton
Co-Advisor	T.P. Stanton

Approved for public release; distribution is unlimited.

T230090

SECURITY CLASSIFICATION OF THIS PAGE

REPORT DOCUMENTATION PAGE

1a REPORT SECURITY CLASSIFICATION: Unclassified
1b RESTRICTIVE MARKINGS
2a SECURITY CLASSIFICATION AUTHORITY
2b DECLASSIFICATION / DOWNGRADING SCHEDULE
3 DISTRIBUTION / AVAILABILITY OF REPORT: Approved for public release; distribution is unlimited
4 PERFORMING ORGANIZATION REPORT NUMBER(S)
5 MONITORING ORGANIZATION REPORT NUMBER(S)
6a NAME OF PERFORMING ORGANIZATION: Naval Postgraduate School
6b OFFICE SYMBOL (If applicable): 68
7a NAME OF MONITORING ORGANIZATION: Naval Postgraduate School
6c ADDRESS (City, State, and ZIP Code): Monterey, California 93943-5000
7b ADDRESS (City, State, and ZIP Code): Monterey, California 93943-5000
8a NAME OF FUNDING / SPONSORING ORGANIZATION
8b OFFICE SYMBOL (If applicable)
9 PROCUREMENT INSTRUMENT IDENTIFICATION NUMBER
8c ADDRESS (City, State, and ZIP Code)
10 SOURCE OF FUNDING NUMBERS

PROGRAM ELEMENT NO	PROJECT NO	TASK NO	WORK UNIT ACCESSION NO

11 TITLE (Include Security Classification): ANALYSIS OF WATER COLUMN STABILITY USING SHIPBOARD AND SUBMARINE DENSITY AND SHEAR MEASUREMENTS
12 PERSONAL AUTHOR(S): Beale, Edward G., Jr.
13a TYPE OF REPORT: Master's Thesis
13b TIME COVERED: FROM ________ TO ________
14 DATE OF REPORT (Year, Month, Day): 1986 December
15 PAGE COUNT: 88
16 SUPPLEMENTARY NOTATION
17 COSATI CODES

FIELD	GROUP	SUB-GROUP

18 SUBJECT TERMS (Continue on reverse if necessary and identify by block number): stability, shear, thermohaline structures

Analysis of water column stability was performed using shipboard and submarine shear and density profile data acquired by U.S.S. DOLPHIN and R/V ACANIA in October, 1984 in the vicinity of Monterey Bay, California. Data was acquired utilizing CTD and acoustic doppler profiler (ADVP) instruments. The upper ocean thermohaline structure and water column stability, over a 10km square domain, was determined from repeated measurements of the conductivity, temperature, and velocity to a depth of 115m. The temporal and spatial variation in the analyzed fields of temperature, salinity, density, and velocity are compared with the constructed profiles of the static stability parameter (E) and gradient Richardson number. The analyzed fields were in turn compared with the larger scale forcing factors of coastal upwelling, current systems, bottom topography, and internal waves. The stability the water column

20 DISTRIBUTION / AVAILABILITY OF ABSTRACT: ☒ UNCLASSIFIED/UNLIMITED ☐ SAME AS RPT ☐ DTIC USERS
21 ABSTRACT SECURITY CLASSIFICATION: Unclassified
22a NAME OF RESPONSIBLE INDIVIDUAL: E. B. Thornton
22b TELEPHONE (Include Area Code): (408) 646-2847
22c OFFICE SYMBOL: 68Tm

DD FORM 1473, 84 MAR
83 APR edition may be used until exhausted
All other editions are obsolete

SECURITY CLASSIFICATION OF THIS PAGE

was found to be both statically and dynamically stable with the exception of thin patches of instability which were determined to be the result of double diffusive processes.

Approved for public release; distribution is unlimited.

Analysis of Water Column Stability Using Shipboard and Submarine Density and Shear Measurements

by

Edward G. Beale, Jr.
Lieutenant, United States Navy
B.S., University of California, Riverside, 1977

Submitted in partial fulfillment of the
requirements for the degree of

MASTER OF SCIENCE IN METEOROLOGY AND OCEANOGRAPHY

from the

NAVAL POSTGRADUATE SCHOOL
December 1986

ABSTRACT

Analysis of water column stability was performed using shipboard and submarine shear and density profile data acquired by U.S.S. DOLPHIN and R/V ACANIA in October, 1984 in the vicinity of Monterey Bay, California. Data was acquired utilizing CTD and acoustic doppler profiler (ADVP) instruments. The upper ocean thermohaline structure and water column stability, over a 10km square domain, was determined from repeated measurements of the conductivity, temperature, and velocity to a depth of 115m. The temporal and spatial variation in the analyzed fields of temperature, salinity, density, and velocity are compared with the constructed profiles of the static stability parameter (E) and gradient Richardson number. The analyzed fields were in turn compared with the larger scale forcing factors of coastal upwelling, current systems, bottom topography, and internal waves. The stability the water column was found to be both statically and dynamically stable with the exception of thin patches of instability which were determined to be the result of double diffusive processes.

TABLE OF CONTENTS

I. INTRODUCTION 8
  A. OBJECTIVE 8
  B. BACKGROUND 9

II. THEORY 13
  A. STATIC STABILITY 13
  B. DYNAMIC STABILITY 14
  C. DOUBLE DIFFUSION 15
    1. Case I: Double Diffusive Instability 15
    2. Case II: Layering 15
    3. Case III: No Motion 16

III. DATA ACQUISITION AND PROCESSING 17
  A. DATA ACQUISITION 17
    1. U.S.S. DOLPHIN Instrumentation 17
    2. R/V ACANIA Instrumentation 18
  B. DATA PROCESSING 20

IV. OBSERVATIONS 23
  A. GENERAL DESCRIPTION 23
  B. STATIC AND DYNAMIC FORCING MECHANISMS 23
    1. Upwelling 24
    2. Bottom Topography 24
    3. Tidal Flow 25
    4. Currents 26
    5. Internal Gravity Waves 27
  C. STATIC AND DYNAMIC STABILITY 28

V. SUMMARY AND CONCLUSIONS 84

LIST OF REFERENCES 86

INITIAL DISTRIBUTION LIST 87

LIST OF FIGURES

1.1 U.S.S. DOLPHIN and R/V ACANIA operation area 11
1.2 Bathymetry of the Monterey Bay in the vicinity of the study area (contours in fathoms) 12
3.1 Illustration of 4-beam Janus configured ADVP 22
4.1 Vertical section of side-averaged temperature 30
4.2 Vertical section of side-averaged salinity 31
4.3 Vertical section of side-averaged sigma-t 32
4.4 Averaged profiles of temperature (northside) 33
4.5 Averaged profiles of temperature (eastside) 34
4.6 Averaged profiles of temperature (southside) 35
4.7 Averaged profiles of temperature (westside) 36
4.8 Averaged profiles of salinity (northside) 37
4.9 Averaged profiles of salinity (eastside) 38
4.10 Averaged profiles of salinity (southside) 39
4.11 Averaged profiles of salinity (westside) 40
4.12 Averaged profiles of sigma-t (northside) 41
4.13 Averaged profiles of sigma-t (eastside) 42
4.14 Averaged profiles of sigma-t (southside) 43
4.15 Averaged profiles of sigma-t (westside) 44
4.16 Vertical section of temperature for circuit 1 45
4.17 Vertical section of temperature for circuit 2 46
4.18 Vertical section of temperature for circuit 3 47
4.19 Vertical section of temperature for circuit 4 48
4.20 Vertical section of temperature for circuit 5 49
4.21 Vertical section of temperature for circuit 6 50
4.22 Vertical section of temperature for circuit 7 51
4.23 Horizontal velocity difference plots for 75-25m levels (circuit 2) 52
4.24 Horizontal velocity difference plots for 75-25m levels (circuit 3) 53
4.25 Horizontal velocity difference plots for 75-25m levels (circuit 5) 54

4.26 Horizontal velocity difference plots for 75-25m levels (circuit 6) 55
4.27 Horizontal velocity difference plots for 75-25m levels (circuit 7) 56
4.28 Vertical section of salinity for circuit 1 57
4.29 Vertical section of salinity for circuit 2 58
4.30 Vertical section of salinity for circuit 3 59
4.31 Vertical section of salinity for circuit 4 60
4.32 Vertical section of salinity for circuit 5 61
4.33 Vertical section of salinity for circuit 6 62
4.34 Vertical section of salinity for circuit 7 63
4.35 Staggered profiles of temperature 64
4.36 Staggered profiles of salinity 65
4.37 Staggered profiles of sigma-t 66
4.38 Vertical section of sigma-t for circuit 1 67
4.39 Vertical section of sigma-t for circuit 2 68
4.40 Vertical section of sigma-t for circuit 3 69
4.41 Vertical section of sigma-t for circuit 4 70
4.42 Vertical section of sigma-t for circuit 5 71
4.43 Vertical section of sigma-t for circuit 6 72
4.44 Vertical section of sigma-t for circuit 7 73
4.45 Average profiles of the static stability parameter (E) for the northside 74
4.46 Average profiles of the static stability parameter (E) for the eastside 75
4.47 Average profiles of the static stability parameter (E) for the southside 76
4.48 Average profiles of the static stability parameter (E) for the westside 77
4.49 Average profiles of the Richardson number (northside) 78
4.50 Average profiles of the Richardson number (eastside) 79
4.51 Average profiles of the Richardson number (southside) 80
4.52 Average profiles of the Richardson number (westside) 81
4.53 Staggered profiles of the static stability parameter (eastside) 82
4.54 Staggered profiles of the static stability parameter (westside) 83

I. INTRODUCTION

A. OBJECTIVE

The objective of this thesis is to examine the static and dynamic stability of the upper 115m of the water column in terms of the spatial and temporal variations in the density and velocity fields. Observations are based upon profile data acquired by the U.S. Navy research submarine U.S.S. DOLPHIN and the Navy Postgraduate School research vessel ACANIA during a series of measurements conducted in Monterey Bay in the vicinity of the Monterey Canyon. From these measurements vertical profiles of the static stability parameter and gradient Richardson number were constructed. Comparison of these profiles with the temperature, salinity, density and velocity fields, as well as the synoptic meteorological analysis and local bathymetry were made in order to determine the effects of atmospheric and oceanographic forcing on the stability of the upper 100m of the water column.

The purpose for the data collection was an experiment lead by T.R. Osborn (Osborn and Lueck, 1985) for submarine measurement of turbulence microstructure in relation to vertical gradients of density and velocity. In order to provide a larger scale context to the submarine measurements, concurrent CTD and acoustic doppler velocity profiler (ADVP) measurements were conducted by the R/V ACANIA. Measurements were acquired within a 10km 'box' centered at 36° 44.5'N, 122° 03.0'W over a 35 hour period from the afternoon of 3 October to the morning of 5 October, 1984 (Fig. 1.1). During this period R/V ACANIA completed seven circuits of the edge of the survey area while U.S.S. DOLPHIN conducted two dives within the interior of the survey area. The separation between the two research vessels was to ensure a margin of safety for the submarine in the event of emergency surfacing. In order to maximize the horizontal resolution of the temperature, salinity and velocity measurements, a CTD was continuously profiled while concurrently recording velocity data from a shipboard ADVP. The resulting space/time series allowed the vertical structure of the upper ocean to be determined over scales of 0.5m to 100m with a near horizontal sampling of 500m. Data collection and processing are discussed further in Chapter 3.

B. BACKGROUND

The waters of the central California coast are subject to many types of dynamic forcing which result in spatial and temporal variations in the thermohaline structure and velocity fields which in turn affect the stability of the water column. The local forcing is dominated by the eastern boundary current system (California current and countercurrent), atmospherically forced coastal upwelling, tidal action, and bottom topography.

The California Current system is composed of a broad, weak equatorward flow near the surface (California Current) and a narrower, submerged poleward counterflow (California Countercurrent) adjacent to the continental slope (Wickham, *et. al.* 1986). In the period from October to March there is typically a decline in the intensity of the northwesterly wind flow near the coast. This acts to reduce coastal upwelling thereby allowing the countercurrent to surface whereupon it is known as the Davidson Current. During this time period, the Davidson Current is present at all depths shoreward of the California Current. It is characterized by a relatively thick homogeneous upper layer and poleward flow of 30 cm/s or less (Blumberg, 1975).

Coastal upwelling intensifies in the spring with the establishment of a strong atmospheric high pressure system/ridge off of the southern and central California coast and the concurrent development of a thermally induced low pressure system (heat low) over the interior region of the state. The northeast-southwest orientation of the pressure gradient results in fairly consistent northwesterly winds along the coast through the spring and summer months. This onshore flow causes offshore Ekman transport in the ocean resulting in coastal upwelling. The upwelling process is very sensitive to the atmospheric forcing and thus varies directly in intensity with the surface wind field with variations observed on the order of several days or less (Breaker, 1983). Upwelling distorts the near surface thermal and salinity fields by transporting colder, more saline water from depth up to the surface, which typically results in density fronts along the coast. During periods of intense upwelling, the Davidson Current is depressed and the California Current may be displaced as much as 200km away from shore (Breaker, 1983).

Bottom topography affects current flow, upwelling, and tidal flow by channeling the flow and by introducing vorticity into the flow. The major bathymetric feature of the Monterey Bay is the Monterey Canyon. The canyon has a northeast-southwest orientation with the maximum depth ranging from 100m near shore to 3600m at the continental slope. Within the study area the canyon axis is somewhat aligned with the NE-SW diagonal of the study area with depth ranges from 200m at northwest and southeast corners to 2000m at the southwest corner (Fig. 1.2). Coastal upwelling has been observed to be greatly intensified over the heads of some submarine canyons due to the channeling effect (Breaker, 1983). Additionally, due to the large topographic variation in the bathymetry current flow perpendicular to the axis of the canyon will tend to be deflected cyclonically due to an increase in positive relative vorticity derived from the increase (stretching) of the water column as the flow crosses over the canyon axis. Flow parallel to the canyon axis will tend to be channelled along the axis.

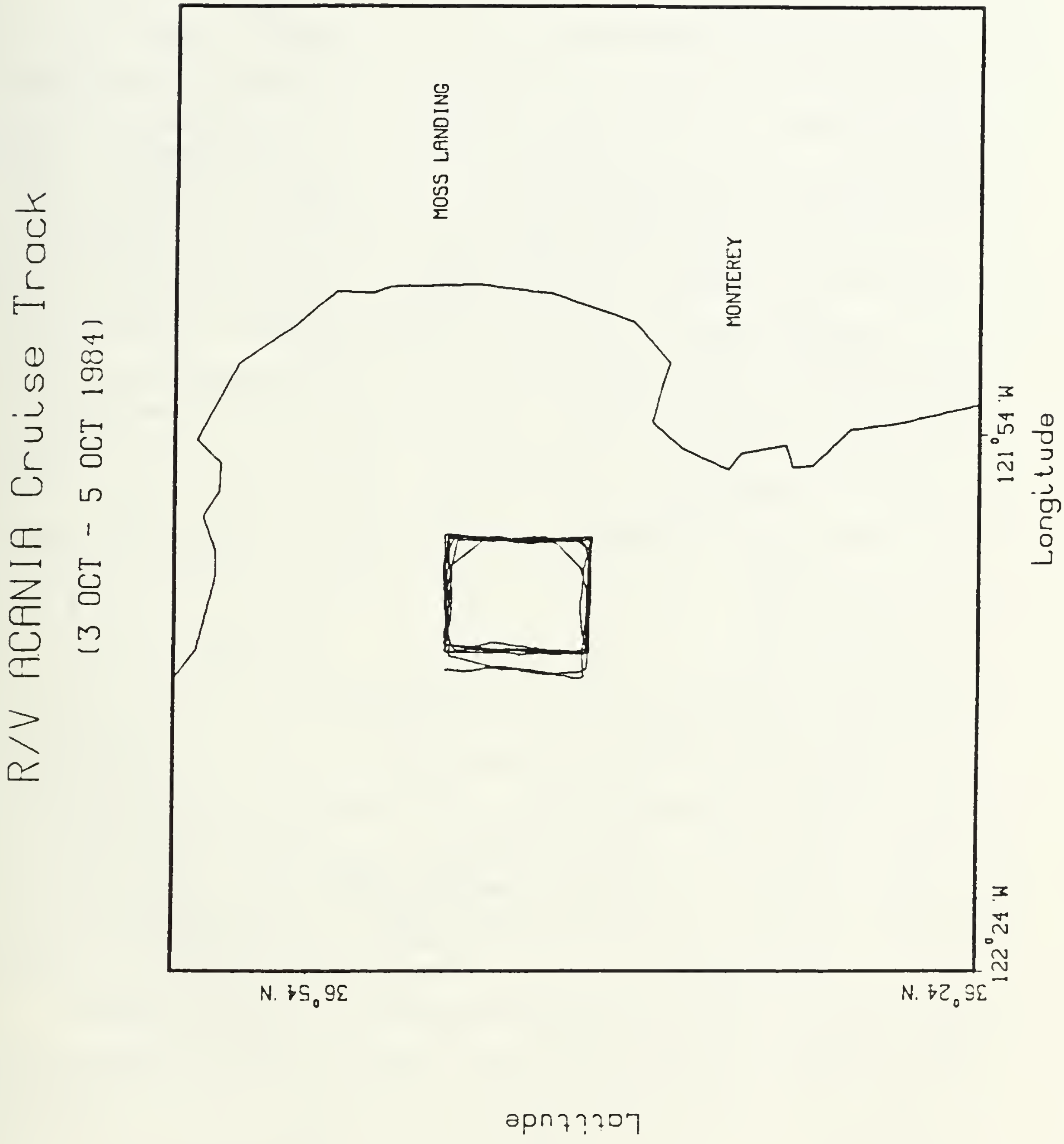

Fig. 1.1 U.S.S. DOLPHIN and R/V ACANIA operation area.

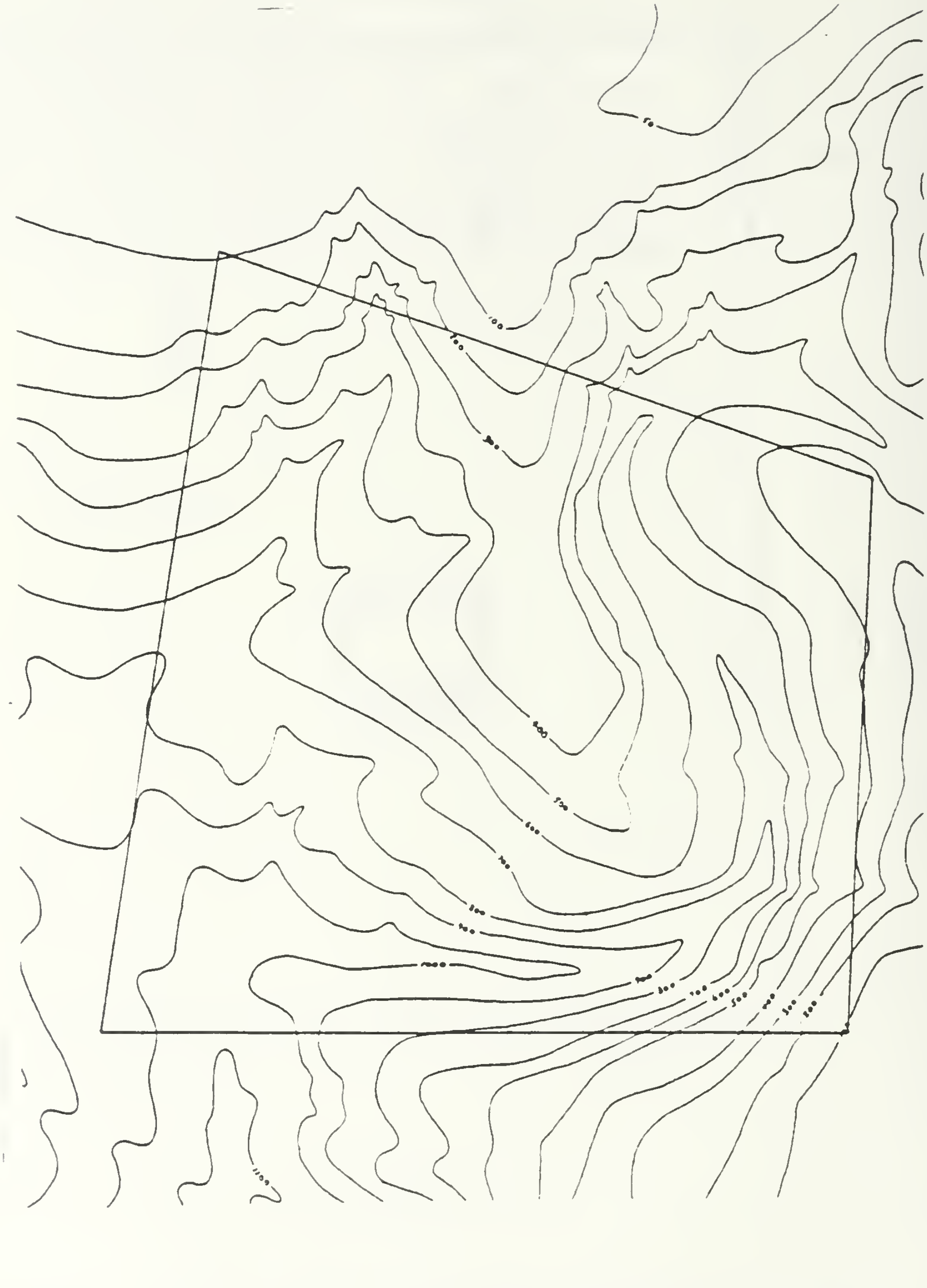

Fig. 1.2 Bathymetry of the Monterey Bay in the vicinity of the study area (contours in fathoms).

II. THEORY

Water column stability is an expression of the likelihood for the occurance of vertical motion of water parcels within the water column. It is a function of the density variation with depth (static stability) and the vertical variation in velocity (shear). Together, the magnitude of these two components provide an indication of the dynamic stability of the water column. Irreversible vertical motion (mixing) of water parcels can occur when there is an imbalance between the horizontal velocity shear and the thermohaline stratification. The result of mixing is to reduce the vertical variation of density thereby making the density of the water column more homogeneous. This results in an increase in the center of gravity of the water column and a consequent increase in the potential energy of the system. The increase in potential energy is derived from the kinetic energy of the vertical motion of the parcels which in turn is derived from the kinetic energy of the force causing the imbalance in the density or velocity profiles (Pond and Pickard, 1983, p.60). Definition of the parameters that define stability as applied to this study are discussed below.

A. STATIC STABILITY

Static stability is strictly a function of the vertical variation in the density field and as indicated by the word 'static' implies no initial motion in the system. Stability is indicated by the variation in density with depth. A stable density profile is one in which density increases with depth. Consequently gravitational forces will not impart any motion to the water parcels. However, if the density profile decreases with depth then heavier water overlies lighter water and the result is for the lighter water to rise while the heavier water sinks (vertical motion) in order to reestablish a gravitational balance.

Density in the ocean is a function of temperature, salinity, and pressure in order of decreasing importance. However a more useful parameter is sigma-t which is defined as:

$$\sigma_t = (\rho(t,s,0) - 1000) \text{ kg/m}^3 \qquad \text{(eqn 2.1)}$$

This parameter is useful in that it allows for a better estimate of what the density difference between two water parcels would be if they were at the same level. Sigma-t values were calculated from the temperature and salinity profiles obtained from the CTD data. The quantitative evaluation of water column static stability is given by the stability parameter "E" which is expressed as follows:

$$E = 1/\rho \; \delta\sigma_t / \delta z \qquad \text{(eqn 2.2)}$$

The $\delta\sigma_t/\delta z$ term represents the vertical gradient of density.

The buoyancy frequency defines the natural or resonant frequency that a parcel would oscillate at if displaced vertically from its stable position within a statically stable fluid. It is quantified as the square root of the product of the static stability parameter "E" and the gravitational constant "g" and is symbolized by "N".

$$N^2 = g \times E \qquad \text{(eqn 2.3)}$$

The buoyancy frequency is also the maximum frequency of internal waves in water of stability "E" (Pond and Pickard, 1983, p.30).

B. DYNAMIC STABILITY

Dynamic stability is an indicator of the effect that the vertical variation in velocity (shear) will have on the generation of vertical motion/turbulence within a water column of stability "E". Therefore it is a function of both the static stability and the magnitude of the shear. A quantitative expression for dynamic stability is the "gradient " Richardson number which is the ratio of the square of the buoyancy frequency to the square of the velocity shear:

$$Ri = (N^2) / (\delta u./\delta z)^2 \qquad \text{(eqn 2.4)}$$

A critical value of 0.25 has been established from turbulence theory as the cutoff between dynamic stability and instability (Pond and Pickard, 1983, p.60). Values of Ri > 1/4 indicate that the vertical gradient of velocity is insufficient to generate sustained turbulence and therefore dynamic stability is is sustained. The converse is true for values below the critical value. This ratio may also be viewed as the ratio of the potential energy of the column expressed by the density field and the kinetic energy expressed by the velocity field.

C. DOUBLE DIFFUSION

Instability in an otherwise statically stable environment may also occur from double diffusion which is the result of the difference in the molecular diffusivities of temperature and salt within a fluid causing an imbalance in the density field. The diffusivity of temperature is approximately 100 times greater than that of salt; thus double diffusion may occur when two masses of approximately the same density, but different temperature and salinity are in contact within a statically stable environment. The difference in the speed of molecular diffusion for temperature and salt results in a relatively rapid exchange of heat without a compensating exchange of salinity thereby resulting in a change in the densities of the two water masses. There are three possible combinations of temperature and salt between the two water masses which result in three entirely different conditions: ie. double diffusive instability, layering, and no motion.

1. Case I: Double Diffusive Instability

Double diffusive instability may occur if there is warmer, saltier water over cooler, fresher water (negative temperature and salinity gradients). The upper layer cools while the lower layer warms however, the salinity exchange is not rapid enough to compensate for the increasing density of the upper layer and the decreasing density of the lower layer. Thus, a negative density gradient is formed, and the boundary between the two layers becomes unstable. Consequently, the lower layer tries to rise while the upper layer tries to sink thereby resulting in mixing. Experiments have shown this mixing to occur as thin columns/filaments of each layer infiltrating the adjacent layer, this type of mixing is described as "salt fingering" (Pond and Pickard, 1983, p.31)

2. Case II: Layering

An intensification of the stable density gradient between layers occurs when cooler, fresher water is over warmer, saltier water (positive temperature and salinity gradients). As the upper layer warms the density decreases while the converse is happening in the lower layer. Again the salinity exchange is not rapid enough to compensate for the density changes. When the temperature difference is large the warming of the upper layer by the lower layer will cause it to rise due to its reduced density . The lower layer will attempt to sink due to cooling and increased density. This will lead to a breakdown in the interface between the layers thereby resulting in mixing.

3. Case III: No Motion

In the case of warmer, fresher water over cooler, saltier water (negative temperature gradient, positive salinity gradient) the density difference is reduced as the upper layer cannot get denser than the layer beneath it. Therefore no motion occurs. In order for double diffusion to result in instability, the gradients of temperature and salt must be the same (Pond and Pickard, 1983,p.32).

III. DATA ACQUISITION AND PROCESSING

A. DATA ACQUISITION

Temperature, conductivity, and velocity data analyzed in this study were acquired from 3 to 5 October, 1984 by the U.S.S. DOLPHIN and R/V ACANIA, which sampled a square-shaped region centered at 36° 44.5′N, 122° 03.0′W, approximately 22 km west of Moss Landing, California (Fig. 1.1). The R/V ACANIA made seven circuits of the edge of the region while U.S.S. DOLPHIN sampled the interior of the region. The vessels were equiped as follows.

1. U.S.S. DOLPHIN Instrumentation

The U.S.S. DOLPHIN was fitted with a 5m high tripod structure near the bow of the submarine. This structure was used to support the temperature, conductivity, and depth sensors. The CTD sensors consisted of Seabird Electronics thermistor and conductivity cell, and a Viatran model 304 strain gauge pressure sensor. The data from these sensors were digitized and stored on 9-track magnetic tape.

Velocity profiles relative to the submarine were measured by T.P. Stanton with an R-D Instruments acoustic doppler profiler mounted at deck level, 2m forward of the base of the instrument tripod. The acoustic profiler had an upward-looking, 4-beam Janus configuration. The beam angles were rotated 45° in azimuth from the forward and cross axes of the submarine in order to minimize acoustic reflection from the instrument tripod. Despite this rotation, reflections from the tripod were received by the aft transducer sidelobes causing the second and third velocity bins to have unreliable data. The acoustic beams were inclined 30° from the vertical axis. Acoustic pulses were transmitted at 1.2 MHz from all four beams at a repetition rate of 5 pings/sec. The received signal was range-gated into 30 sections corresponding to 1m length vertical bins, providing profiles of doppler velocities in the 30m above the hull of the submarine. The radial doppler shifts were resolved into orthogonal velocity components by differencing the doppler shifts of each bin in opposing beams using the relationship:

$$V_{13} = ((f_1 - f_3)/4f_0) \times C_0 \sin(\theta) \qquad \text{(eqn 3.1)}$$

$$V_{24} = ((f_2 - f_4)\ 4f_0) \text{ x } C_0 \sin(\theta) \qquad \text{(eqn 3.2)}$$

V_{ij}: velocity component resolved from the "i"th and "j"th beams

f_0: transmitted frequency

f_i: received doppler shifted frequency from the "i"th beam

C_0: velocity of sound at the transducer face

θ: beam inclination from the vertical

These two orthogonal velocity measurements were then rotated by 45° to give the forward and cross velocities. Velocity components were averaged for 10 seconds to reduce the high noise level inherent in pulsed incoherent acoustic doppler systems which principally arises from trying to resolve small doppler frequency shifts within short range intervals. The platform referenced velocity components were recorded and displayed on a Hewlett-Packard 216 computer.

Other instrumentation onboard R/V DOLPHIN, though not used in this study, included microstructure measuring equipment used by T.R. Osborn and R.G. Lueck. These consisted of 3 fast response thermistors, 2 airfoil shear probes and 3-axes accelerator. The airfoil probes were used to measure the time derivative of orthogonal components of horizontal velocity (du/dt, dv/dt). The time derivative is then converted into a measurement of shear. The scales of the shear measured by this method is on the order of 0.01m to 0.5m. Use of these instruments is described in detail by Osborn and Lueck (1985). The fast response thermistors were used to measure fine-structure temperature gradients. The analysis of these measurements of mixing activity is being performed by T.R. Osborn and E.C. Itsweire.

Additionally, there were two acoustic transducers which transmitted an 80 KHz pulse in the forward and vertical directions with the intent of measuring the scattering cross-section of the backscatterers in the volume ahead and above the submarine. These were used by D. Farmer and C. Crawford to investigate the nature of acoustic back and side scatter at this frequency.

2. R/V ACANIA Instrumentation

R/V ACANIA utilized several types of instruments to measure the temperature and conductivity of the upper ocean between the surface and in excess of 115m depth. Ocean skin temperature was measured with a Rosemont platinum resistance thermometer (5.0 mdeg absolute calibration) suspended from a boom over the side of the ship such that the thermometer remained within the upper few centimeters of the surface. Near surface (2m) temperatures and conductivities were measured with a pump-through Seabird thermistor and conductivity cell located in the ship's seachest. Continuous measurement of temperature and conductivity between 5 and 115 meters was made by towyoing a Neil Brown Instrument Systems Mk III CTD. The CTD consisted of a combination thermistor and platinum resistance thermometer (0.5 mdeg resolution, 5.0 mdeg absolute calibration), platinum electrode conductivity cell (0.001 mmho resolution, 0.01 nominal accuracy), and an electrical strain gauge pressure sensor (10 cm resolution). During the towyo the CTD package was raised and lowered between specified depth limits while maintaining a constant ship speed of approximately 5 knots. By this method a continuous series of near vertical temperature and conductivity profiles were obtained. A spatial resolution for the vertical section was achieved on the order of 0.5km by 0.5m based on the distance covered in the time to complete an upcast/downcast and the binning of temperature and conductivity every 0.5m of depth. This sampling resolution was used to determine the T, S, σ_t, and N structure of the upper 100m of the water column on a scale comparable with the shipboard ADVP measurements. Thus a valid comparison around the perimeter of the study area could be made between the static stability as determined from the CTD data and the shear stability determined from the ADVP data. Location (latitude/ longitude) information for each CTD profile was obtained from an Internav LC408 LORAN C receiver (25m resolution, 100m accuracy).

Velocity profile measurements below the ship were made with an Ametek-Straza acoustic doppler profiler model DCP4015 (ADVP). This profiler has a 4-beam Janus configuration transducer aligned with the forward and cross axes of the ship (Fig. 3.1). Acoustic pulses were transmitted at 300KHz every 0.6 seconds (1.67 pings/sec) with a 5 msec pulse duration. The received signal was range-gated into 32 bins giving a 3m vertical bin size; the shallowest range bin was centered at 7.5m depth. The forward and cross velocity components for each depth level were computed by differencing doppler shifts from complementary beams as in the U.S.S. DOLPHIN (section A.). Forward and cross velocity estimates from each ping were rotated into a North-South coordinate system using heading information from the ship's Mk9 Sperry gyro. The resolved velocity components were then averaged over 2 minutes in order to reduce the doppler frequency noise level as well as noise due to the pitch and roll of the platform. As indicated by Kosro (1985), when using comparable averaging intervals and moderate sea conditions, pitch and roll affects the vertical velocity component the most with velocity overestimates on the order of 3 - 4 cm/sec. However, the horizontal velocity components are affected on the order of less than 1 cm/sec; thus the horizontal velocity estimates may be calculated with minimal error when pitch and roll corrections are ignored, particularly for the low sea states encountered during these measurements.

The ADVP measures velocity profiles relative to the vessel. Absolute current profiles may be derived by measuring and removing the ground referenced ship's velocity. In this study only the shear profiles will be used as high resolution profiles were needed for the construction of Richardson Number profiles and the ship's velocity cannot be determined to comparable accuracy with only two minutes averages; typically 15 minutes are needed to resolve the ship's velocity to 10 cm/sec using LORAN C.

B. DATA PROCESSING

The stability of the water column and the processes affecting it were examined by analyzing the temperature, salinity, sigma-t, and velocity fields. Stability is a function of the vertical gradients of density and velocity, but since the water mass structure is not readily apparent in the density field alone, the temperature and salinity fields were also analyzed. Analysis was accomplished by the construction of graphical displays of contoured vertical sections, profile plots, and horizontal vector plots. The temperature, salinity, sigma-t, and static stability fields were constructed from the R/V ACANIA CTD data, which provided information from 5.0m to 115.0m depths. These fields are displayed as both contoured vertical sections and profile plots. U.S.S. DOLPHIN CTD data was not used in the construction of these fields as information was limited to the cruise depth of the submarine and thus had limited vertical range. Velocity fields were constructed from both the R/V ACANIA and U.S.S. DOLPHIN ADVP data sets and were displayed as profile plots and horizontal vector plots. Richardson number fields were constructed by combining the sigma-t and velocity fields from the R/V ACANIA CTD and ADVP data sets and are displayed as profile plots.

Contoured vertical sections were chosen for the temperature, salinity, and sigma-t fields because they provided a ready depiction of the spatial variability of a parameter within a particular section as well as an indication of the temporal variability through successive vertical sections. The vertical sections were constructed from 2.0m vertical averages of the R/V ACANIA CTD data. Vertical averaging was necessary in order to reduce the noise level in the contouring procedure. Individual vertical sections may be considered to be approximate "snapshots" of the variability expressed in the temperature, salinity, and sigma-t fields as they represent data collected within approximately one hour along a 8km horizontal section.

Averaged and staggered profile plots were constructed for the parameters of temperature, salinity, sigma-t, velocity, static stability, and Richardson number. The plots are useful in that they provide a more detailed depiction of the vertical variation of a parameter than does the contoured vertical section. Thus, small scale vertical variability associated with some processes such as internal waves and double diffusion are more readily apparent. Also, in combination with the contoured vertical sections, a better understanding of the temporal and spatial variability of the fields of interest may be made. The averaged profiles of temperature, salinity, and sigma-t were constructed by side-averaging the vertical profiles of these parameters at 2.0m vertical resolution. The standard deviation about these profiles was also calculated and depicted by dashed profiles on either side of the averaged profile. Included with the side-averaged profiles is a composite profile which represents the mean of the side-averaged profiles. Averaged profiles of static stability were constructed from 3.0m vertical resolution side-averaged profiles to correspond with the resolution of the ADVP data used in the calculation of the Richardson number; standard deviation was not calculated. Critical value limits are expressed on the E and Ri plots by a vertical dotted line. Staggered profiles were constructed for temperature, salinity, sigma-t, and static stability from the 0.5m resolution CTD data.

Horizontal vector plots of velocity were constructed for the 25m and 75m depth levels from the R/V ACANIA ADVP data for the second through seventh transits of the study area. The velocity difference between these two levels (shear) was also constructed. Together these plots served to provide information on the tidal and large-scale current flow. The 25m and 75m depth level was chosen because they defined the upper and lower depth limits of the section of the water column exhibiting the greatest activity in terms of temperature and salinity variability. This permitted a comparison between the dynamic (velocity) forcing and the static forcing on stability.

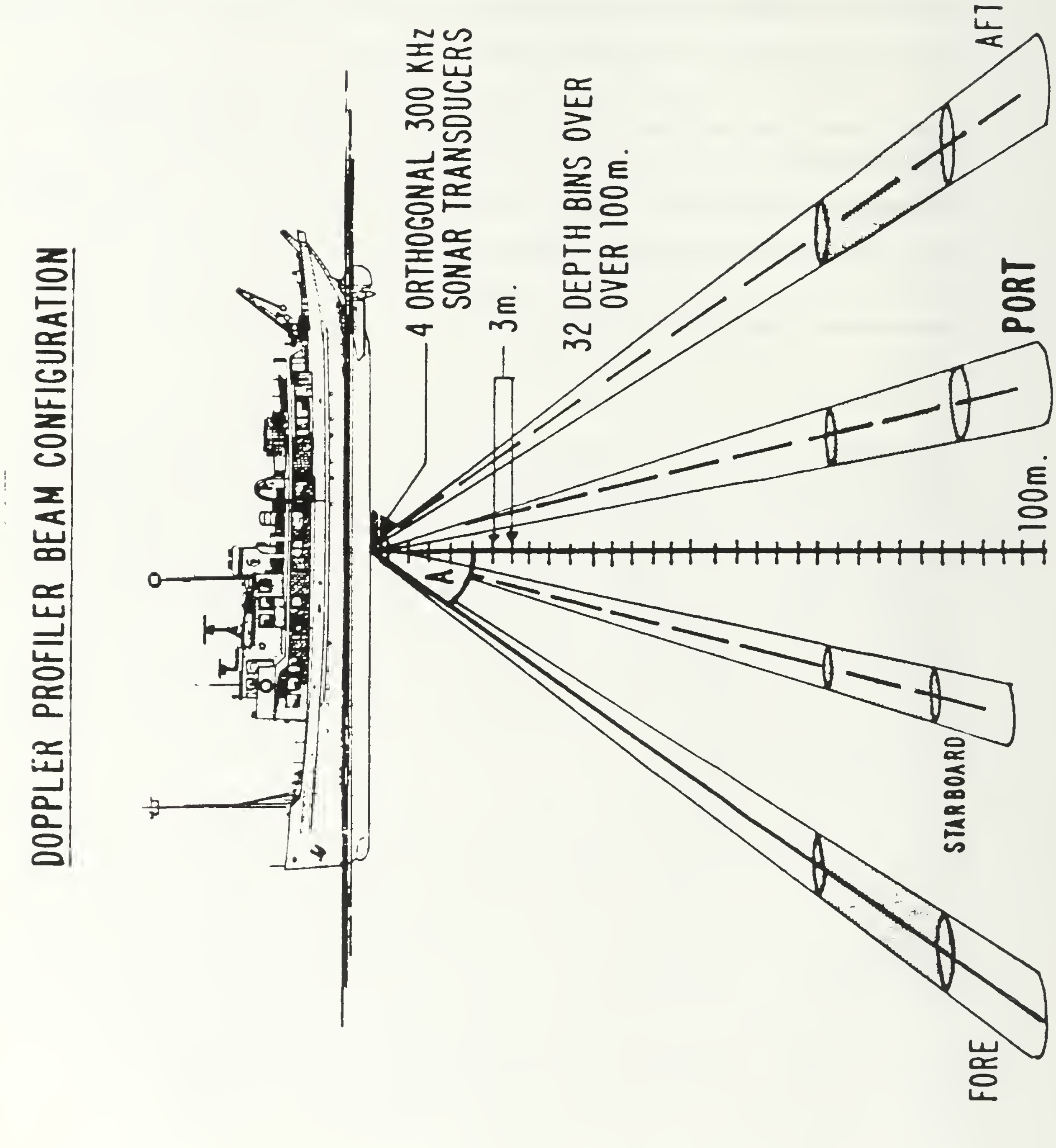
DOPPLER PROFILER BEAM CONFIGURATION
4 ORTHOGONAL 300 KHz SONAR TRANSDUCERS
3m.
32 DEPTH BINS OVER OVER 100m.
A
100m.
FORE
STARBOARD
PORT
AFT

Fig. 3.1 Illustration of 4-beam Janus configured ADVP.

IV. OBSERVATIONS

A. GENERAL DESCRIPTION

A general depiction of the spatial variability present in the analyzed fields of temperature, salinity and sigma-t are presented in the side-averaged contoured vertical sections (Figs. 4.1 - 4.3). It is readily apparent that there is considerably more variability in the temperature and salinity vertical sections than in the density/sigma-t vertical section. This is due to a tendency for the variations in temperature and salinity to compensate each other resulting in a more consistent density field. This is evidenced particularly by the compensation exhibited in the eastern side panel comparing the strong thermal gradient between 35m and 45m with the salinity minimum at the same depth levels. Overall, the density field strongly reflects the temperature field; however, where there are strong salinity gradients, salinity variations are reflected in the density field.

Mean profiles of temperature, salinity, and sigma-t for each side and transit of the study area depict the temporal variability in the vertical variation of these parameters (Figs. 4.4 - 4.15). Of note are the consistently strong thermal gradients between 15m and 35m depicted in the profiles for the east and south sides (Figs. 4.5 and 4.6). The north and west sides exhibit considerably more temporal variability in their temperature profiles (Figs. 4.4 and 4.7). This variability is oscillatory such that the composite profile (average of all seven circuits of a side) has nearly constant slope. The salinity profiles (Figs. 4.8 - 4.11) suggest a migration of parcels of less saline water between 25m and 65m through the study area. Sigma-t profiles for the east and south sides (Figs. 4.13 and 4.14) reflect the temperature profiles especially with regard to the strong thermal gradients as was indicated in the contoured vertical sections. The sigma-t profiles for the north and west sides (Figs. 4.12 and 4.15) however do not tend to reflect the vertical variability evident in the temperature profiles, and instead tend to monotonically increase with depth. This may be attributed to compensation by the salinity field.

B. STATIC AND DYNAMIC FORCING MECHANISMS

As discussed in Chapter I, there are several forcing mechanisms which can induce variability in the temperature, salinity, density, and velocity fields and thus ultimately the stability of the water column. The mechanisms investigated in this study were upwelling, bottom topography, tidal flow, current systems, and internal gravity waves. Analysis of the temperature, salinity, sigma-t, and velocity fields in conjunction with the atmospheric and tidal conditions present during the study indicated that all of these mechanisms were present with the exception of upwelling. Evidence for these mechanisms is discussed below.

1. Upwelling

The atmospheric conditions several days prior to and during the study period were characterized by a high pressure ridge off the central California coast with a weak pressure gradient over the coastal areas. The resulting low level winds were from the north-northwest at approximately 5 - 8 knots. This weak NNW flow was modified by the diurnal land-sea breeze fluctuations. A sea breeze regime commenced in the early afternoon with a backing and increase in wind speed to WNW at 8 - 14 knots. This regime persisted until midnight when the winds veered back to NNW and diminished to 2 - 4 knots (weak land breeze regime). The synoptic scale flow resumed in the early morning just prior to sunrise. The low winds and generally offshore flow resulted in an absence of the summertime pervasive coastal status and fog . Low winds also provided for calm sea conditions. Due to the weak NNW flow, coastal upwelling was severly diminished and thus deemed to be negligible as a forcing mechanism during the study period.

2. Bottom Topography

The bottom topography of the study area, as mentioned previously, was dominated by the steep slopes of the Monterey Canyon (Fig. 1.2) The canyon axis roughly corresponded with the NE-SW diagonal of the study area with slope towards the southwest, but is deflected somewhat from the NE-SW orientation by the presence of a large topographic ridge projecting southward into the study area from near the midpoint of the north side. Evidence of the effects of bathymetry on the analyzed fields is demonstrated in the contoured vertical sections of temperature (Figs. 4.16 - 4.22). Particularly evident is the mass of colder water between 40m and 95m in the eastern side. This mass is expressed in the vertical section by an upward bulging of the 11.5 and 12.0°C isotherms in the northern half of the eastern side. The bathymetry of the eastern side is nearly constant at approximately 400 fathoms (800m) for the northern three-forths of the side then rises to 100 fathoms (200m) at the southeast corner. Therefore, this colder mass would be indicative of a trapped pool of colder water. Analysis of the 12°C isotherm in the northern side sections also show evidence of bathymetric channeling as expressed by an downward bulging in the isotherm. The location of the bulging corresponds with the axis of the canyon and would seem to represent the channeling of warmer water along the canyon axis. The combination of the warmer pool in the eastern portion of the northside with the cooler pool in the northern portion of the eastern side indicates that warmer water is being advected along the canyon axis while the cooler water is displaced along the sides of the canyon. Channeling of water flow by the canyon may also affect the velocity field, especially with regard to the oscillatory tidal flow.

3. Tidal Flow

Tidal flow along the California Coast is characterized by two high and two low tides every 25 hours, occurring about 50 minutes later every day. The heights of the two high tides and the heights of the two low tides are not equal in magnitude or in time between them. During the study period the higher high tide occurred in the early evening at about 1900 while the lower low tide occurred shortly after midnight. Actual tide times at Moss Landing were high tide at 1818, 3 Oct and 0839 and 1924, 4 Oct; low tide occurred at 0140 and 1403, 4 Oct and 0240, 5 Oct.

Tidal effects are most noticeable on the temperature and velocity fields. This is demonstrated in the contoured vertical sections of temperature (Figs. 4.16 - 4.22) and the horizontal vector plots of velocity (Figs. 4.23 - 4.27). With regard to the temperature field, tidal effects are especially evident in the vertical sections for the northern side expressed by the variability in the 12° and 14°C isotherms. This may be due to the near parallel orientation of the section with the predominantly east-west fluctuations in the near surface tidal flow. In circuit 1 (Fig. 4.16) the 12° isotherm is nearly flat across the northern section at a depth of approximately 60m during a time corresponding to a period of slack water at high tide. By circuit 2 (Fig. 4.17), the 12° isotherm slopes upward to the east and a patch of warmer water is evident in the eastern portion of the section between 60 and 80m; this is during a period of ebb flow. In circuit 3 (Fig. 4.18), a period of flood flow, the 12° isotherm is deeper and slopes in the opposite direction to the previous circuit, but exhibits a bulge in the isotherm to representing an intrusion of warmer water. At low tide (Fig. 4.20) the 12° isotherm is again nearly flat as in circuit 1, however the depth is nearly 15m deeper indicating the ebb flow introduced warmer water into the study area which depressed the 12° isotherm. The tilt of the 14° isotherm also reflects the tidal flow. During periods of ebb flow (Fig. 4.17 and 4.22), the isotherm slopes downward to the east whereas the slope is reversed for flood flow (Fig. 4.18 and 4.21). The 14° isotherm is approximately horizontal during periods of slack water (Fig. 4.16 and 4.20). Tidal flow may also distort the temperature and salinity fields through the advection of water parcels such that the advected parcels have different temperature and salinity characteristics than the host water. Evidence of tidal induced advection was discussed above with regard to the influence of bottom topography.

The horizontal velocity plots (Figs. 4.23 - 4.27) exhibit fluctuations in direction and magnitude corresponding to the tidal period. This is particularly evidenced by the eastern and western sides. The western side shows a consistent westerly flow , however the magnitude varies in direct relationship to the east-west flow reversals observed on the eastern side. The period between the flow reversals is on the order of 13 hours which corresponds well with the tidal period. The northern and southern sides, on the other hand, exhibit consistent southerly flow through the study period; this could therefore be indicative of a general southerly flow (California Current) with a tidally induced fluctuating east-west velocity component. Bottom topography induced channeling results in the flow fluctuations being greater along the eastern side.

4. Currents

Current systems of interest to this study included the California and Davidson Currents. The Davidson Current is usually dominant during periods of reduced upwelling as occurred during this study. However, the horizontal vector velocity plots (Figs. 4.23 - 4.27) along the northern and southern sides of the study area do not give any indication of the presence of the northward flowing Davidson Current within the study area, but rather depict a consistent southward flow characteristic of the California Current. As mentioned above the flow along the eastern and western sides appears to be modified by tidal flow. Additionally, the current velocities are greater at 25m than at 75m resulting in a negative velocity gradient and providing for shear as a dynamical forcing on stability. Average velocity differences between the 25m and 75m depth levels was on the order of 5 cm/sec.

Currents also affect the temperature and salinity fields through advection of water parcels. This appears evident in the contoured vertical sections of salinity (Figs. 4.28 - 4.34) where a lens shaped minimum in salinity is described by the 33.3 ppt isohaline at between 25m and 55m depth. Advection of this less-saline lens by the large-scale current flow may be observed in the vertical sections for the north and east sides where the lens, which initially spans the northside at approximately 45m, is observed in successive sections to reduce in size and migrate to the east and south. This southward migration is also evident in the vertical sections for the south and westsides where smaller parcels of less-saline water are observed to migrate across the side during the course of the study. An estimate of the speed of migration is approximately 0.5 km/hr (14cm/s). This is only a crude estimate considering the other processes which may distort the parcels. The overall southward migration apparent in these vertical sections is consistent with the general southerly flow observed in the velocity plots and may be attributed to the California Current system.

5. Internal Gravity Waves

Internal gravity waves affect the temperature, salinity, and density fields through the intensification and weakening of gradients caused by wave induced displacements of the density interface. The movement of the internal wave intensifies temperature, salinity, and density gradients in the direction of movement as the density interfaces oscillates vertically. A concurrent weakening of gradients occurs behind the movement of the density interface. The frequency of internal waves is bounded at the upper end by the buoyancy frequency. A mean buoyancy frequency of approximately 0.6 cph was calculated for the study area though this represents a low value for the upper bound of the buoyancy frequency as individual profiles values were higher. This frequency corresponds to a period of 1.7 hours indicating that the shorter period internal waves should be adequately represented by these diagrams. The lower bound on the frequency for internal waves is the inertial frequency. The inertial frequency for the latitude of the study area (36.75°N) was calculated to be 0.0498 cph. The corresponding inertial is 20.06 hours.

While wave-like features appear evident in the contoured vertical sections, they are especially evident in the staggered profile plots. This is particularly noticeable in the staggered profile plots for the eastern and western sides (Figs. 4.35 - 4.37). In the staggered temperature profiles for the eastside, the area of strongest thermal gradient (between 15m and 35m depth) is observed to oscillate in a wave-like pattern with a wavelength of approximately 7km. A second wave pattern is evident between 65m and 85m and is in phase with the upper wave pattern. Similar wave patterns are exhibited in the staggered profiles of salinity and sigma-t. The western side staggered temperature profiles exhibit two sets of waves at between 10m and 30m for the upper wave and between 75m and 95m for the lower wave pattern. These two wave patterns are 180° out of phase which results in a stronger alternating intensification and weakening of density gradients between them. As in the staggered profiles for the eastern side, the western side salinity and sigma-t profiles exhibit similar wave patterns to that displayed in the temperature profiles. This similarity in wave patterns between all three parameters is due to the movement of internal gravity waves along density interfaces resulting in an oscillatory or wave motion expressed in the density profiles. Since the density is not changed by the motion of the internal wave, the temperature and salinity profiles should exhibit similar wave patterns.

C. STATIC AND DYNAMIC STABILITY

The variability expressed in the displays of temperature and salinity were for the most part compensating such that the displays of sigma-t exhibited a more uniform field. This is exemplified in the contoured vertical section of sigma-t (Figs. 4.38 - 4.44). Consequently, the static stability field could be expected to be stable overall as exhibited by displays of the static stability parameter (E) and the dynamic stability parameter (Ri) or Richardson number. Comparison of the averaged profiles of the static stability parameter (E) (Figs 4.45 - 4.48) and the Richardson number (Ri) (Figs. 4.49 - 4.52) provide an indication of the relative importance between the vertical density gradient and the velocity gradient on the stability of the water column. The E and Ri average profiles are calculated from 3m vertically averaged density differences to coincide with the 3m vertical resolution of the velocity data. Consequently, because gradients of density and shear can occur on scales smaller than this 3m differencing interval, the Ri profile values represent an upper bound. Many of the maximums in the Ri profiles correspond with the maximums in the E profiles indicating that the strength of the density gradient is driving the dynamic stability. Maximums in the Ri profiles which do not correspond to maximums in the E profiles indicate that there is a relative minimum in the vertical gradient of velocity (shear) in that portion of the water column as well as a weak density gradient. Minimums in the Ri profiles indicate that the relative magnitude of the shear is greater than the density gradient. Values of Ri below the critical value indicate that the shear is greater than twice the density gradient. Of note are the below critical Ri values observed near the top of most profiles. This is a manifestation of the acoustic profiler caused by sidelobe interference in the upper bins of the shipboard ADVP.

The averaged profiles of the static stability parameter indicate stability through the vertical extent of the water column. However, the staggered profiles of E indicate thin patches (< 2.0m thick) of static instability. This is exemplified in the staggered profiles for the east (Fig. 4.53) and west sides (Fig. 4.54). As was noted in the discussion of internal waves, wave like patterns are also exhibited in the staggered E profiles. The thin unstable patches are indicative of double diffusive processes acting upon the disturbances in the density field caused by the static and dynamic forcing mechanisms of bottom topography, tidal and current flow, and internal waves. Preferred locations of instability and double diffusive processes are in regions of strong, but opposing temperature and salinity gradients. However, despite the extreme variability observed in the temperature and salinity fields, the density fields were for the most part consistent with monotonically increasing gradients, and consequently the water column is predominantly stable.

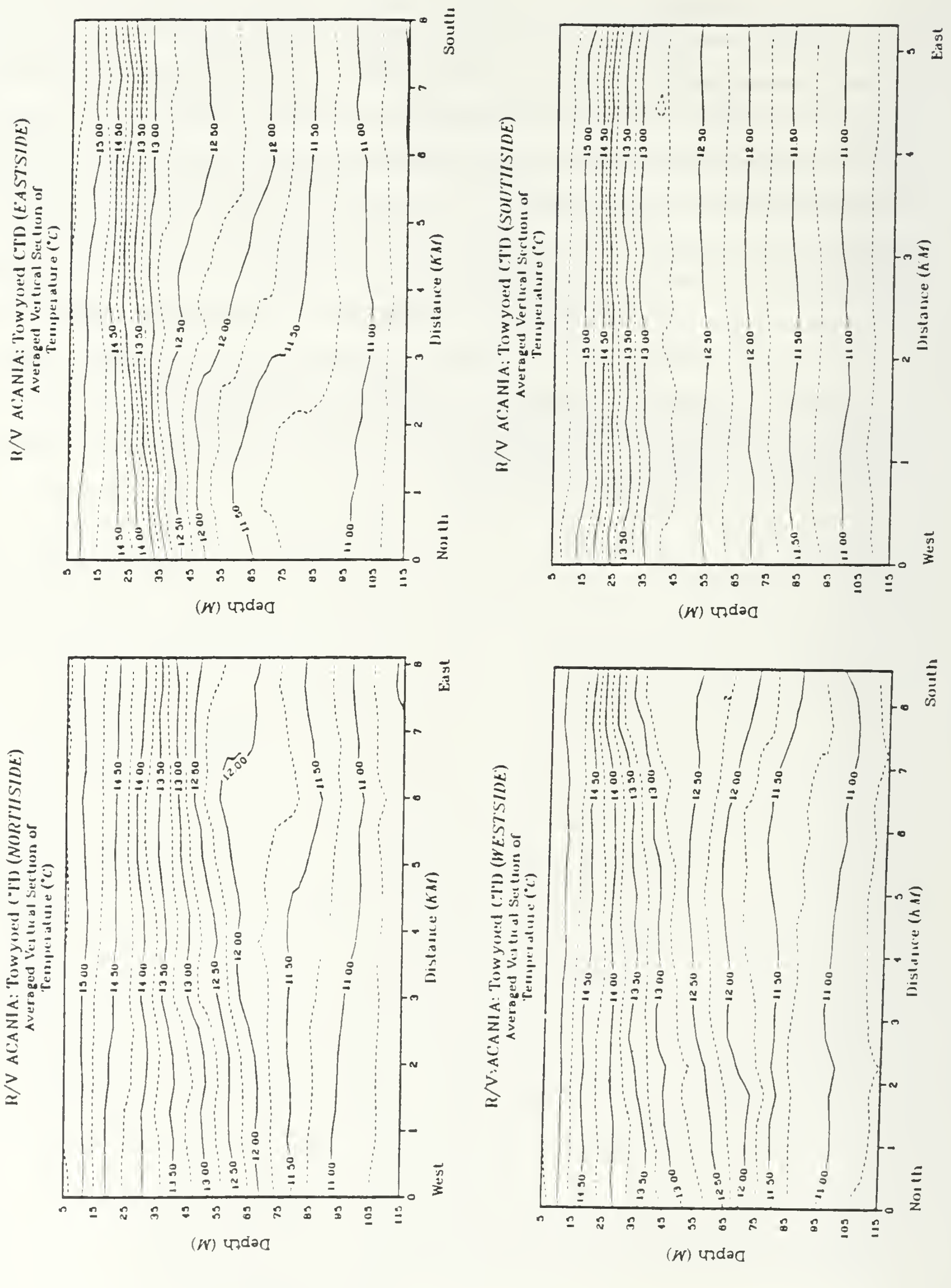

Fig. 4.1 Vertical section of side-averaged temperature.

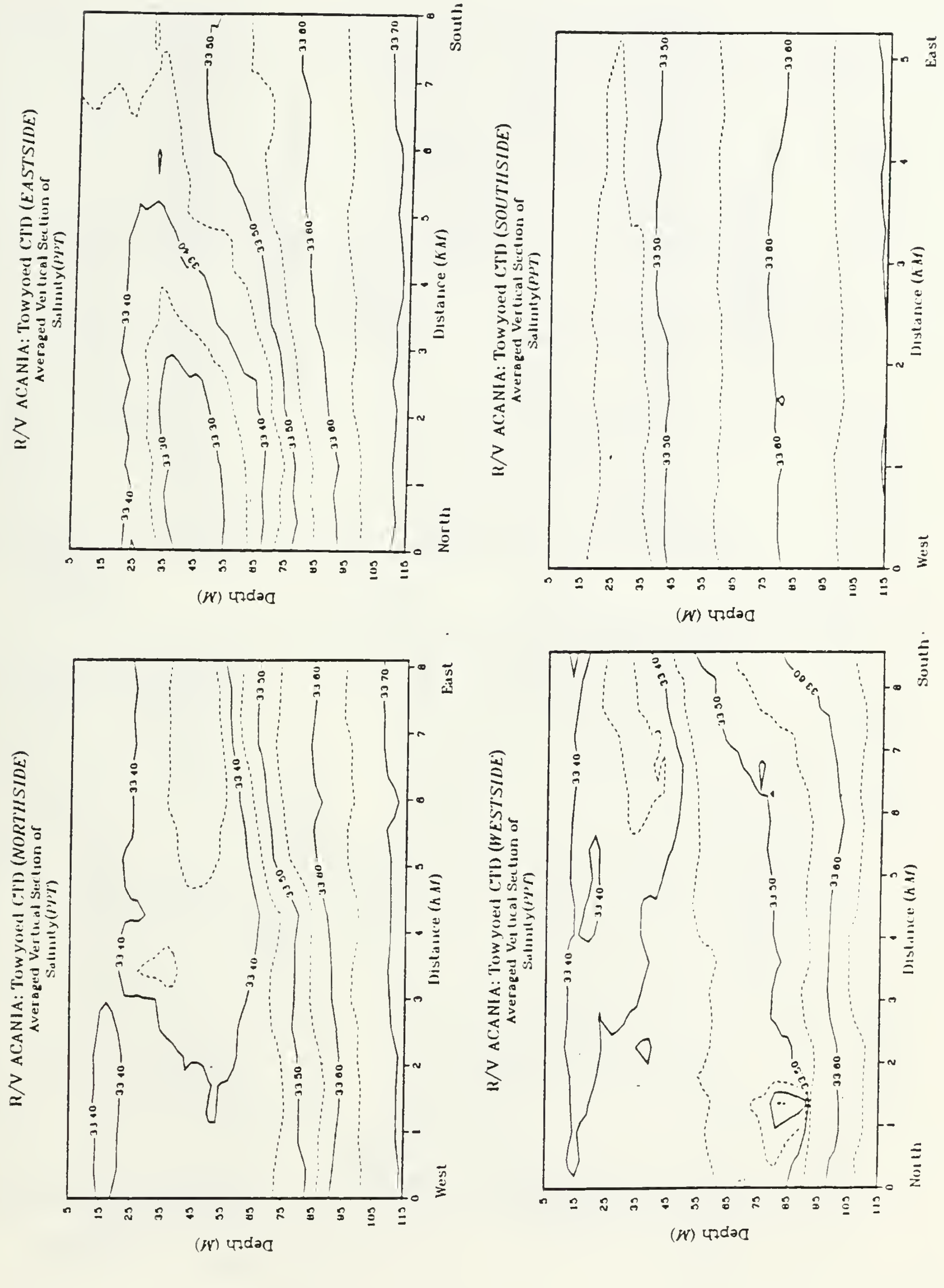

Fig. 4.2 Vertical section of side-averaged salinity.

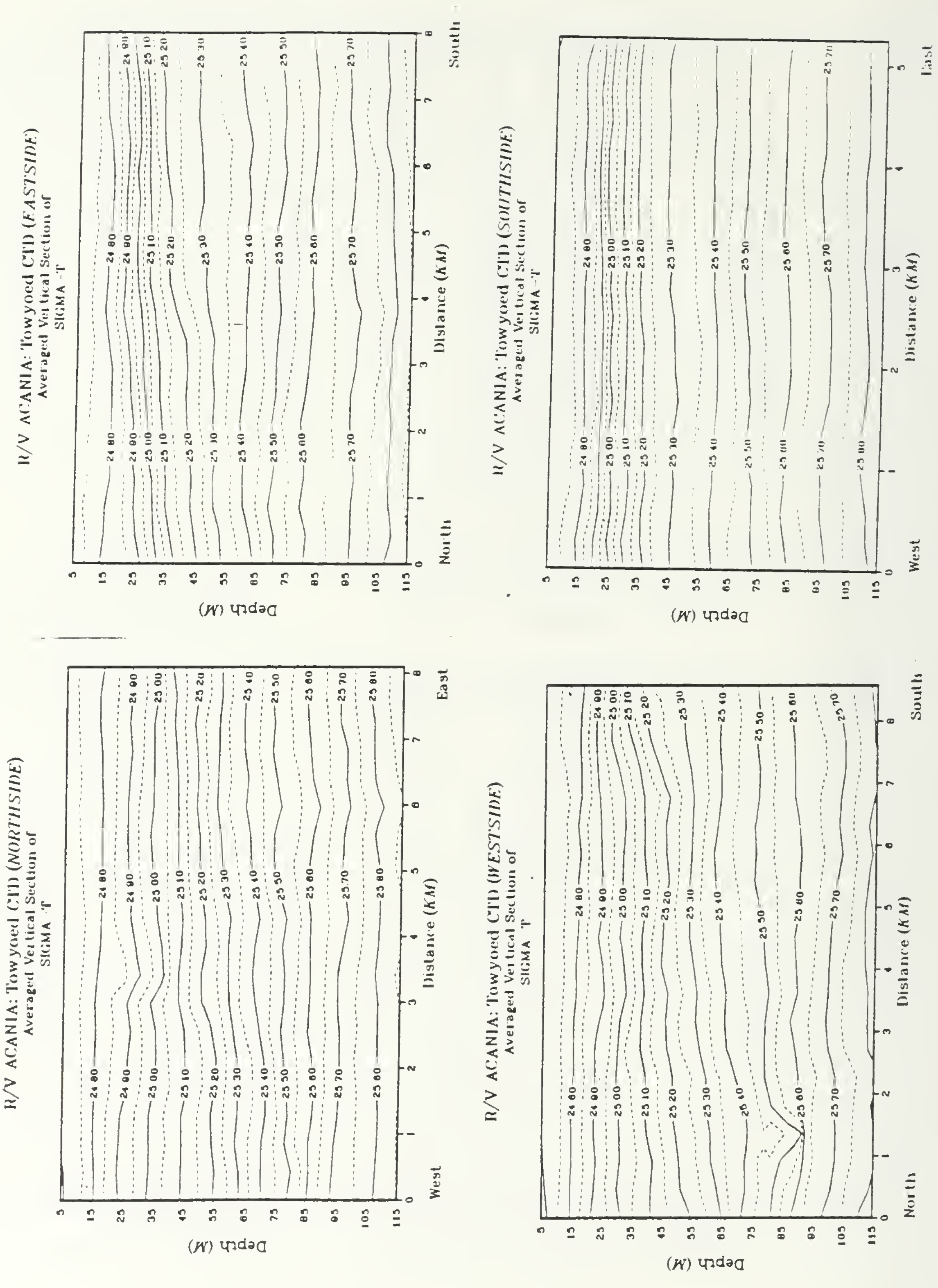

Fig. 4.3 Vertical section of side-averaged sigma-t.

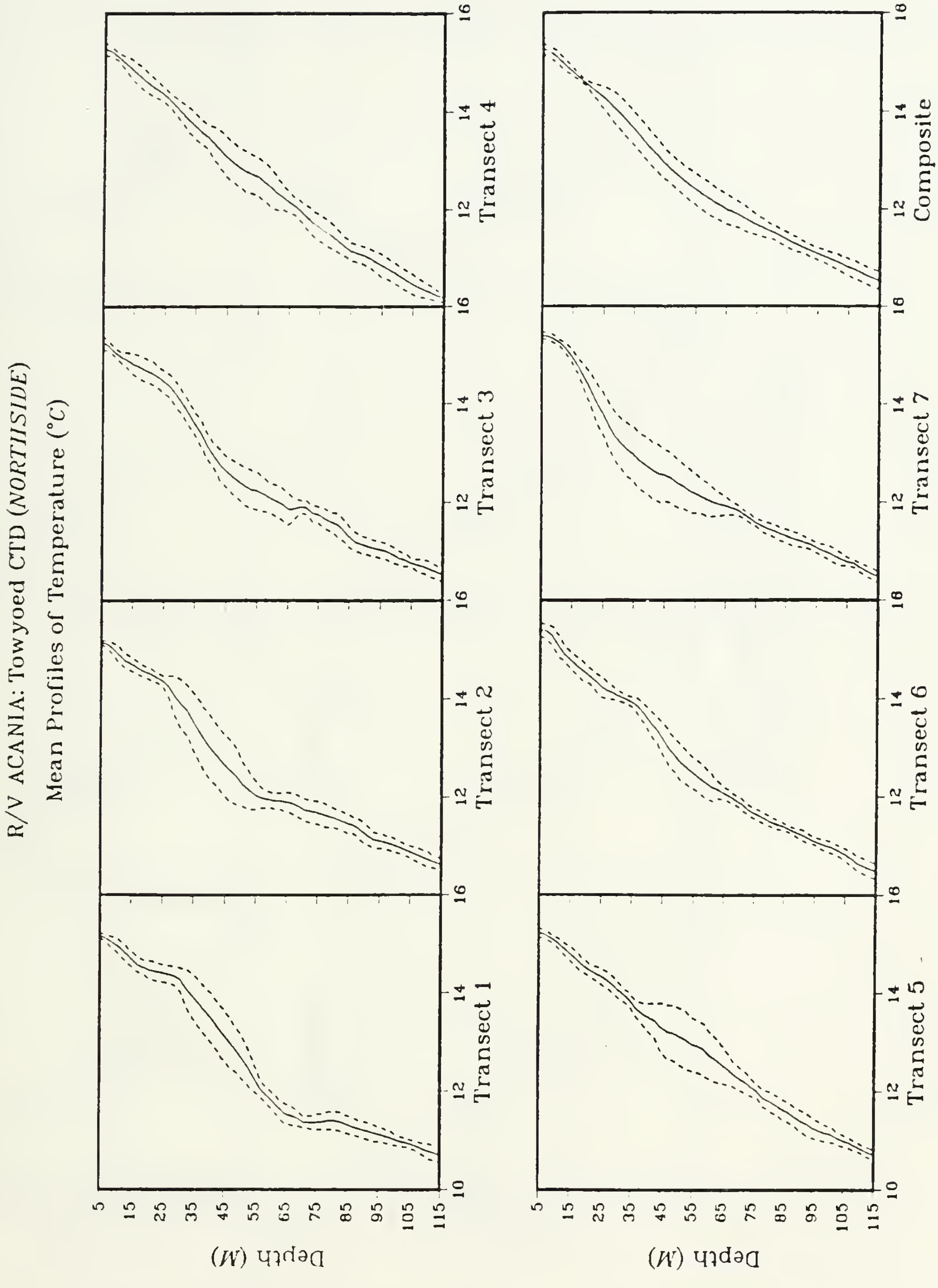

Fig. 4.4 Averaged profiles of temperature (northside).

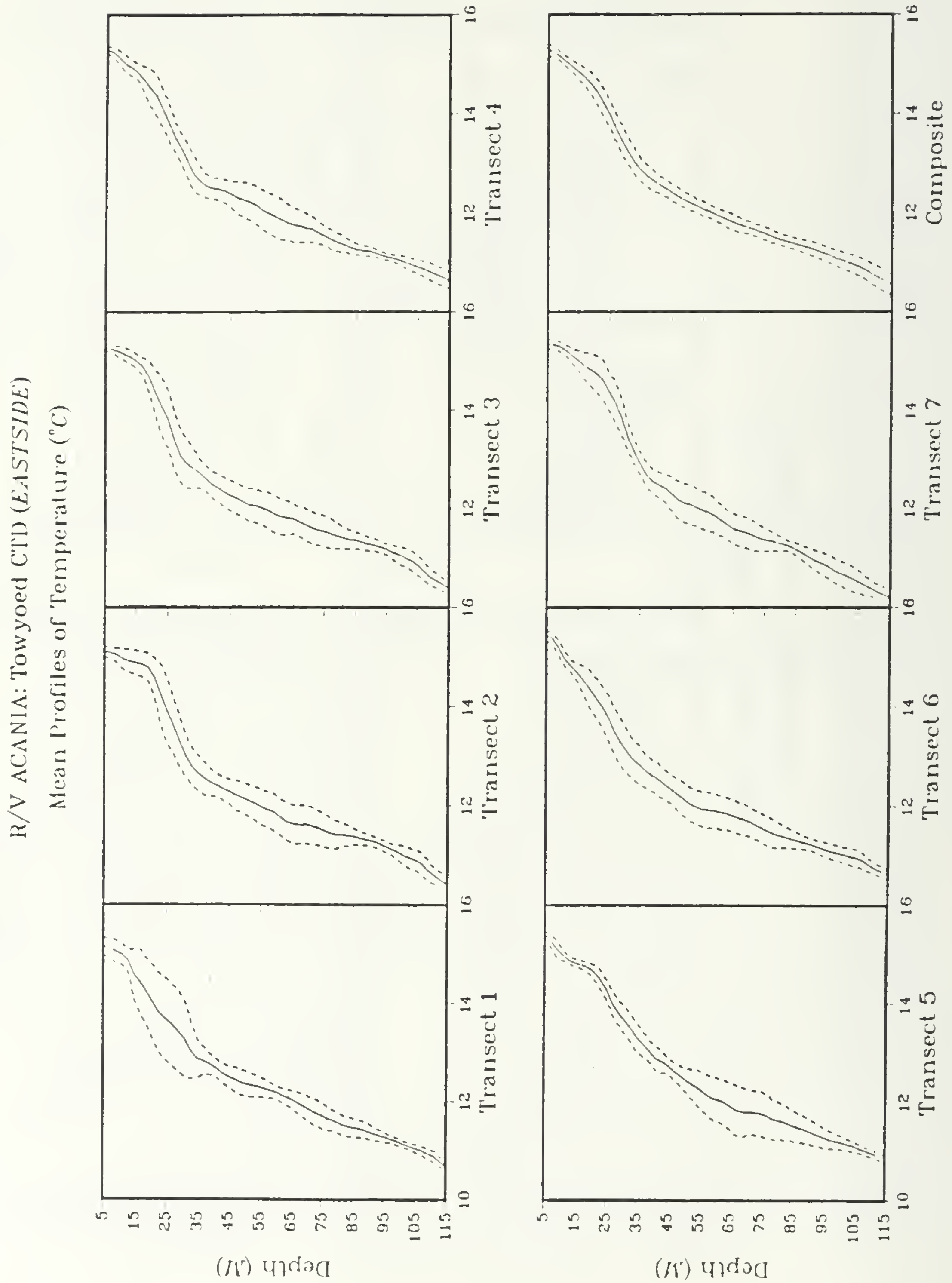

Fig. 4.5 Averaged profiles of temperature (eastside).

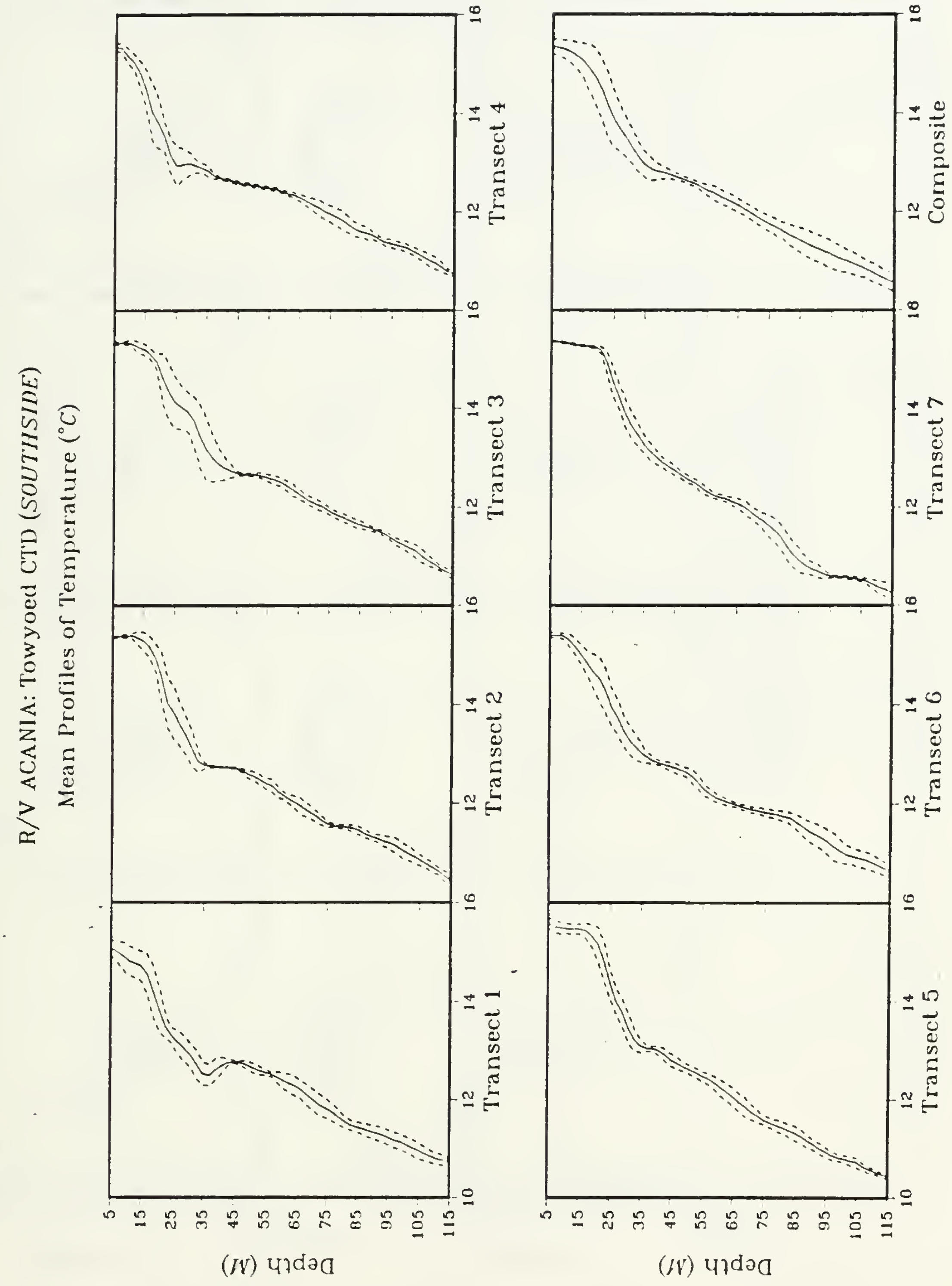

Fig. 4.6 Averaged profiles of temperature (southside).

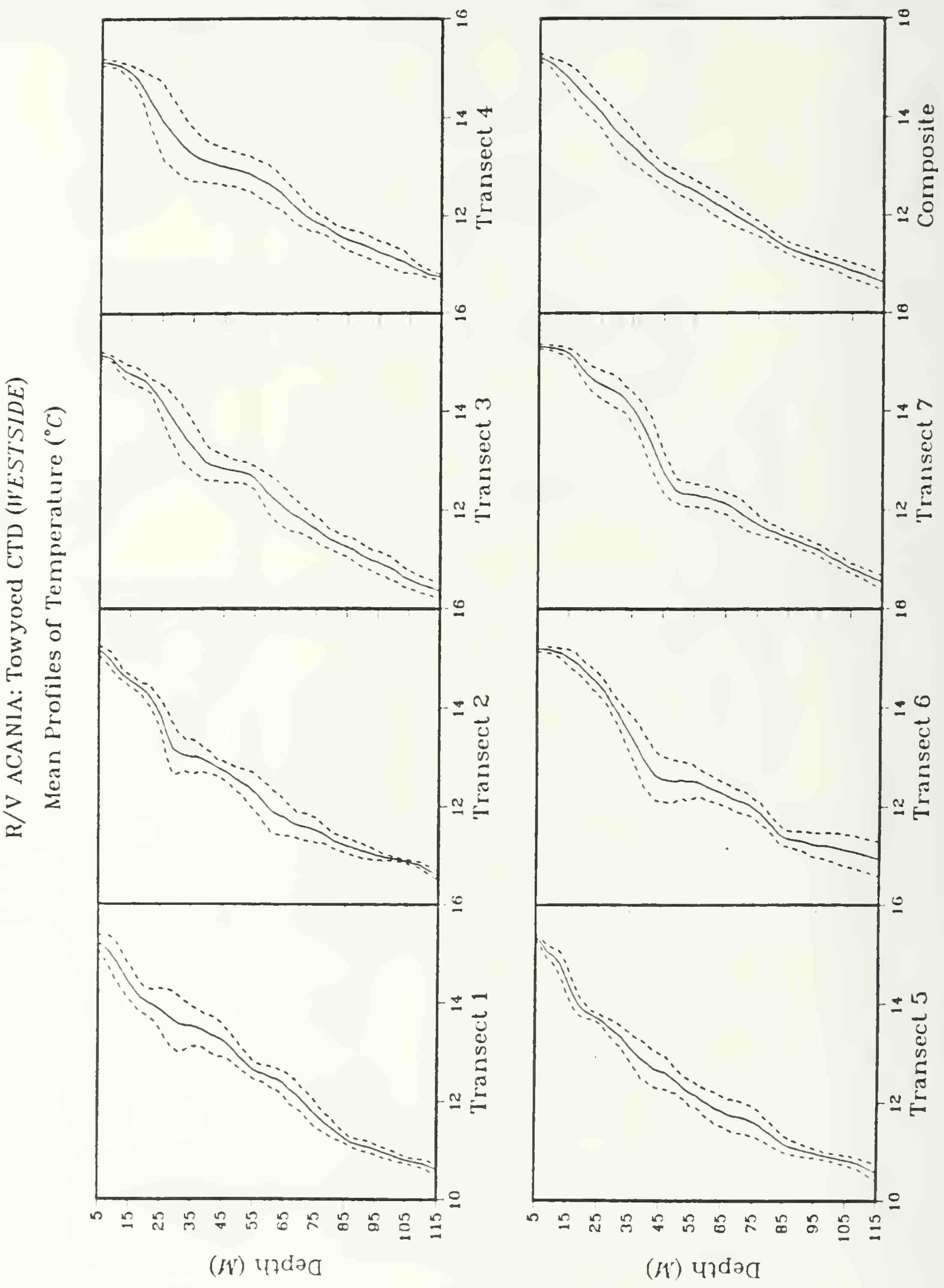

Fig. 4.7 Averaged profiles of temperature (westside).

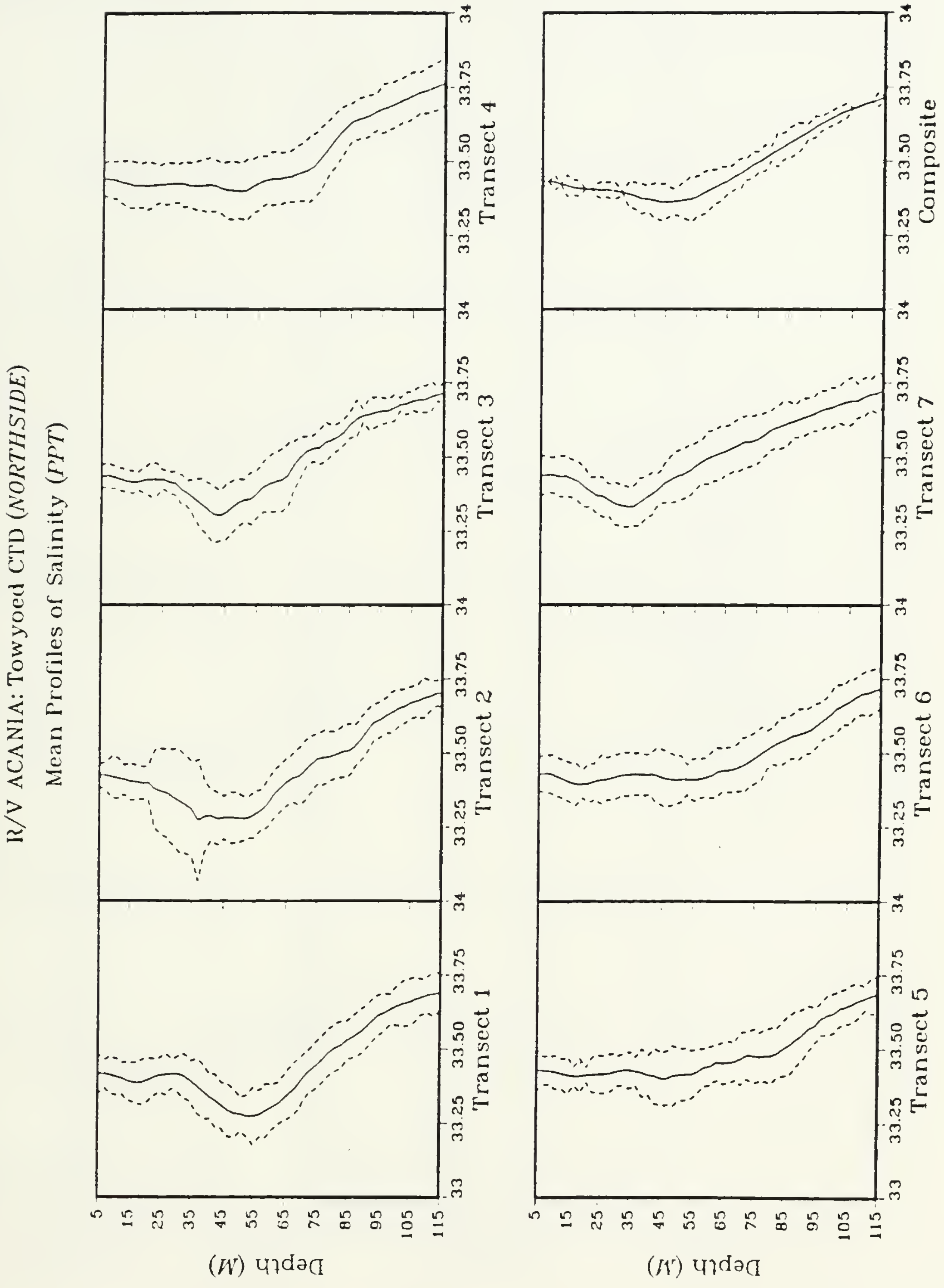

Fig. 4.8 Averaged profiles of salinity (northside).

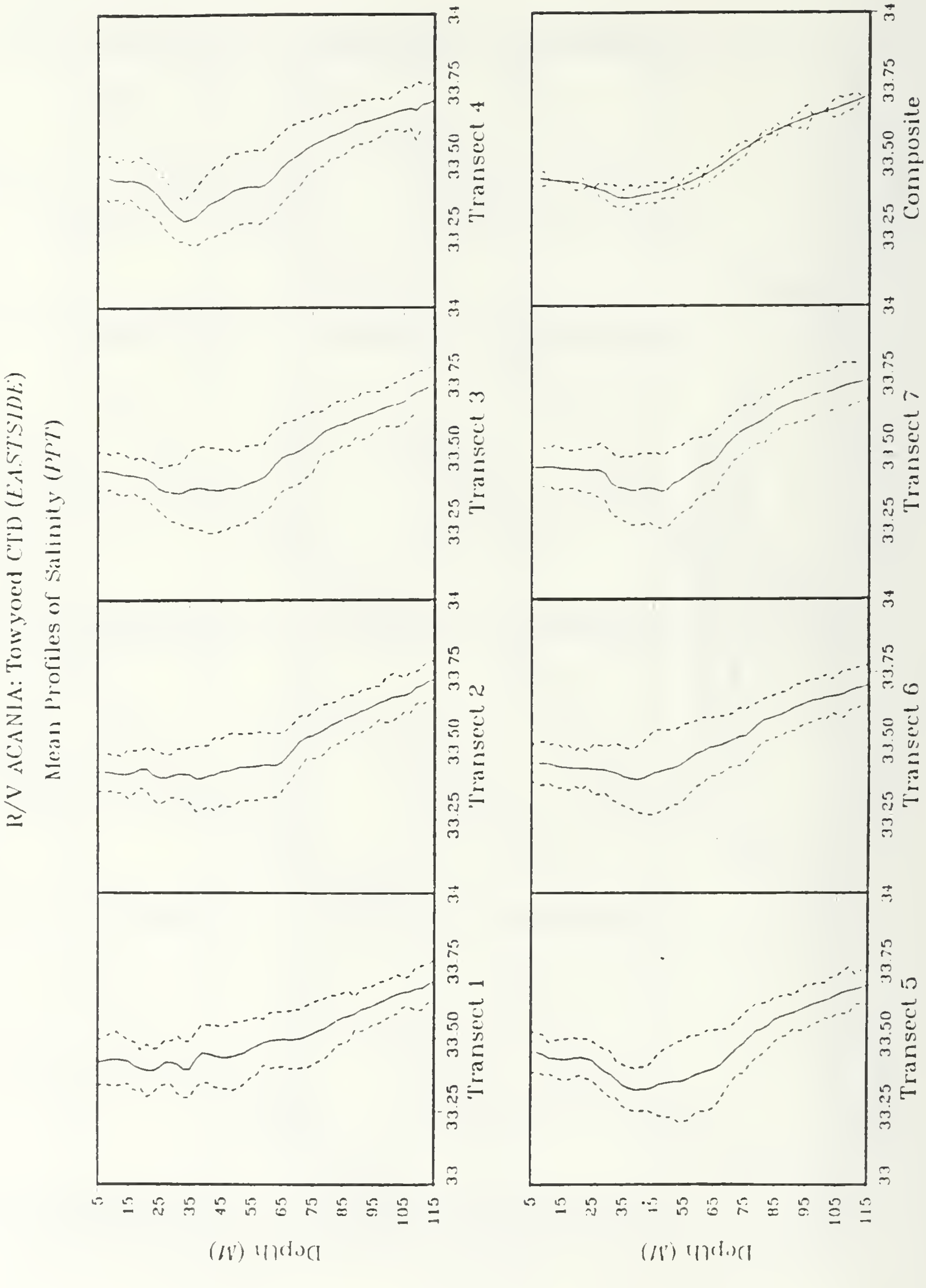

Fig. 4.9 Averaged profiles of salinity (eastside).

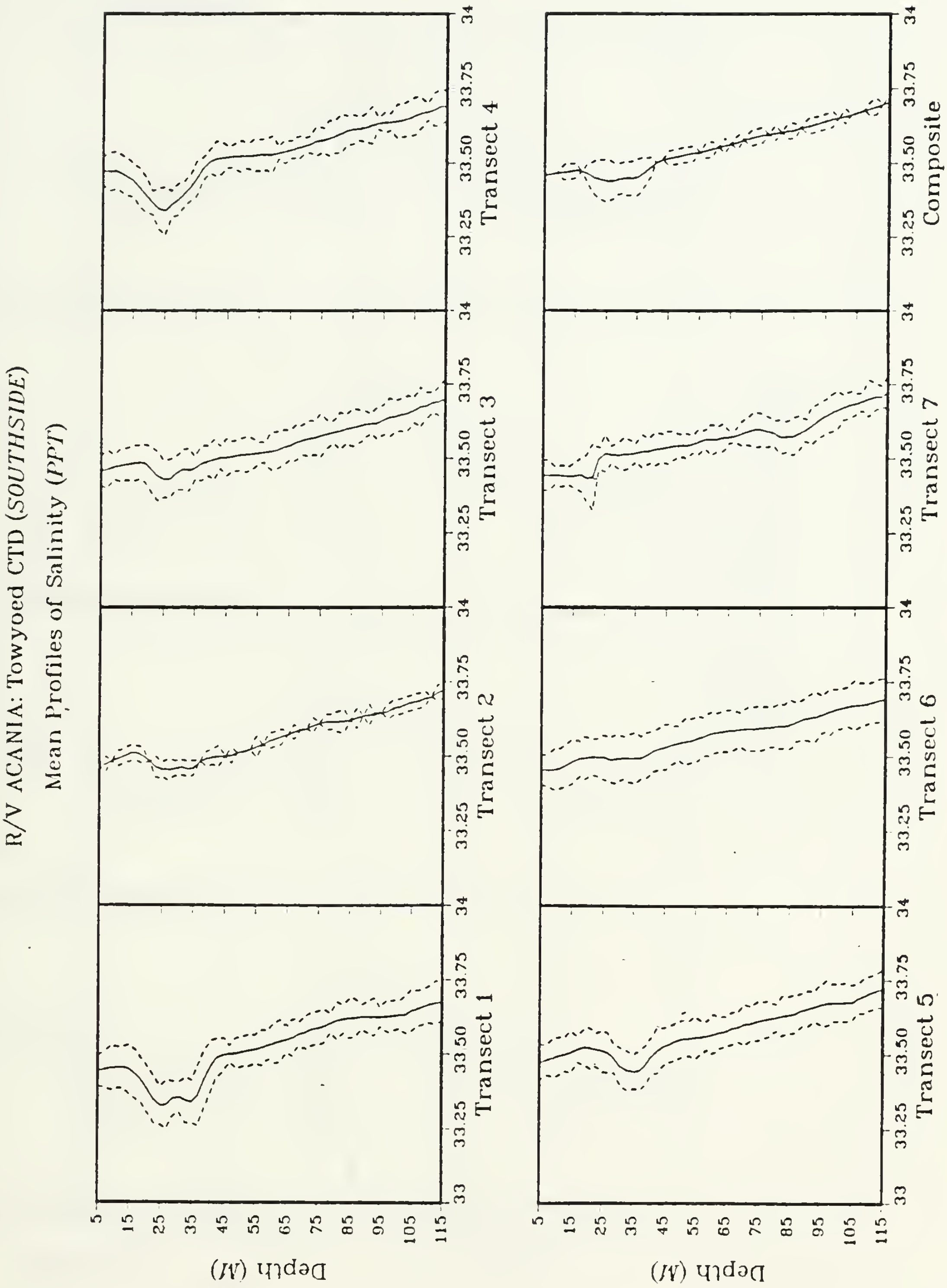

Fig. 4.10 Averaged profiles of salinity (southside).

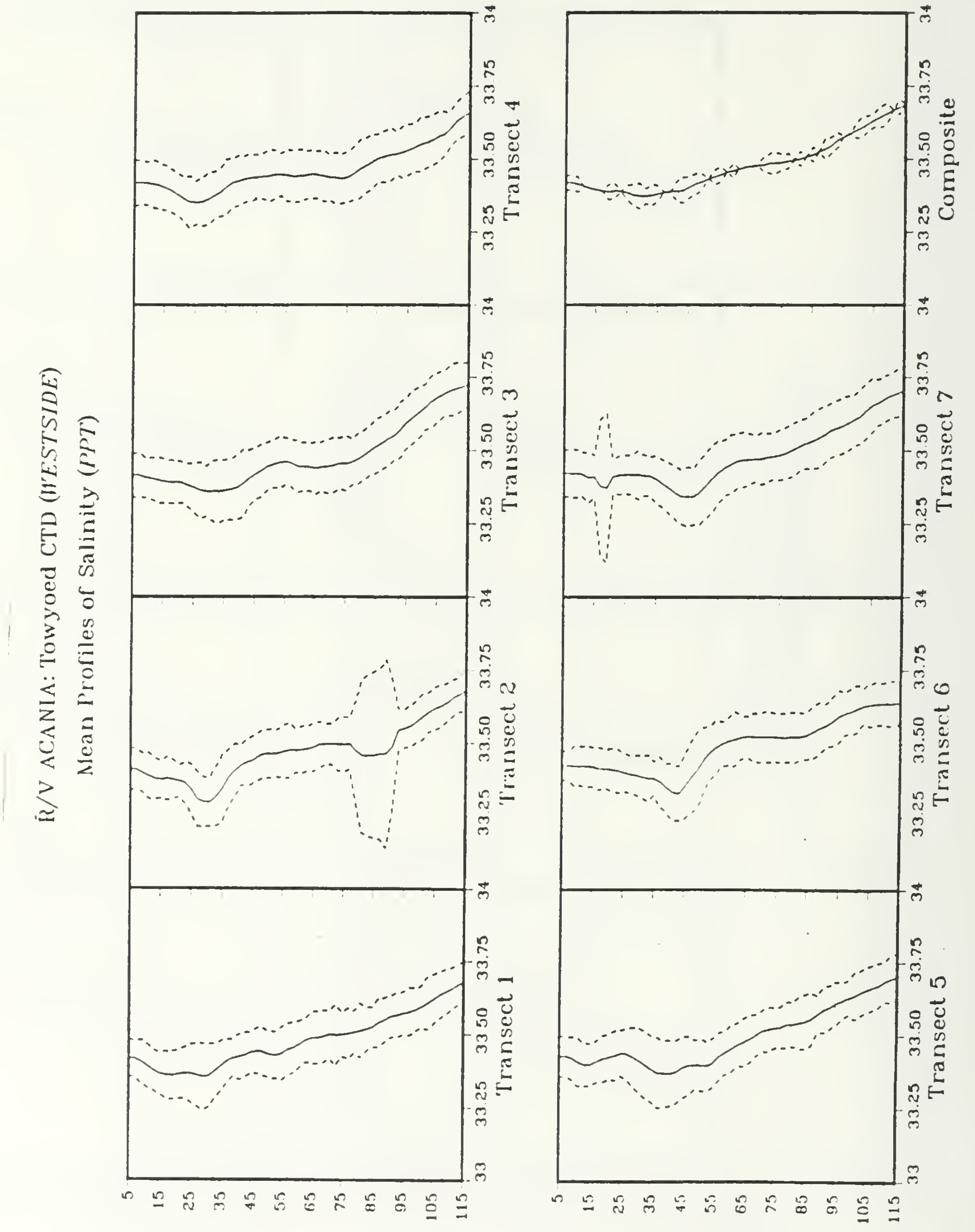

Fig. 4.11 Averaged profiles of salinity (westside).

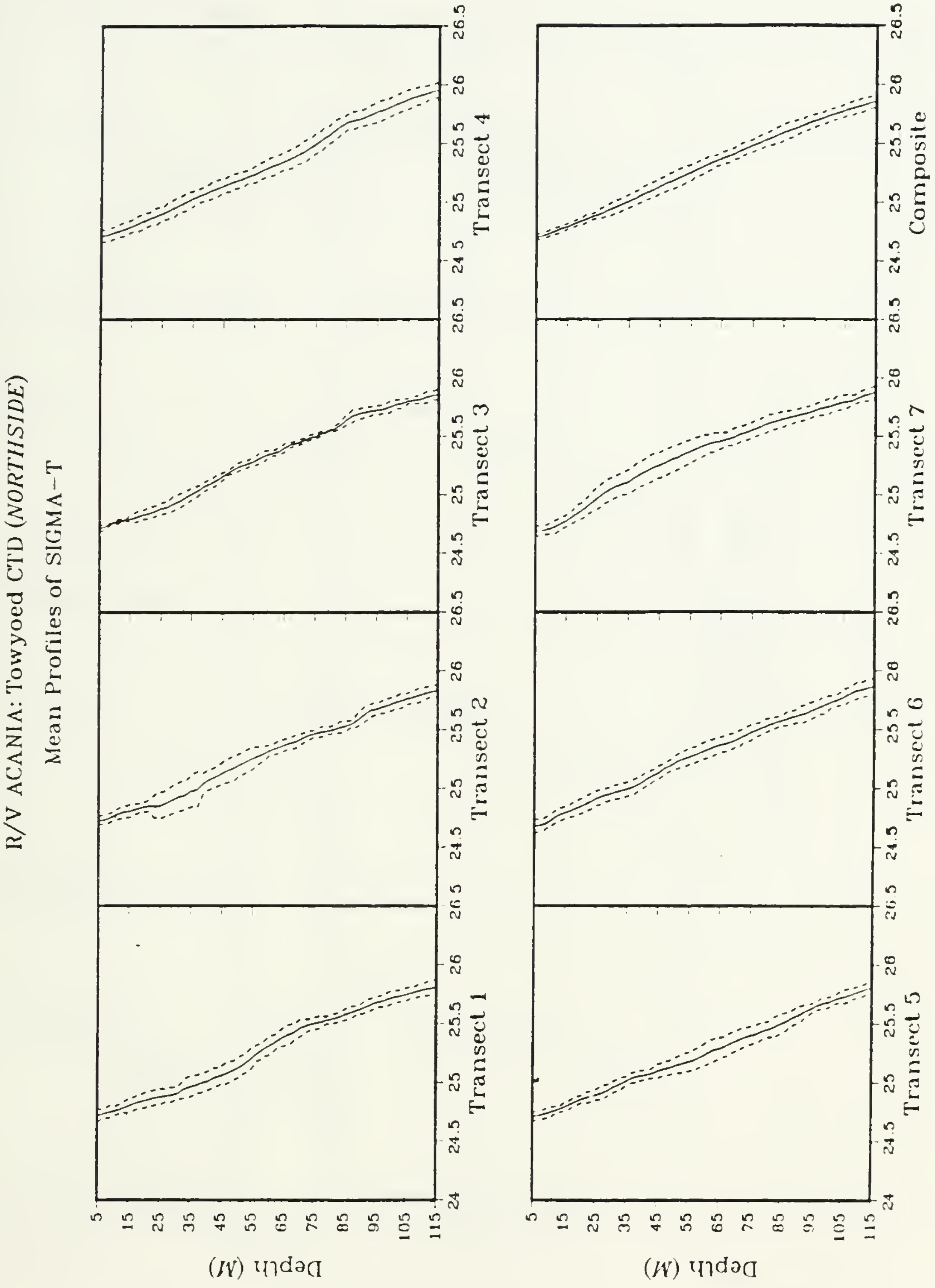

Fig. 4.12 Averaged profiles of sigma-t (northside).

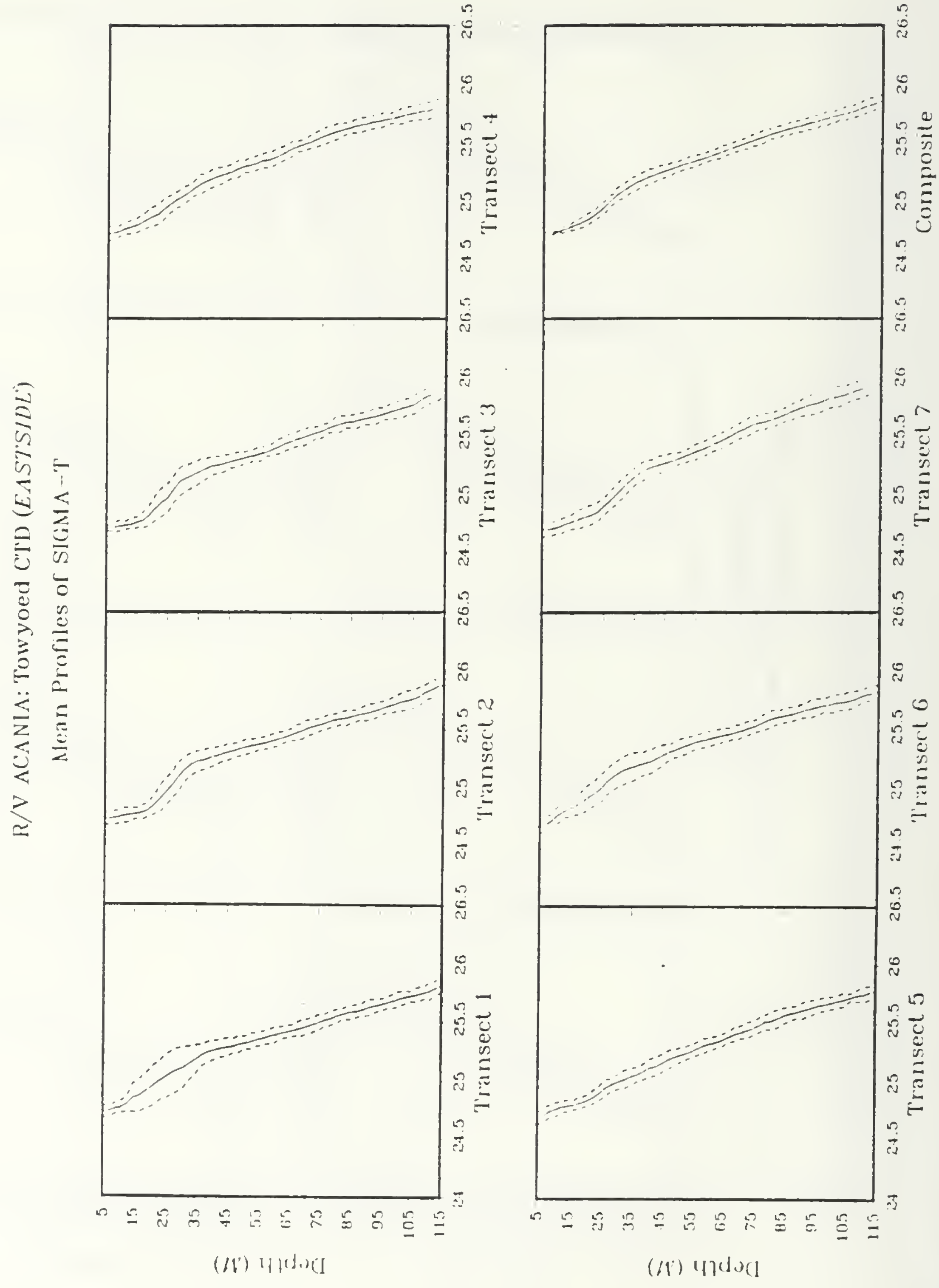

Fig. 4.13 Averaged profiles of sigma-t (eastside).

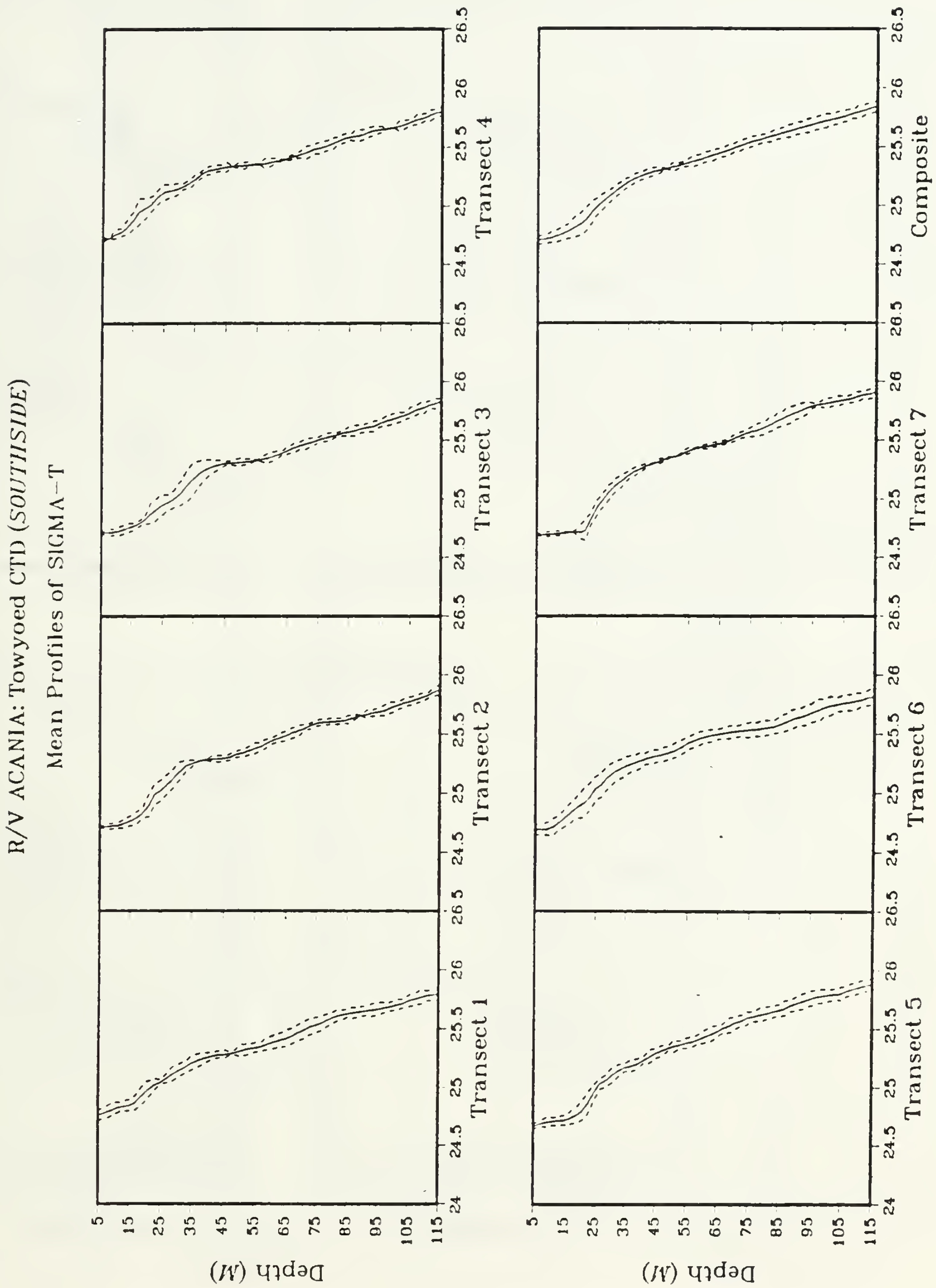

Fig. 4.14 Averaged profiles of sigma-t (southside).

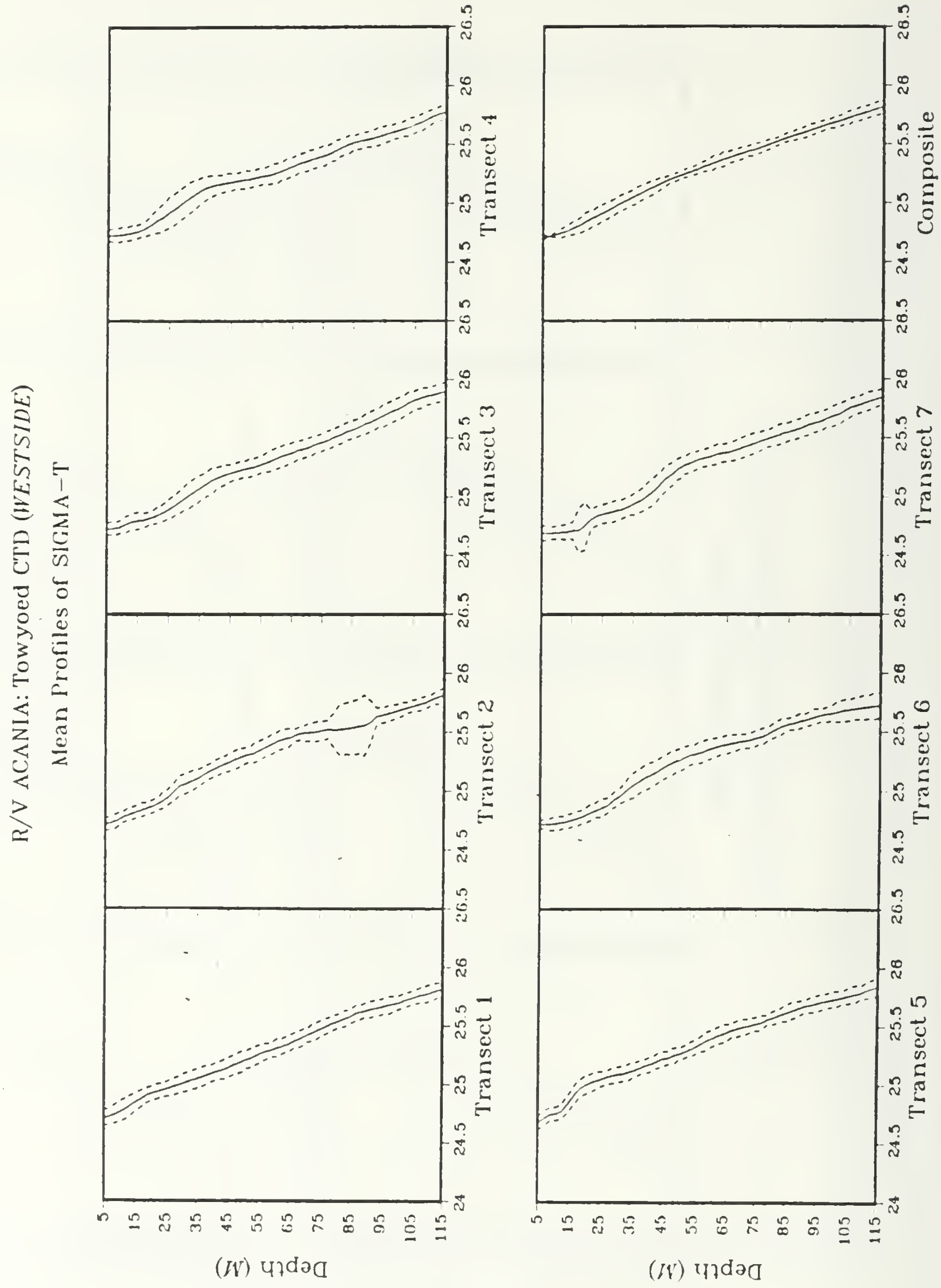

Fig. 4.15 Averaged profiles of sigma-t (westside).

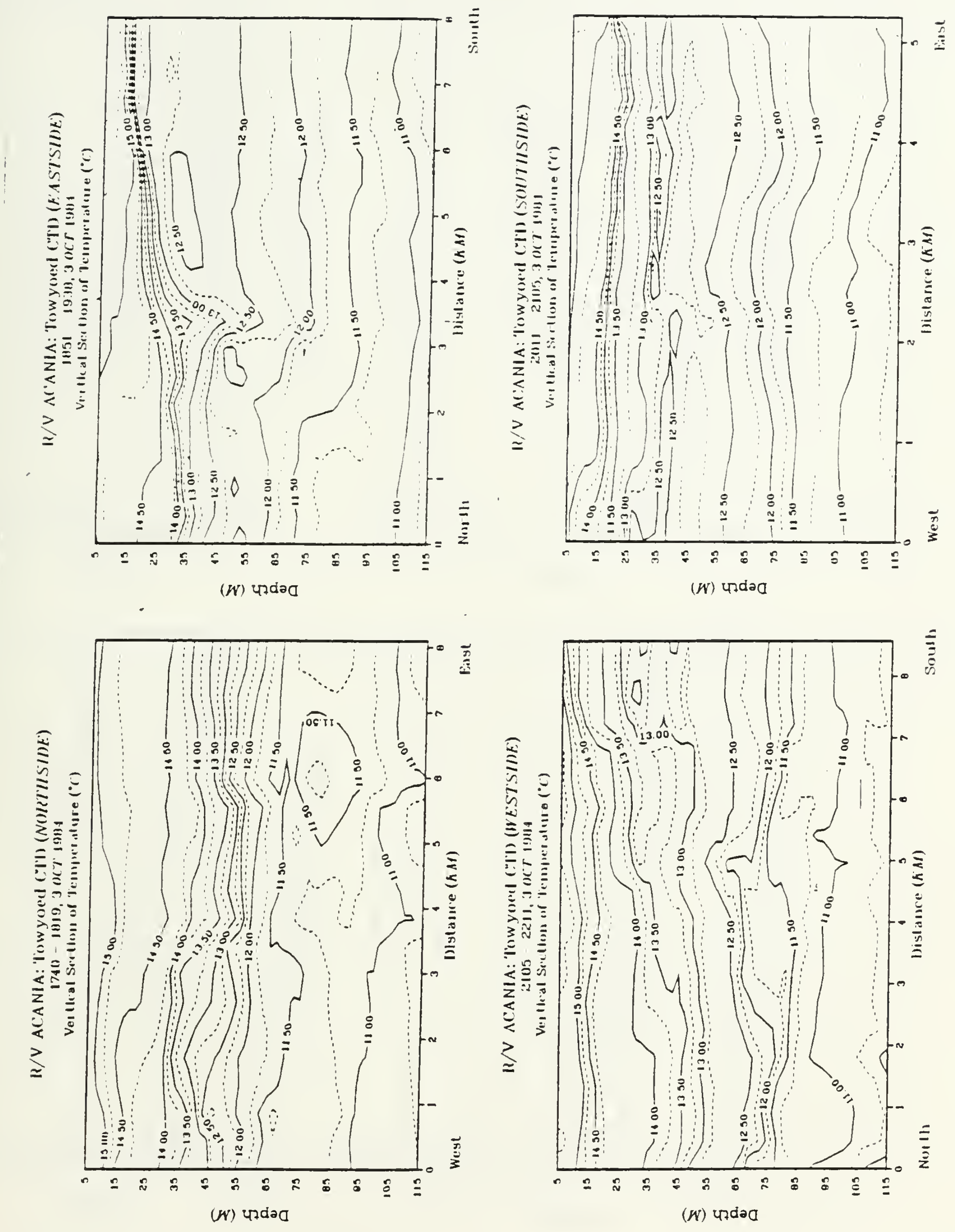

Fig. 4.16 Vertical section of temperature for circuit 1.

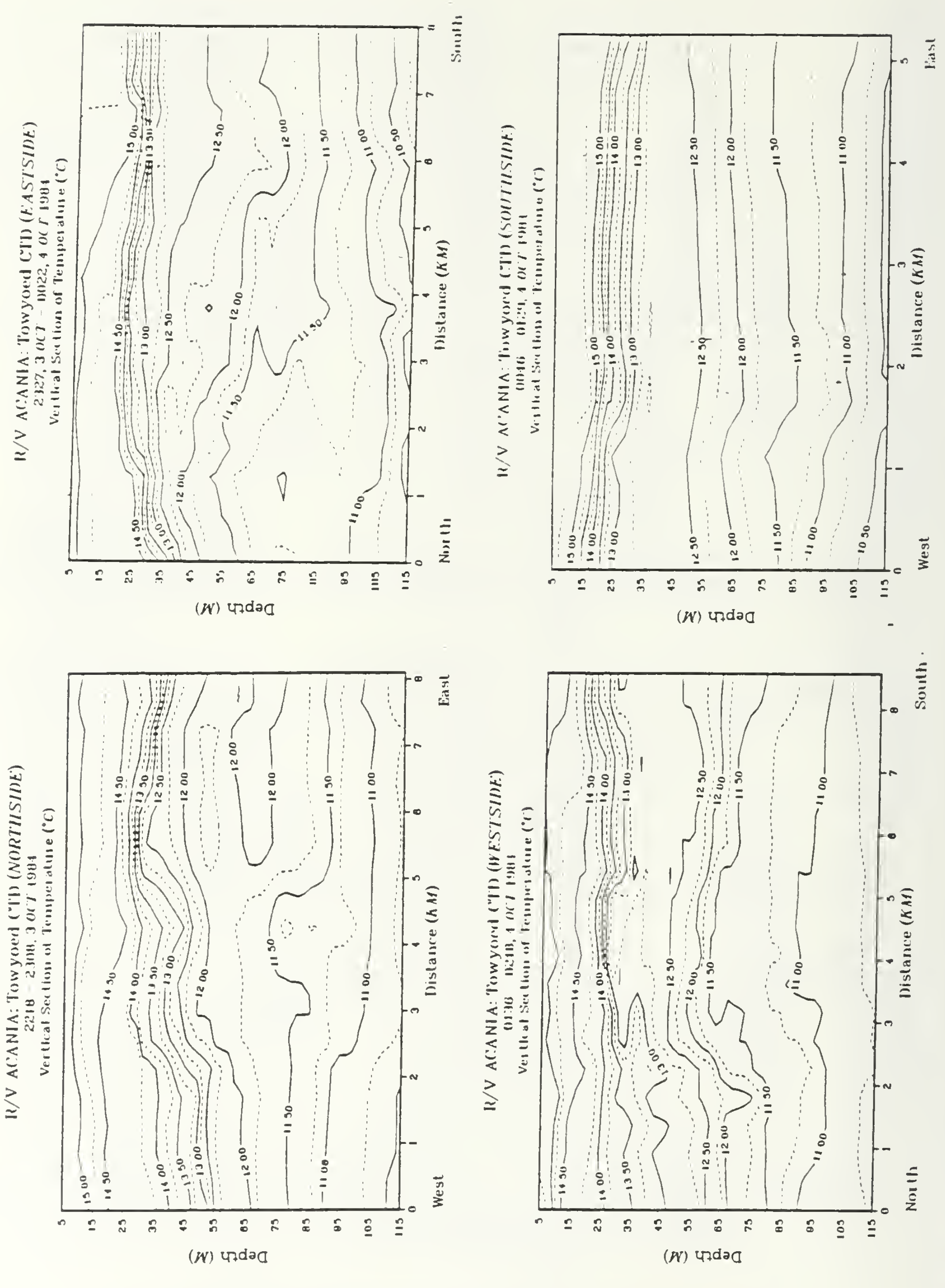

R/V ACANIA: Towyoed CTD (NORTHSIDE) 2218 - 2308, 3 OCT 1984 Vertical Section of Temperature (°C)

R/V ACANIA: Towyoed CTD (EASTSIDE) 2327, 3 OCT - 0022, 4 OCT 1984 Vertical Section of Temperature (°C)

R/V ACANIA: Towyoed CTD (WESTSIDE) 0138 - 0218, 4 OCT 1984 Vertical Section of Temperature (°C)

R/V ACANIA: Towyoed CTD (SOUTHSIDE) 0046 - 0129, 4 OCT 1984 Vertical Section of Temperature (°C)

Fig. 4.17 Vertical section of temperature for circuit 2.

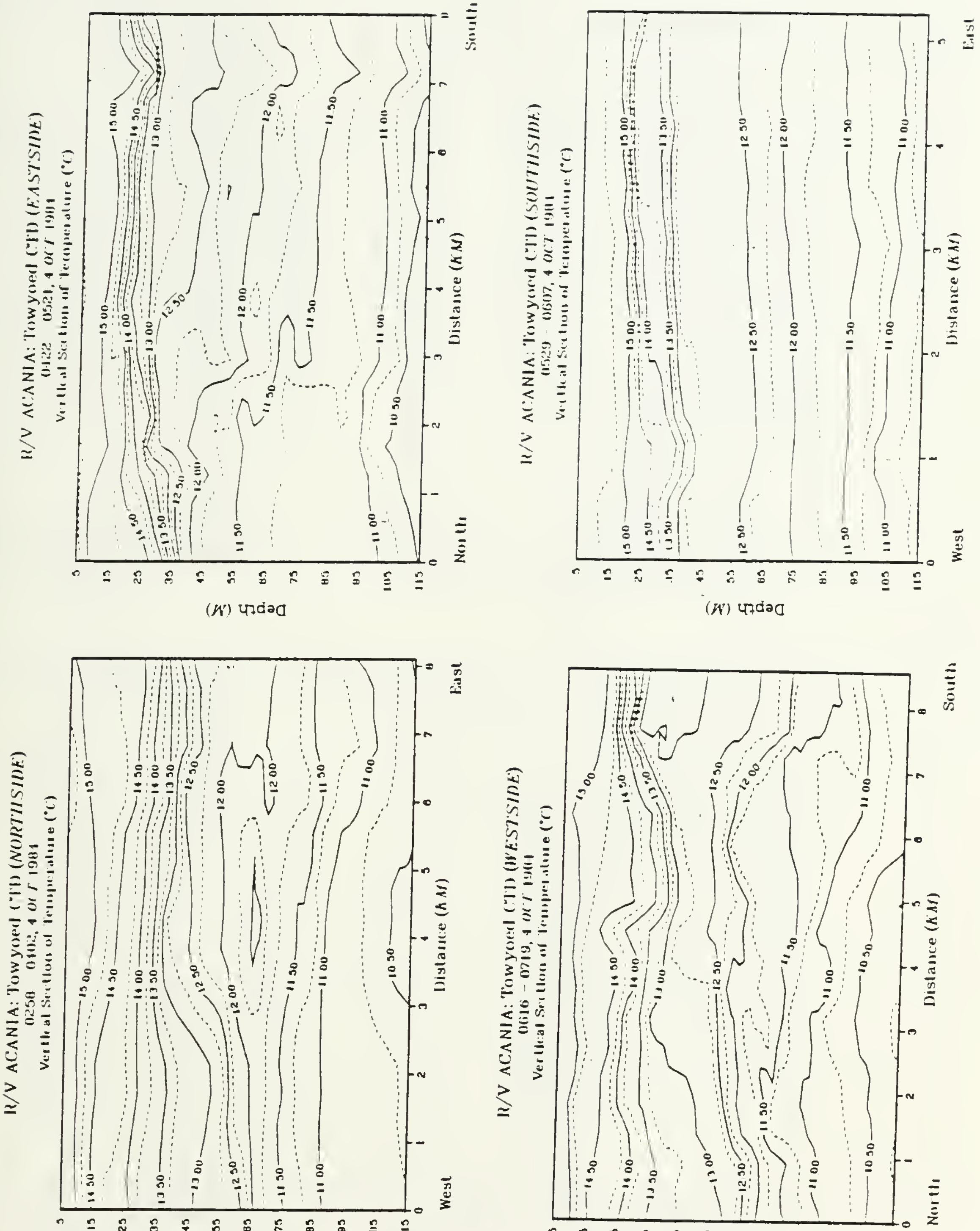
R/V ACANIA: Towyoed CTD (*NORTHSIDE*)
0258 - 0402, 4 *OCT* 1981
Vertical Section of Temperature (°C)

R/V ACANIA: Towyoed CTD (*EASTSIDE*)
0422 - 0521, 4 *OCT* 1981
Vertical Section of Temperature (°C)

R/V ACANIA: Towyoed CTD (*WESTSIDE*)
0616 - 0719, 4 *OCT* 1981
Vertical Section of Temperature (°C)

R/V ACANIA: Towyoed CTD (*SOUTHSIDE*)
0529 - 0607, 4 *OCT* 1981
Vertical Section of Temperature (°C)

Fig. 4.18 Vertical section of temperature for circuit 3.

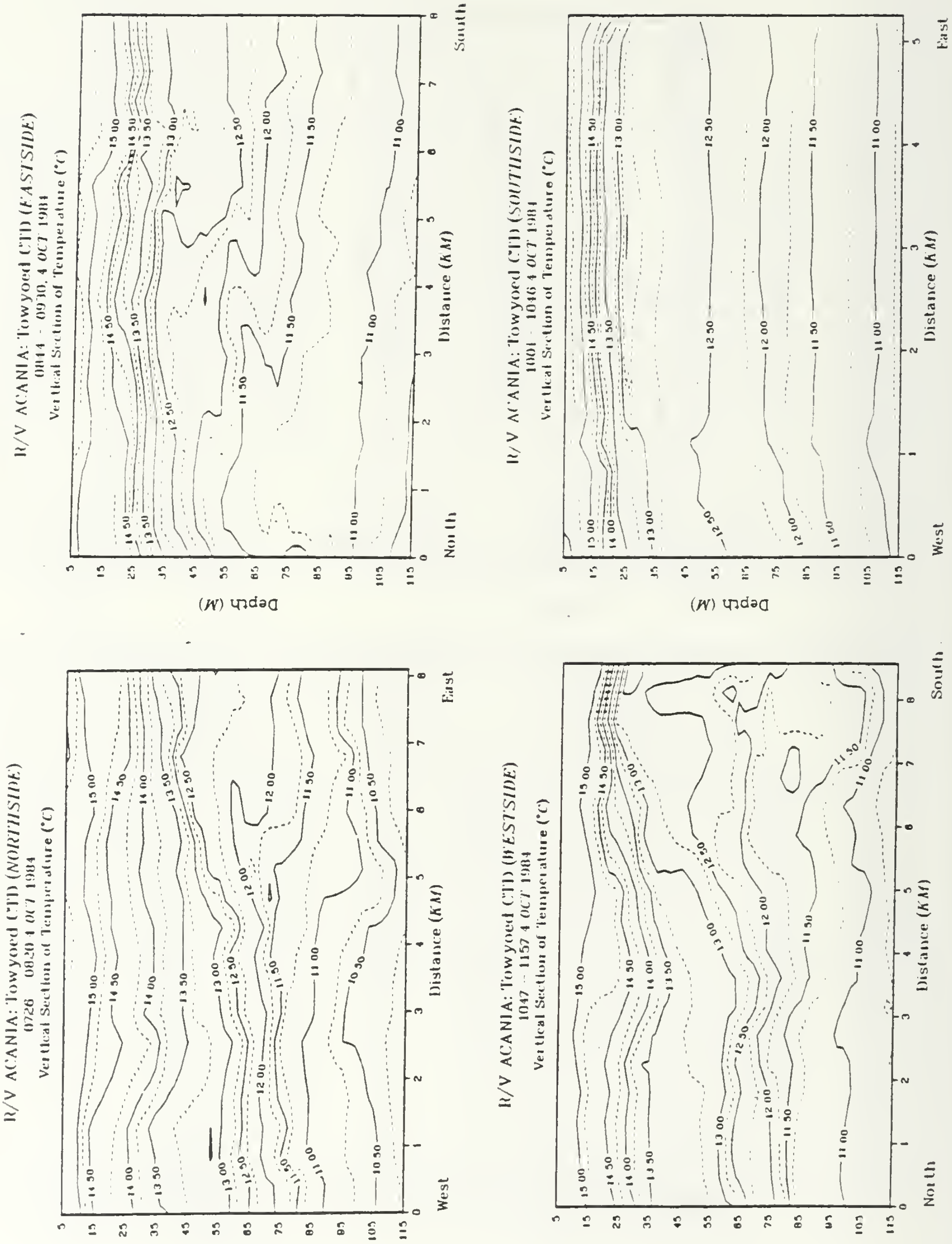

Fig. 4.19 Vertical section of temperature for circuit 4.

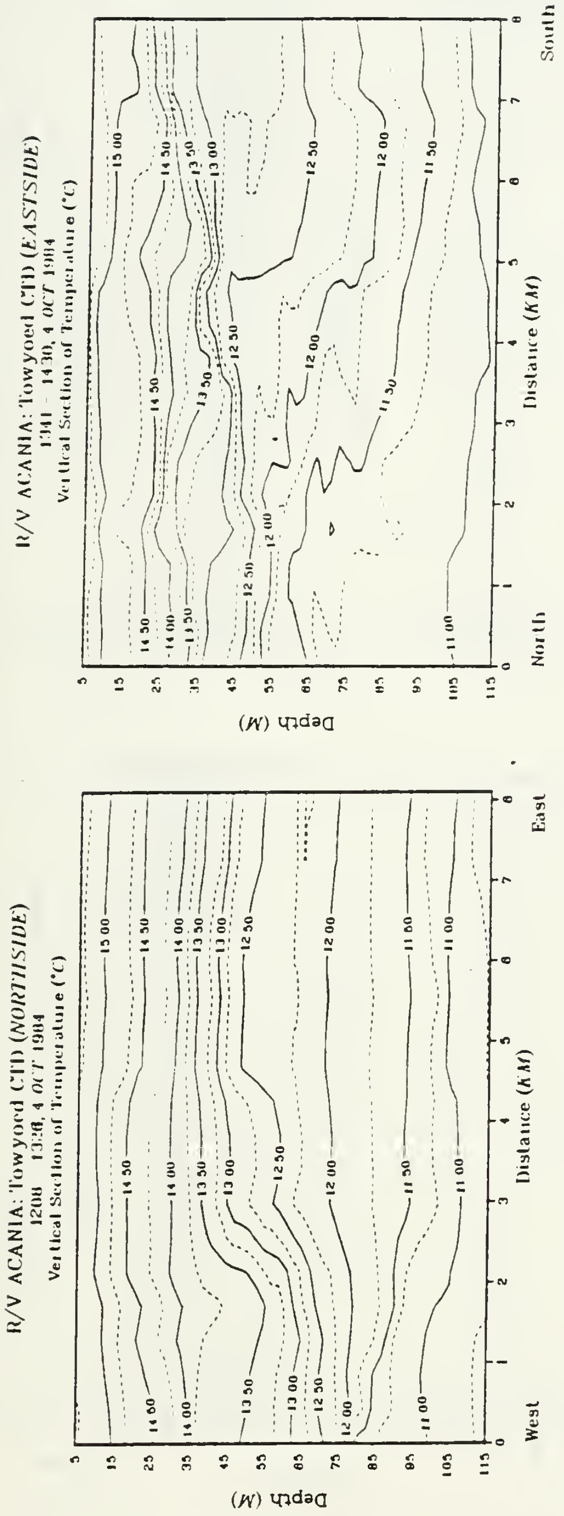

Fig. 4.20 Vertical section of temperature for circuit 5.

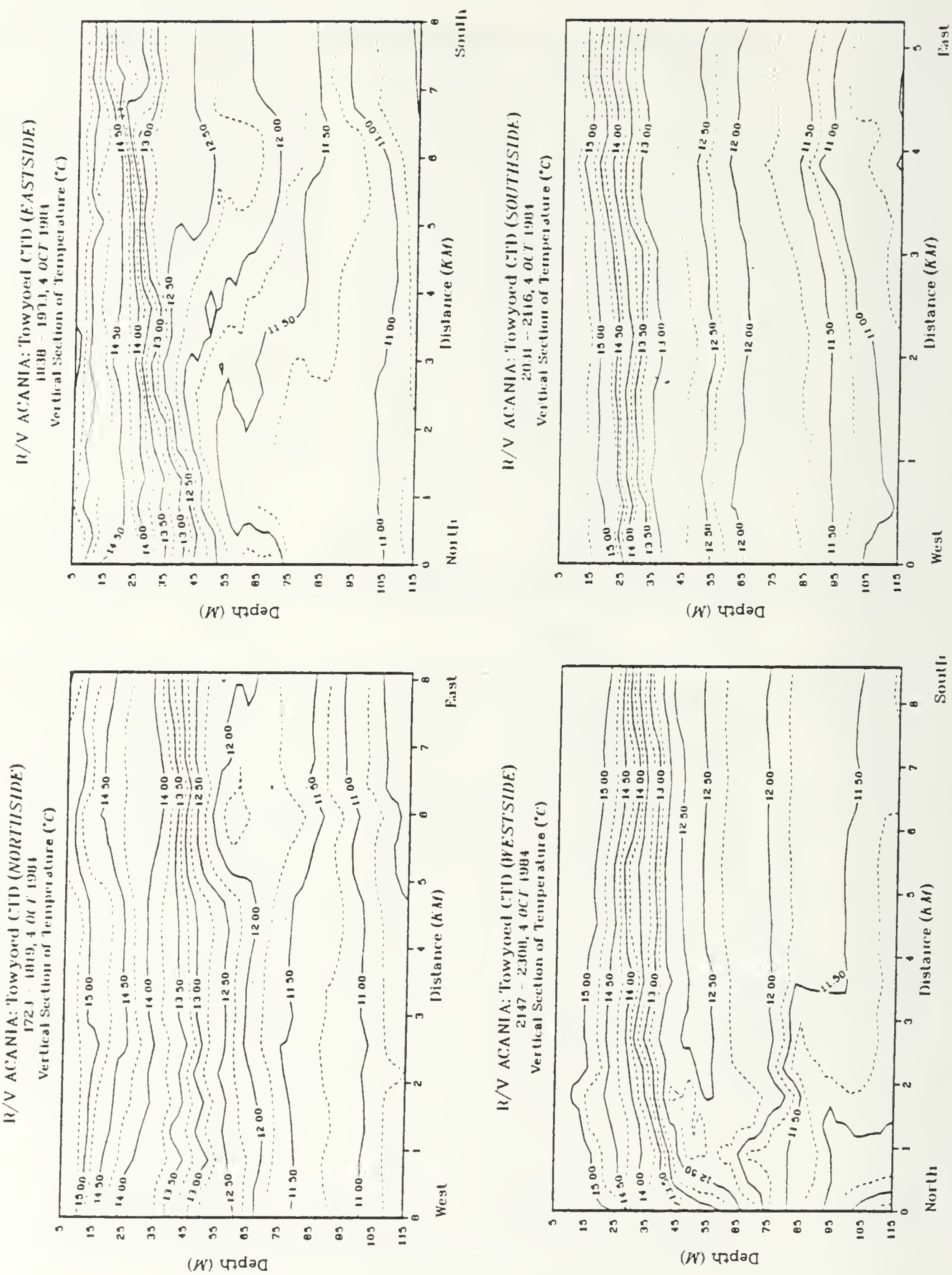

Fig. 4.21 Vertical section of temperature for circuit 6.

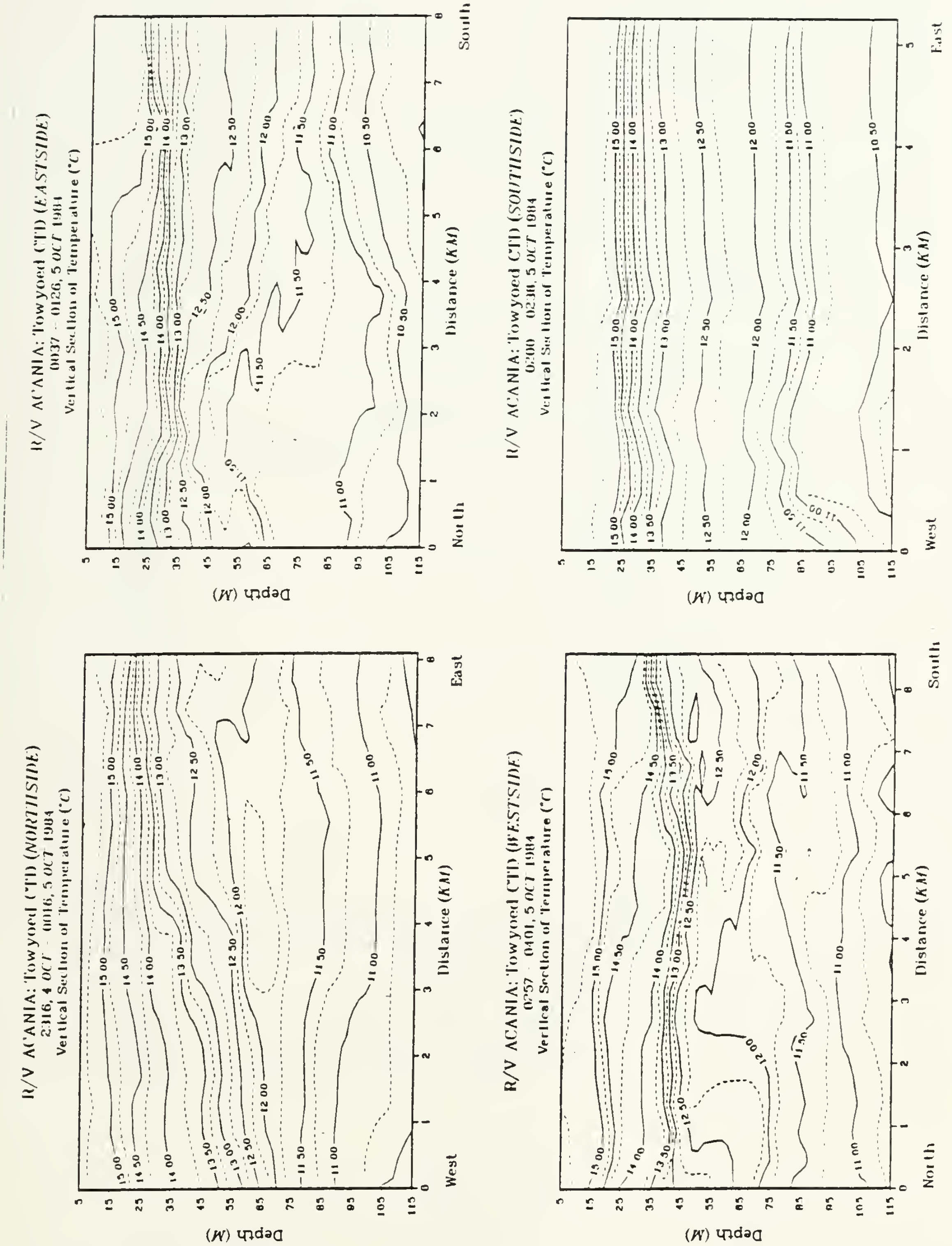

Fig. 4.22 Vertical section of temperature for circuit 7.

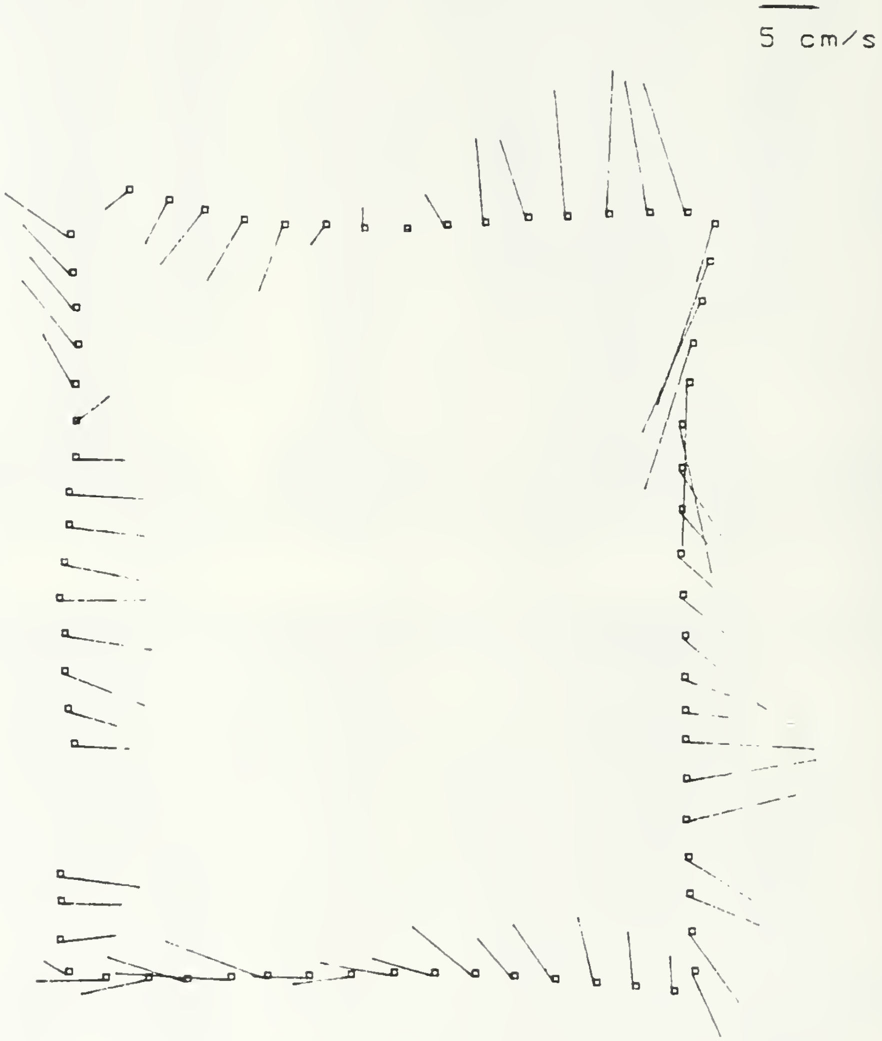

Fig. 4.23 Horizontal velocity difference plots for 75-25m levels (circuit 2).

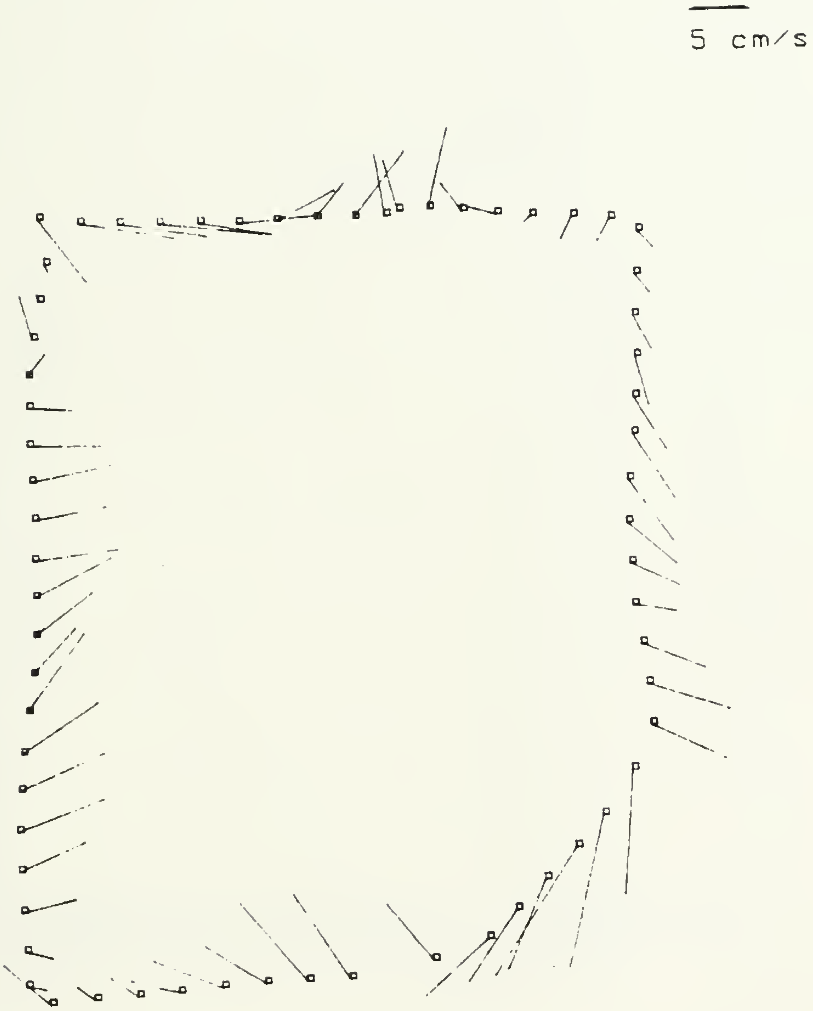

Fig. 4.24 Horizontal velocity difference plots for 75-25m levels (circuit 3).

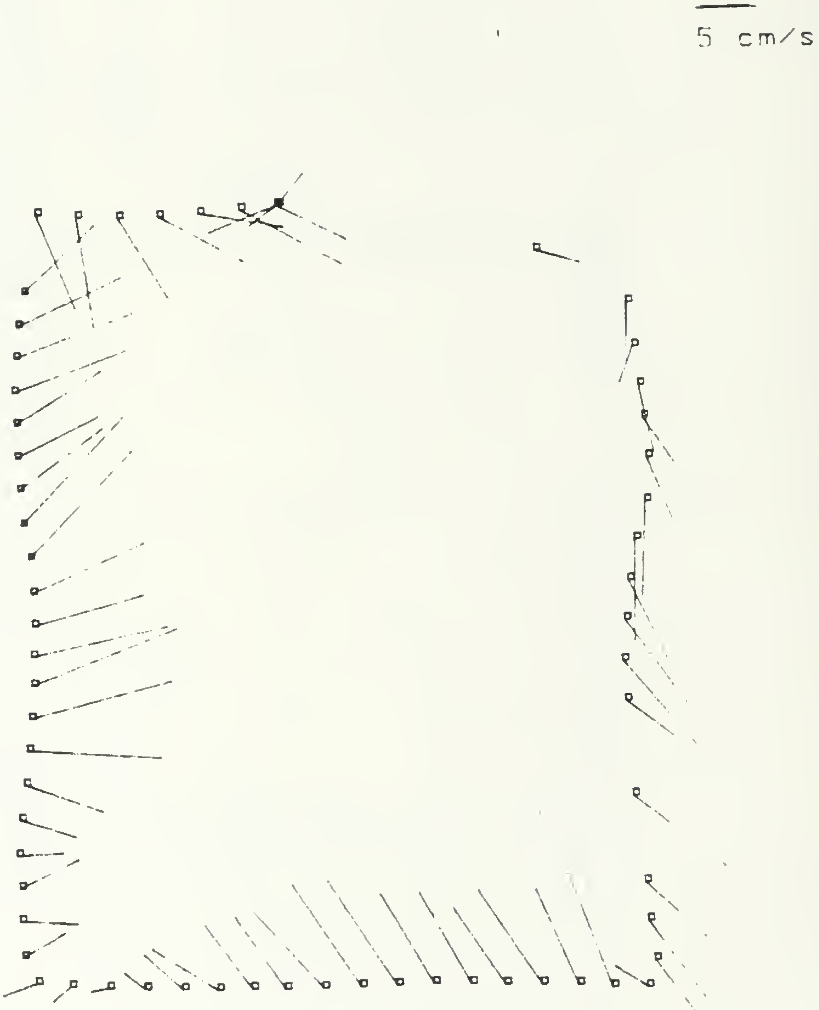

Fig. 4.25 Horizontal velocity difference plots for 75-25m levels (circuit 5).

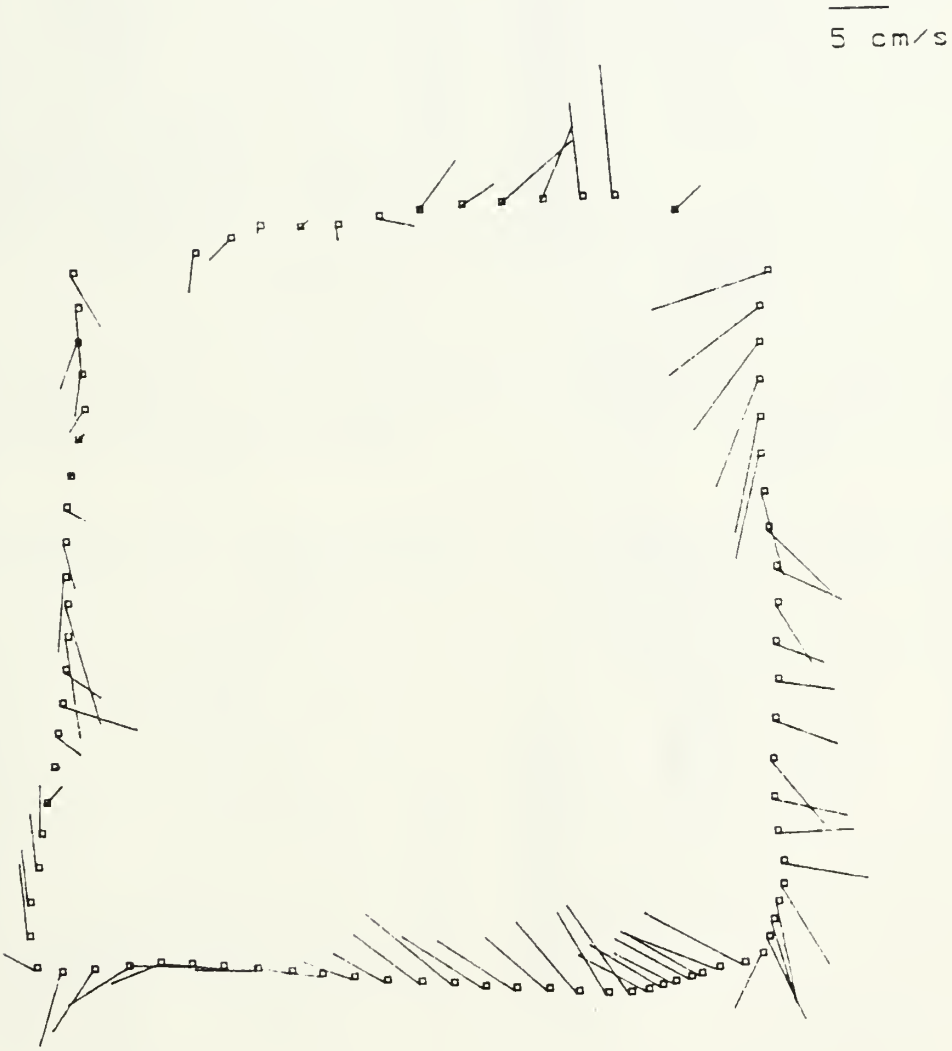

Fig. 4.26 Horizontal velocity difference plots for 75-25m levels (circuit 6).

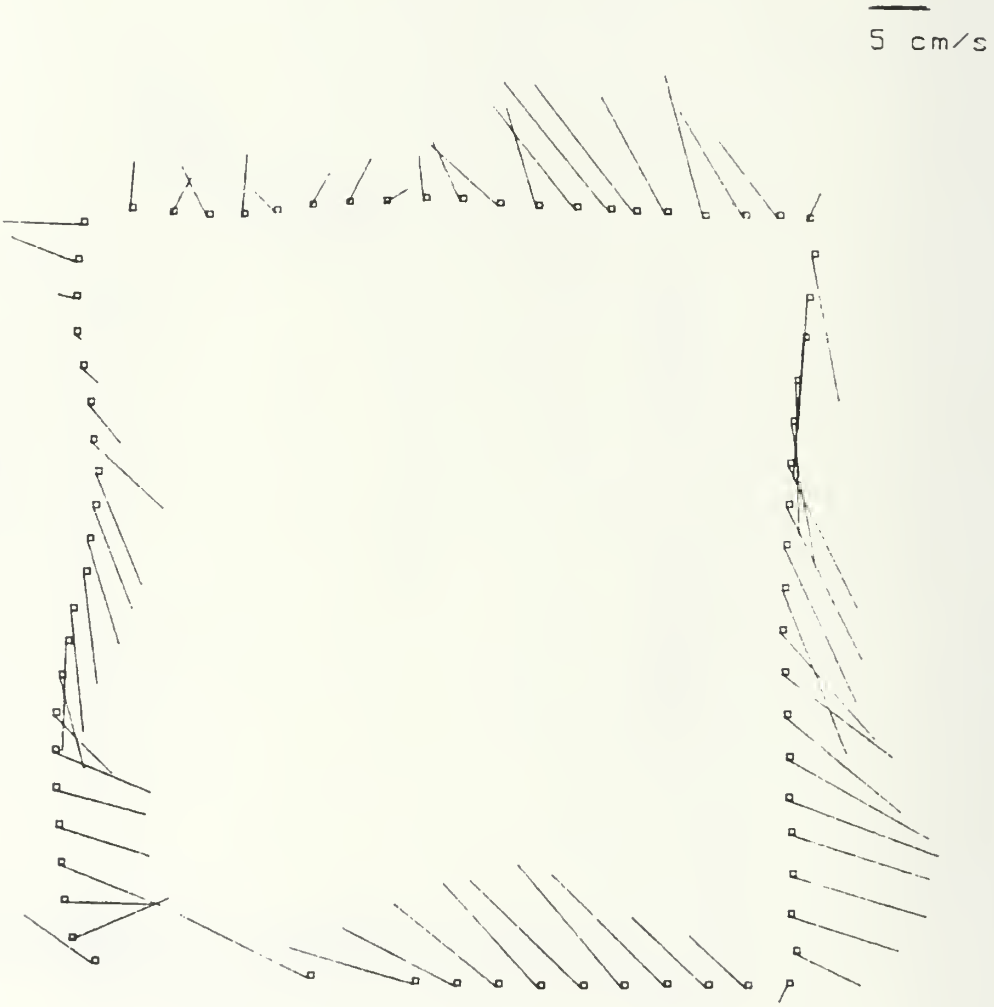

Fig. 4.27 Horizontal velocity difference plots for 75-25m levels (circuit 7).

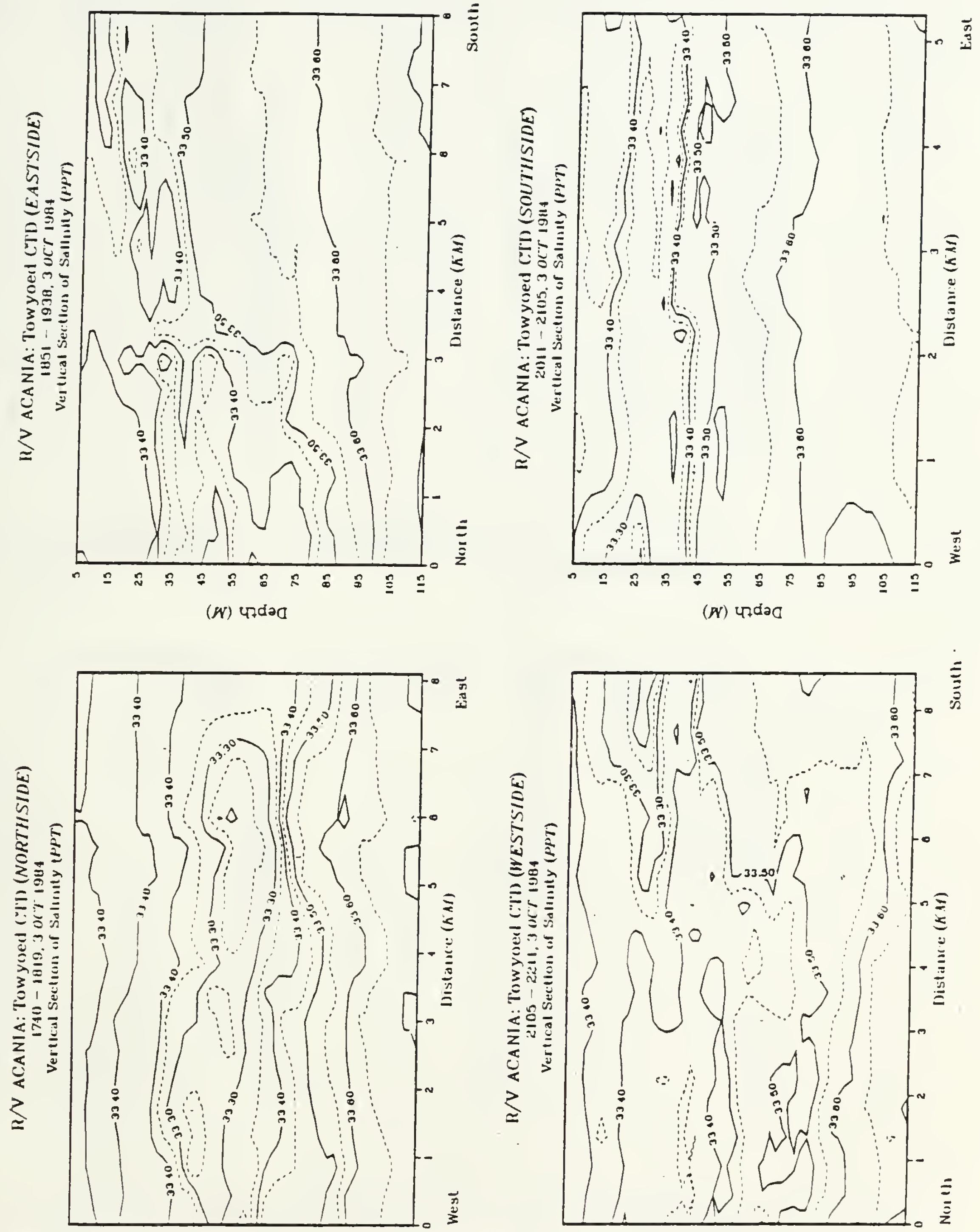

Fig. 4.28 Vertical section of salinity for circuit 1.

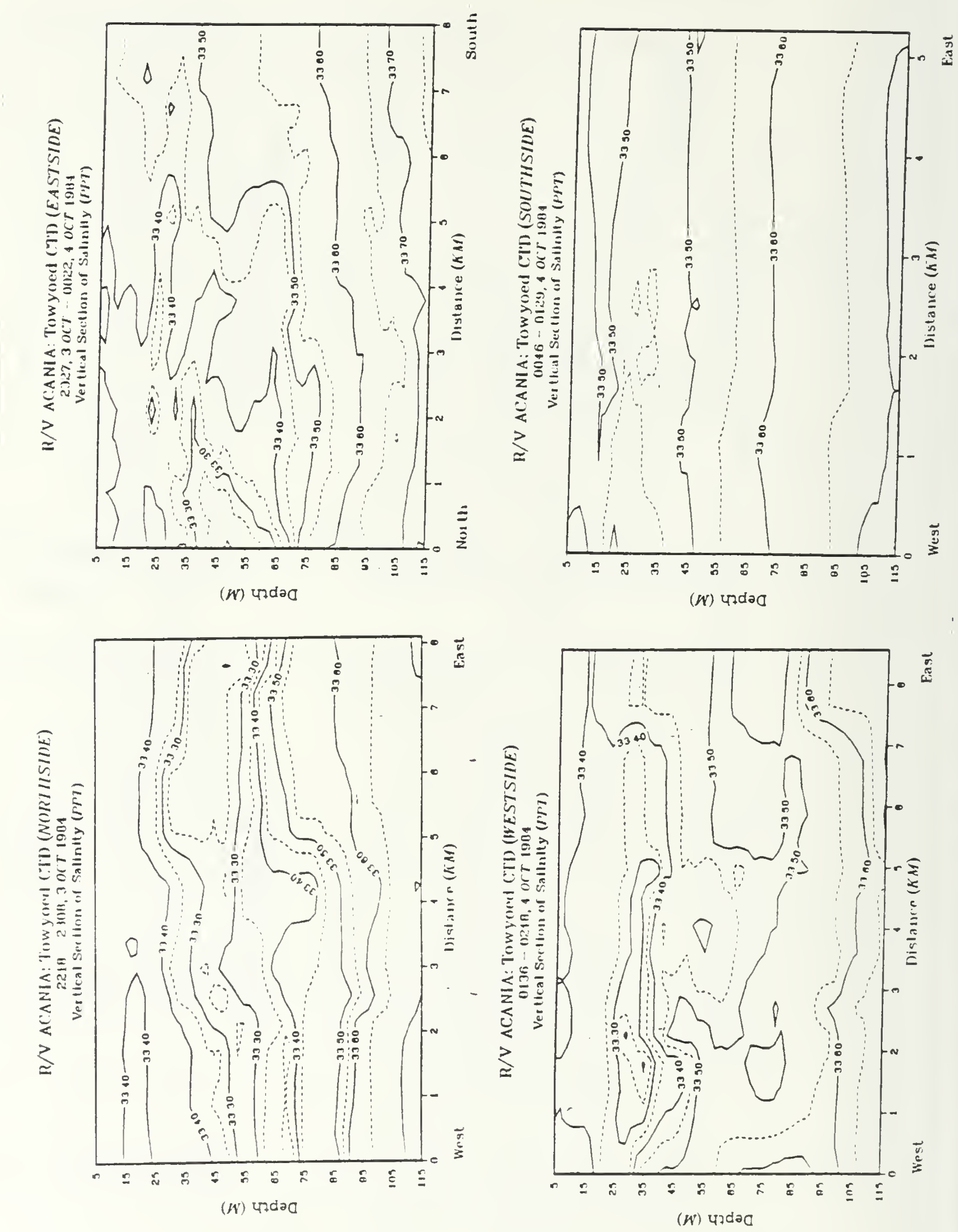

Fig. 4.29 Vertical section of salinity for circuit 2.

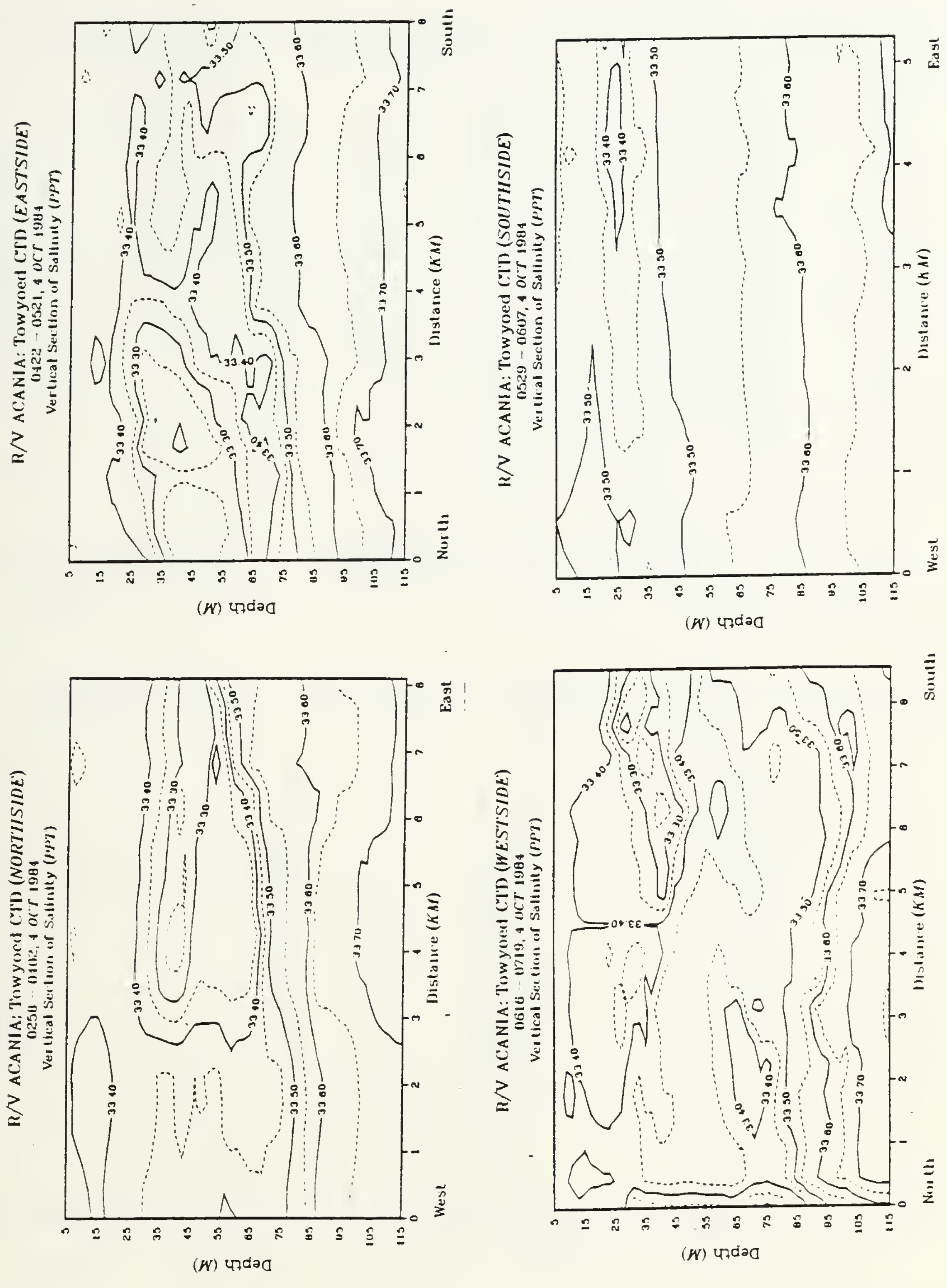

Fig. 4.30 Vertical section of salinity for circuit 3.

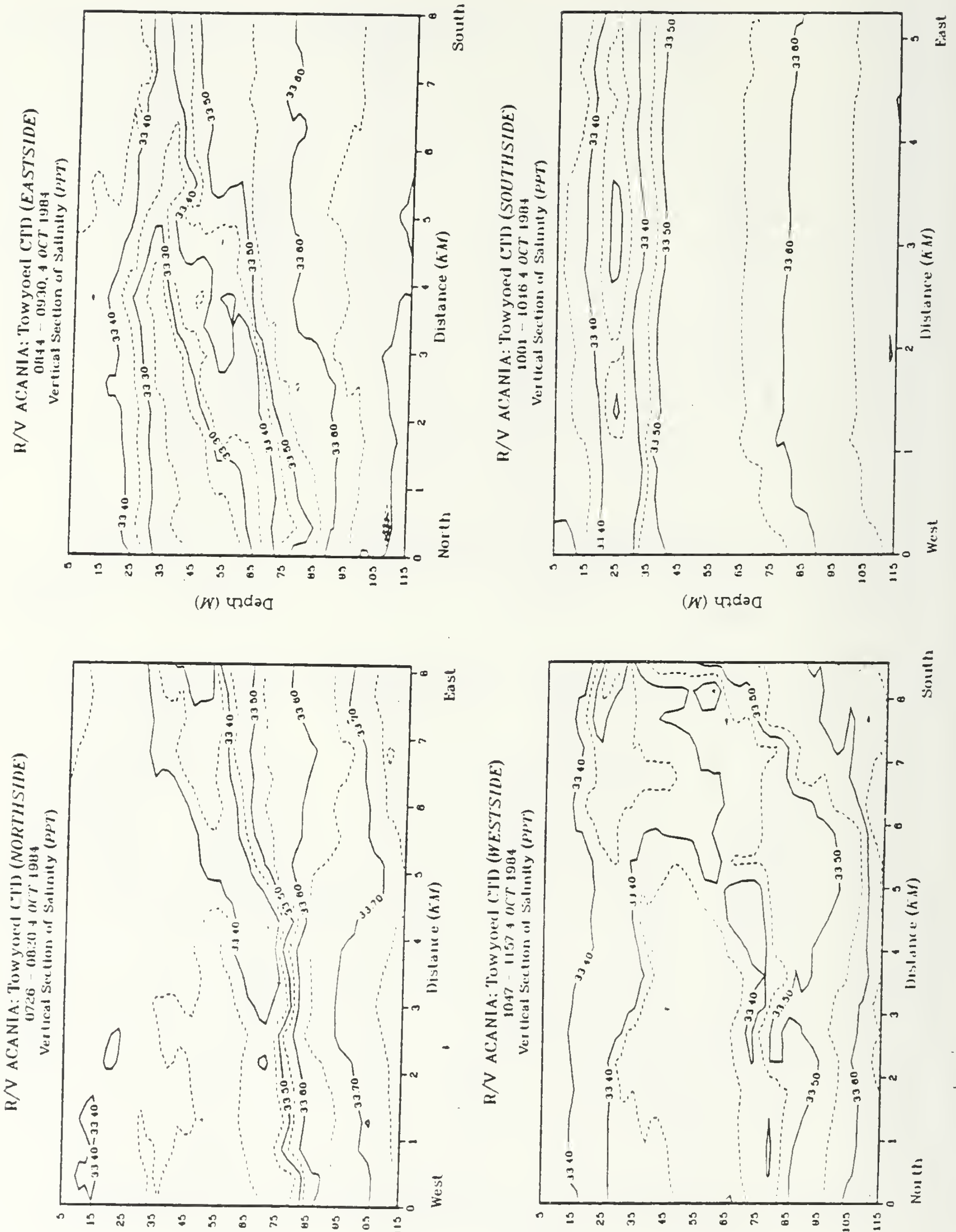

Fig. 4.31 Vertical section of salinity for circuit 4.

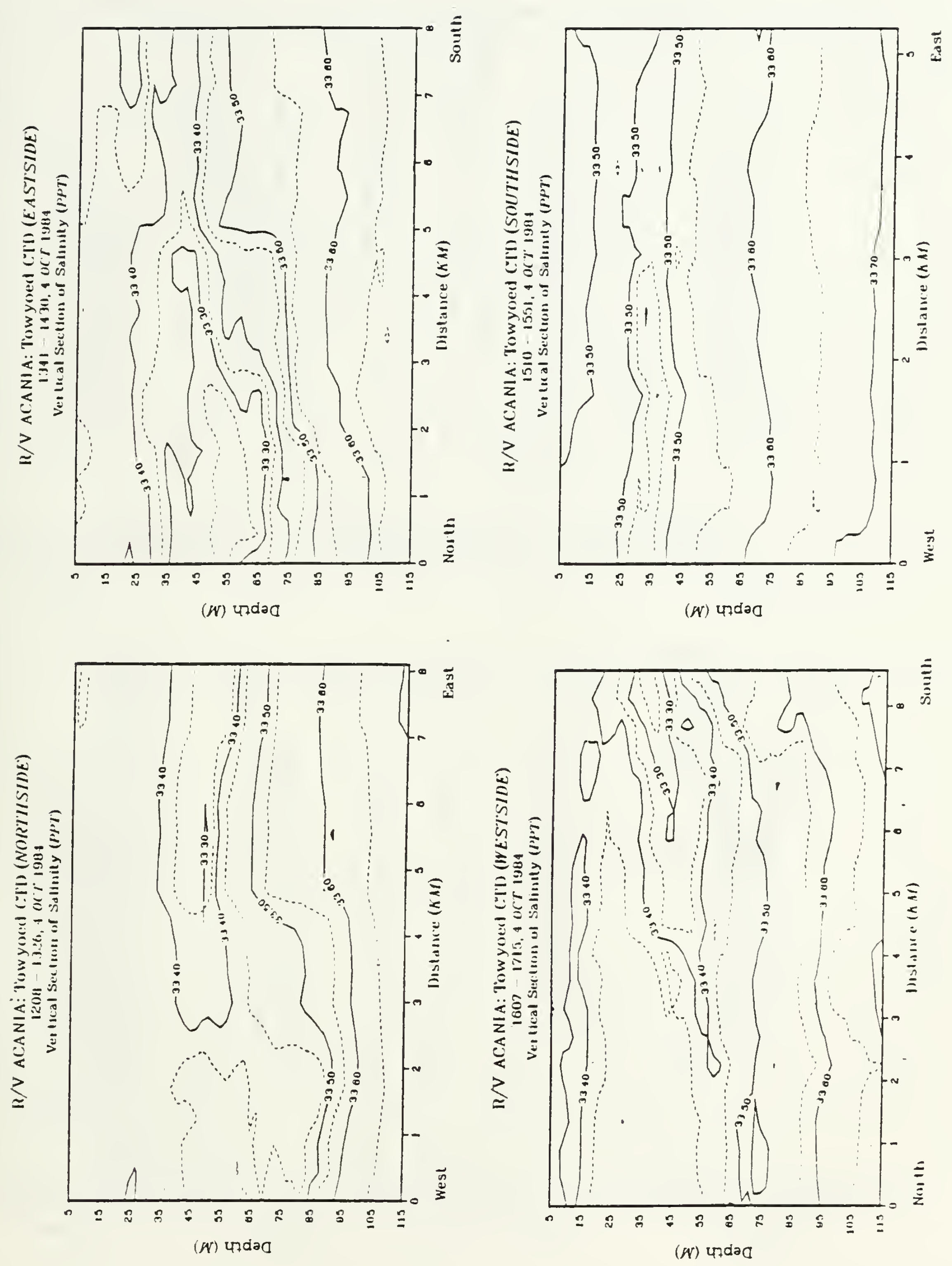

Fig. 4.32 Vertical section of salinity for circuit 5.

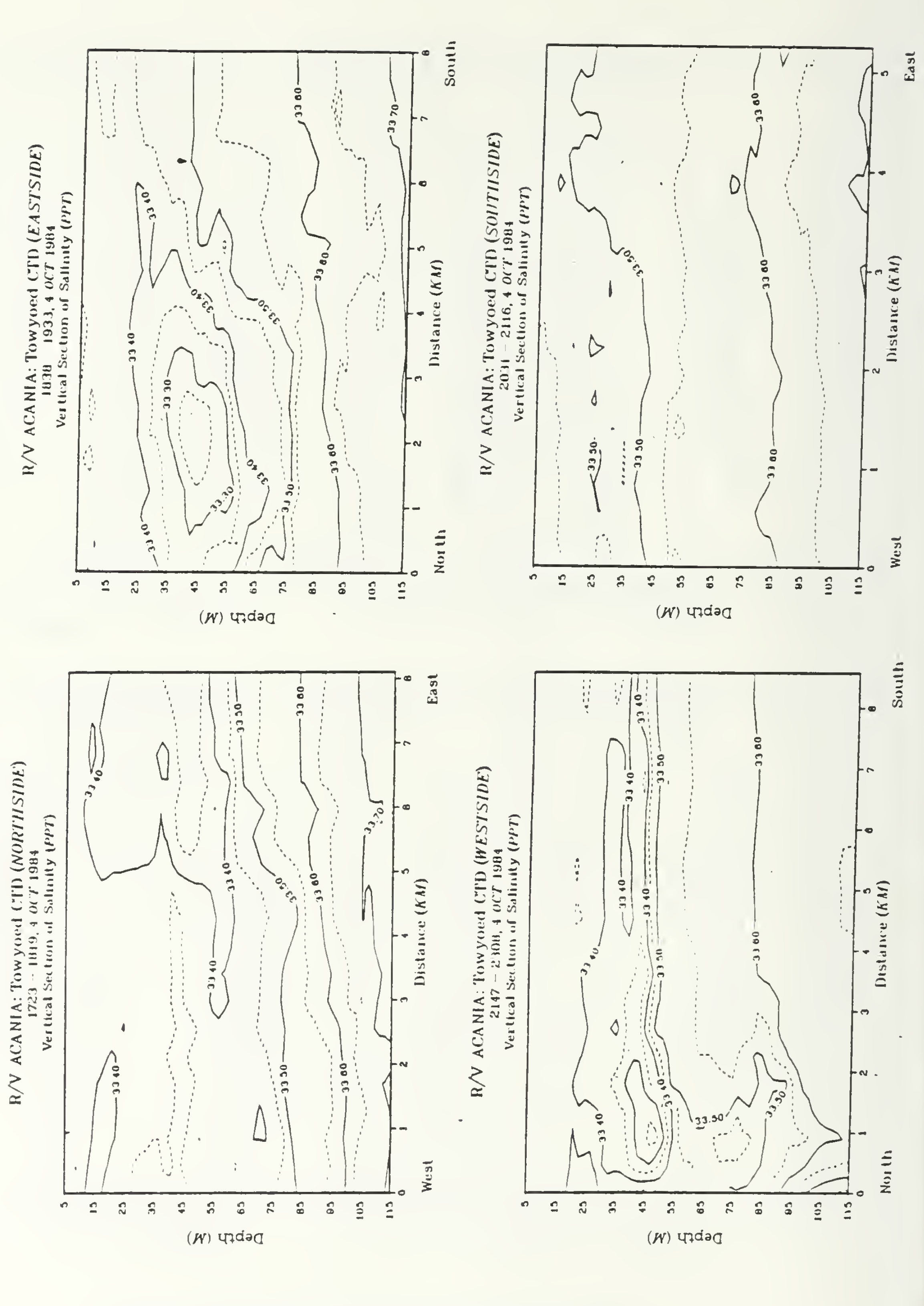

Fig. 4.33 Vertical section of salinity for circuit 6.

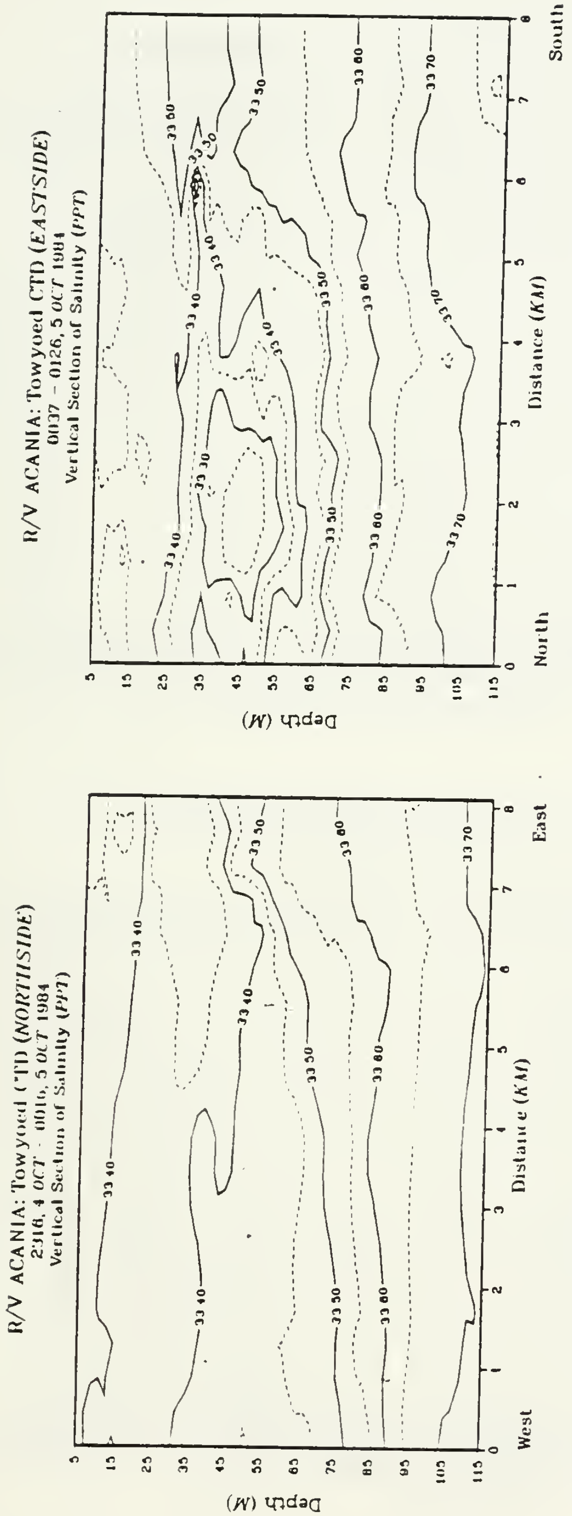

Fig. 4.34 Vertical section of salinity for circuit 7.

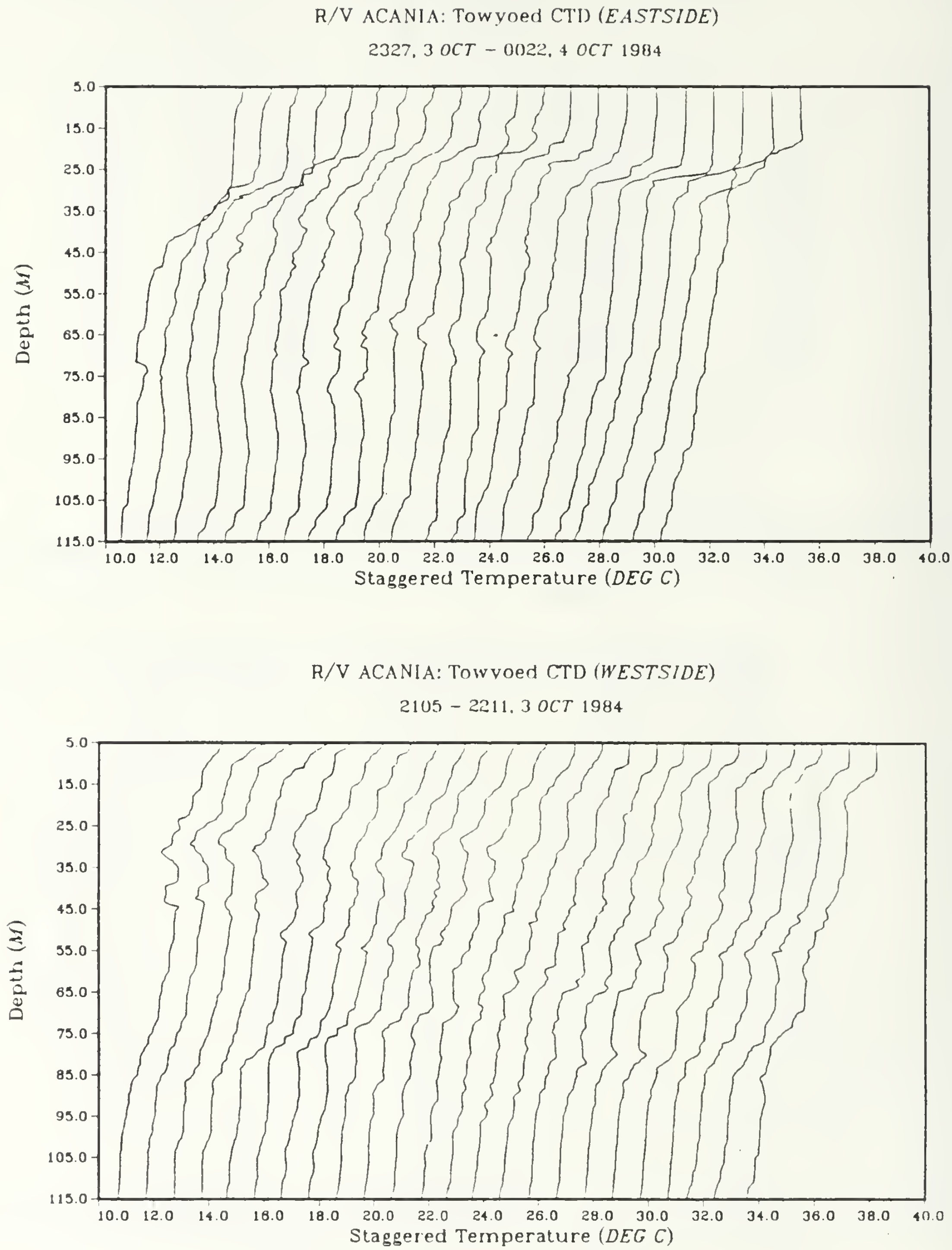

Fig. 4.35 Staggered profiles of temperature.

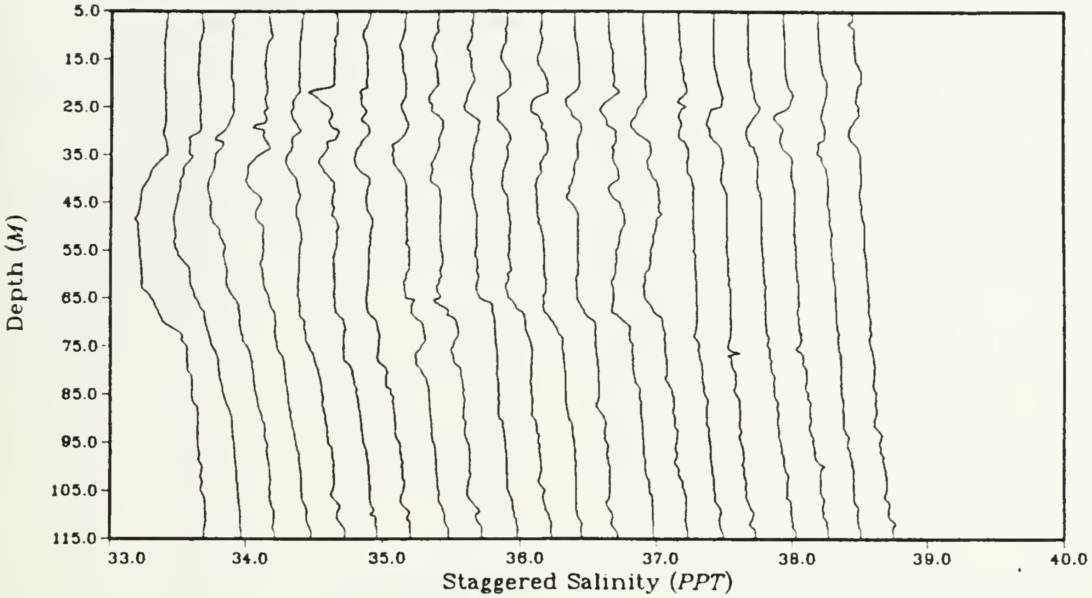

R/V ACANIA: Towyoed CTD (*EASTSIDE*)

2327, 3 *OCT* – 0022, 4 *OCT* 1984

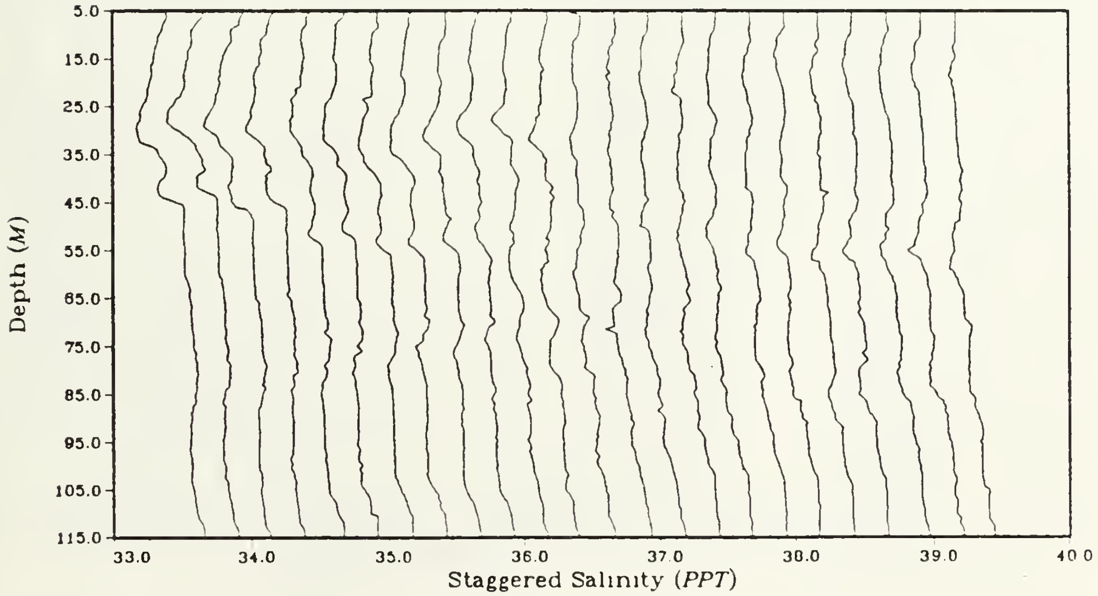

R/V ACANIA: Towyoed CTD (*WESTSIDE*)

2105 – 2211, 3 *OCT* 1984

Fig. 4.36 Staggered profiles of salinity.

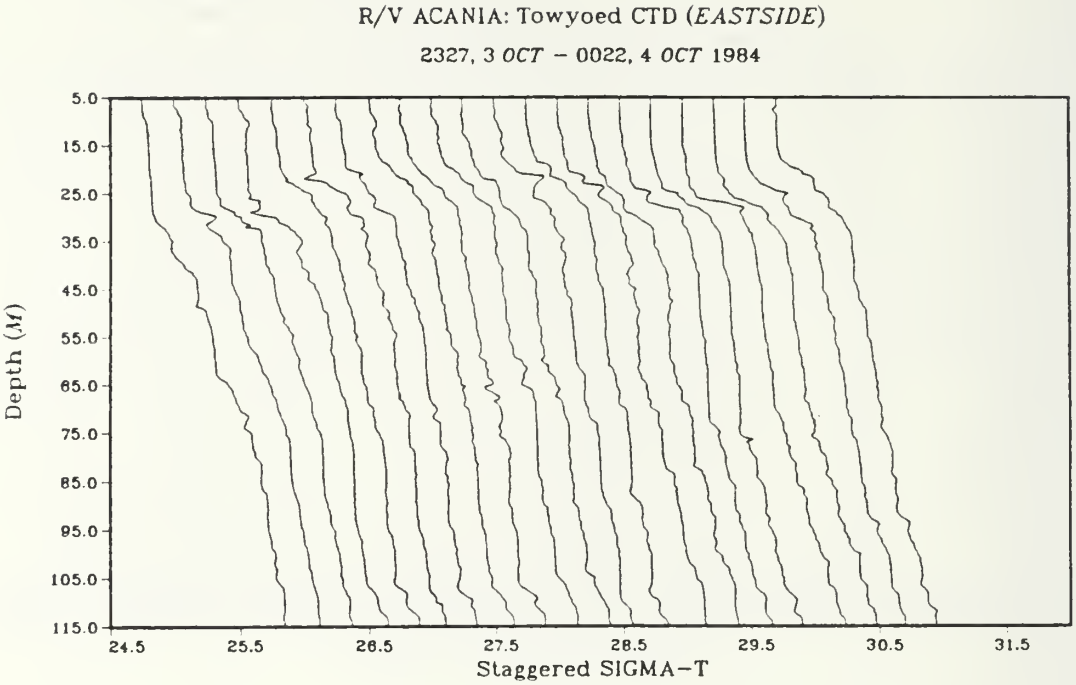

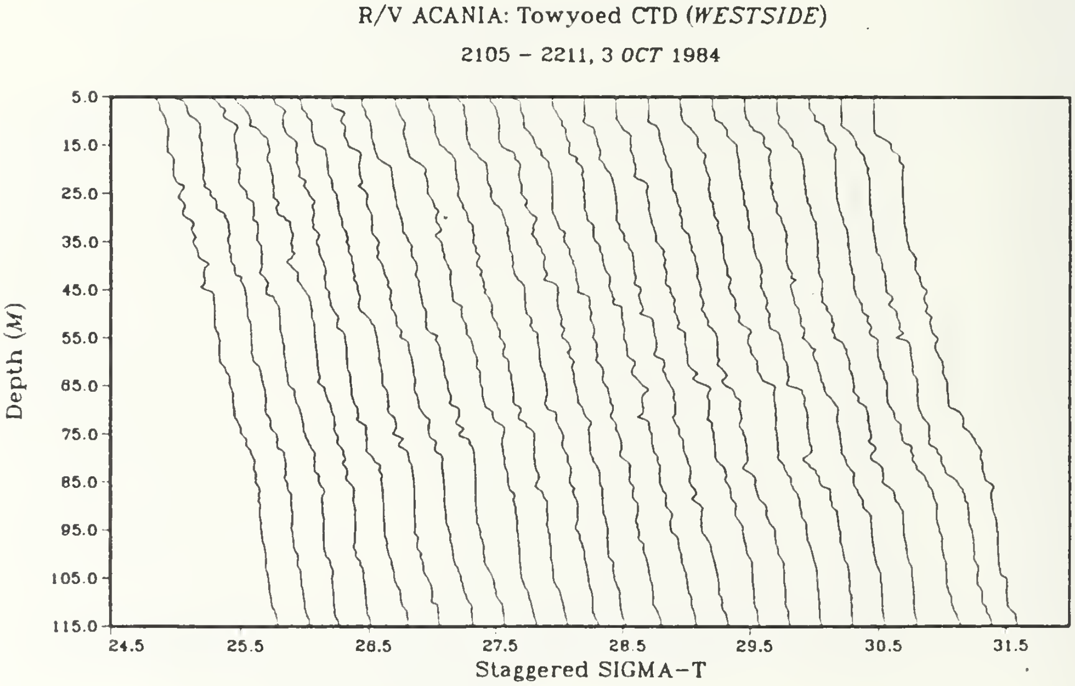

Fig. 4.37 Staggered profiles of sigma-t.

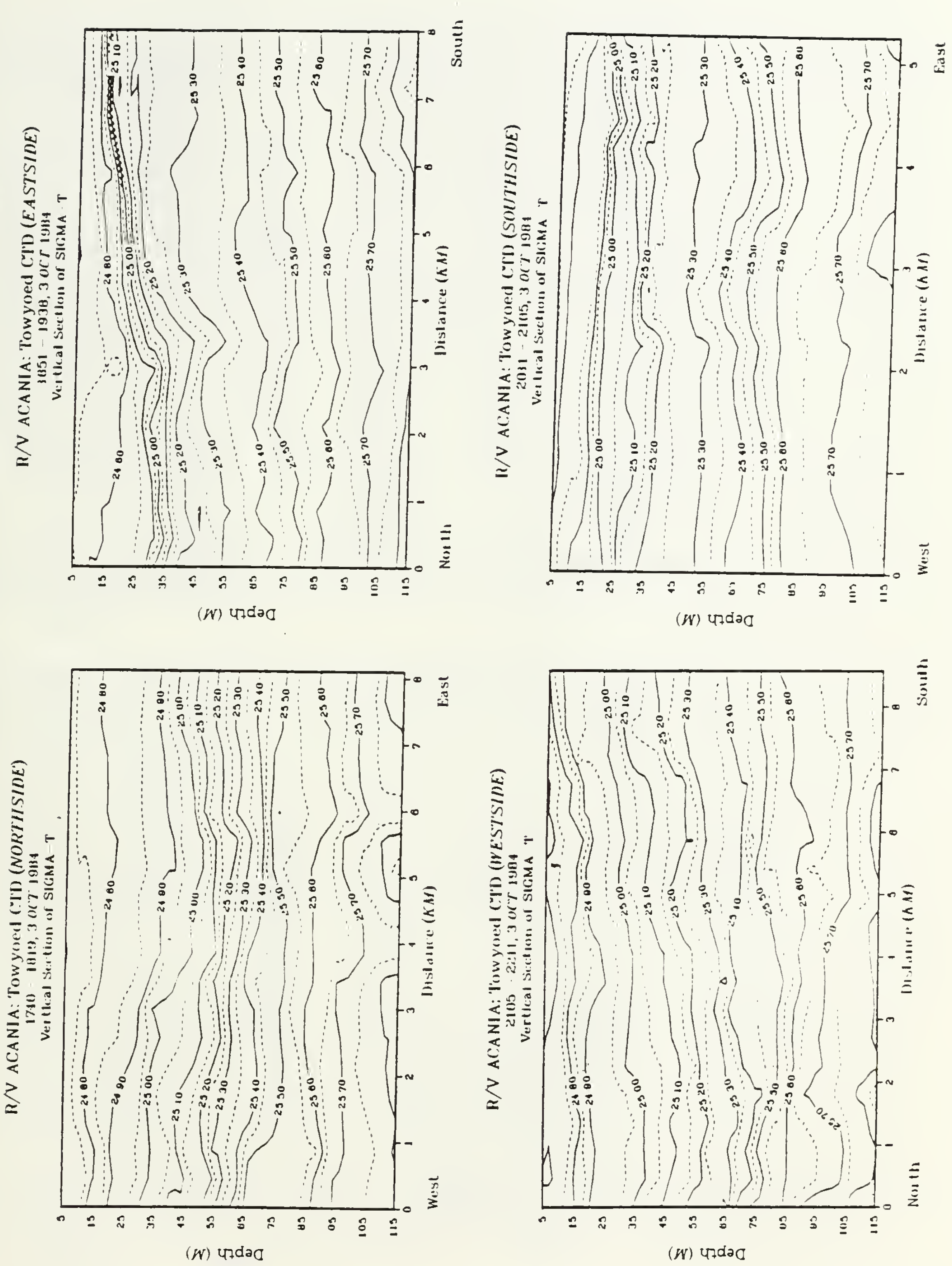

Fig. 4.38 Vertical section of sigma-t for circuit 1.

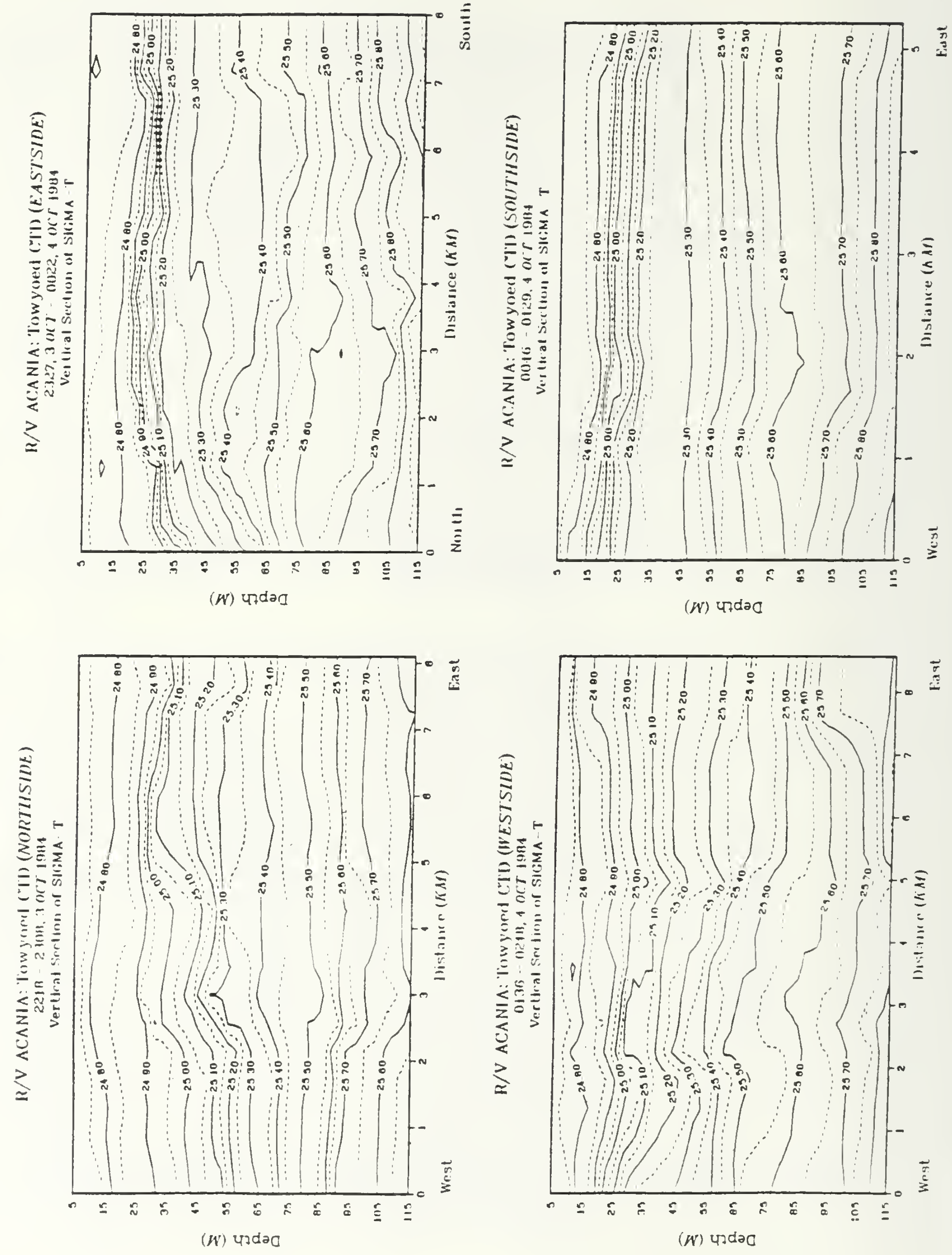

Fig. 4.39 Vertical section of sigma-t for circuit 2.

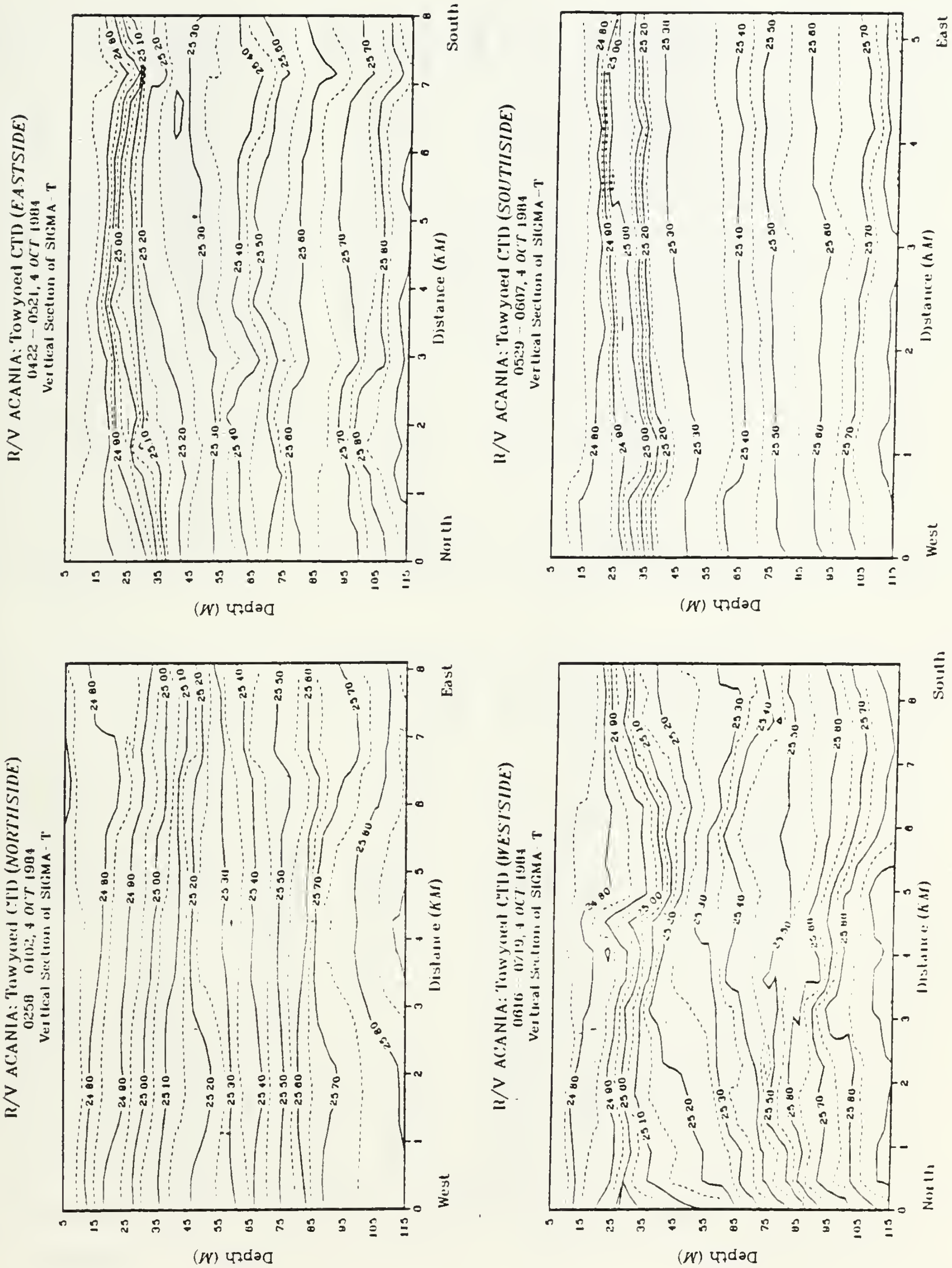

Fig. 4.40 Vertical section of sigma-t for circuit 3.

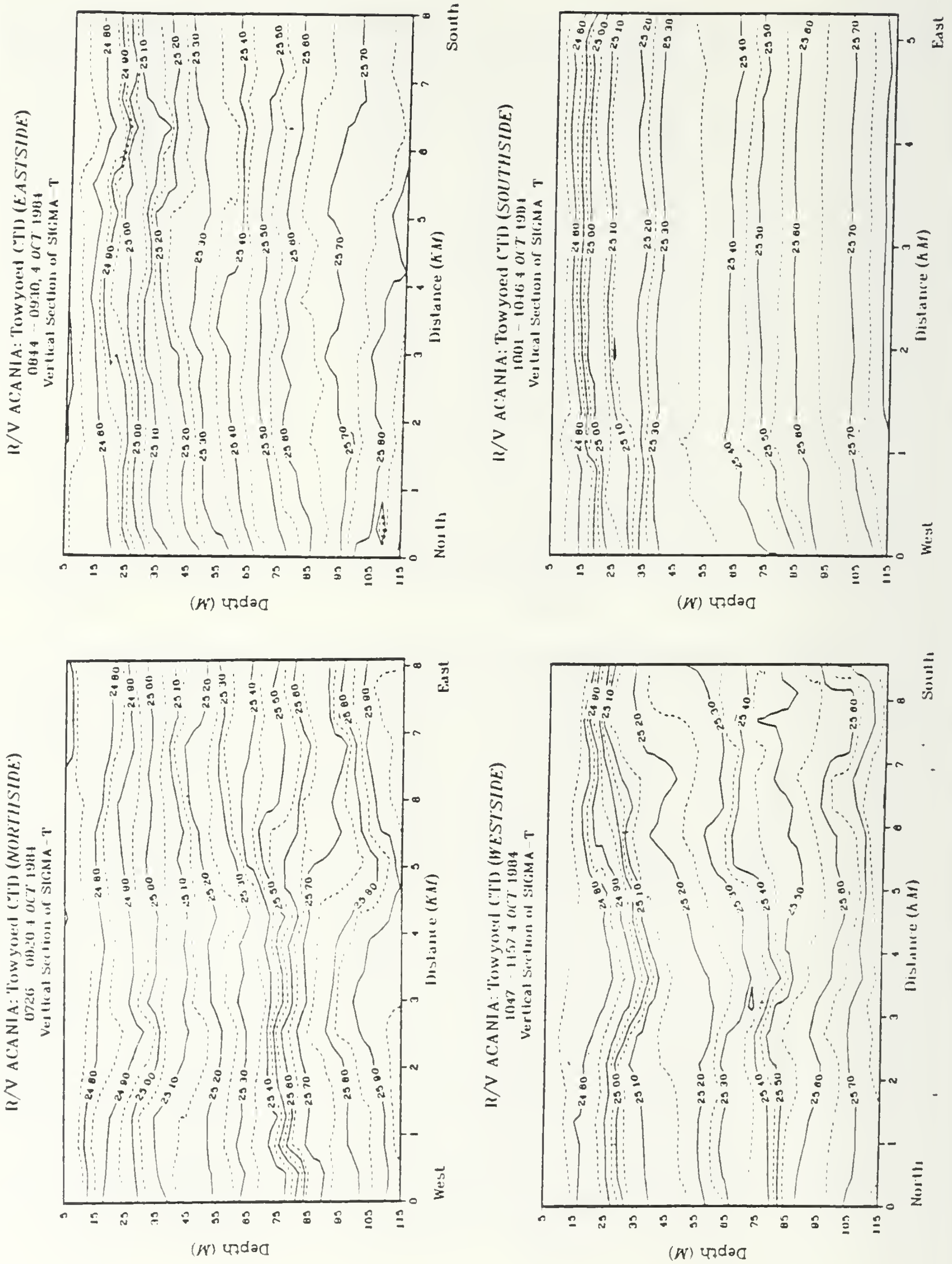

R/V ACANIA: Towyoed CTD (*NORTHSIDE*)
0726 - 0820 4 *OCT* 1984
Vertical Section of SIGMA-T

R/V ACANIA: Towyoed CTD (*EASTSIDE*)
0844 - 0930, 4 *OCT* 1984
Vertical Section of SIGMA-T

R/V ACANIA: Towyoed CTD (*WESTSIDE*)
1047 - 1157 4 *OCT* 1984
Vertical Section of SIGMA-T

R/V ACANIA: Towyoed CTD (*SOUTHSIDE*)
1001 - 1046 4 *OCT* 1984
Vertical Section of SIGMA-T

Fig. 4.41 Vertical section of sigma-t for circuit 4.

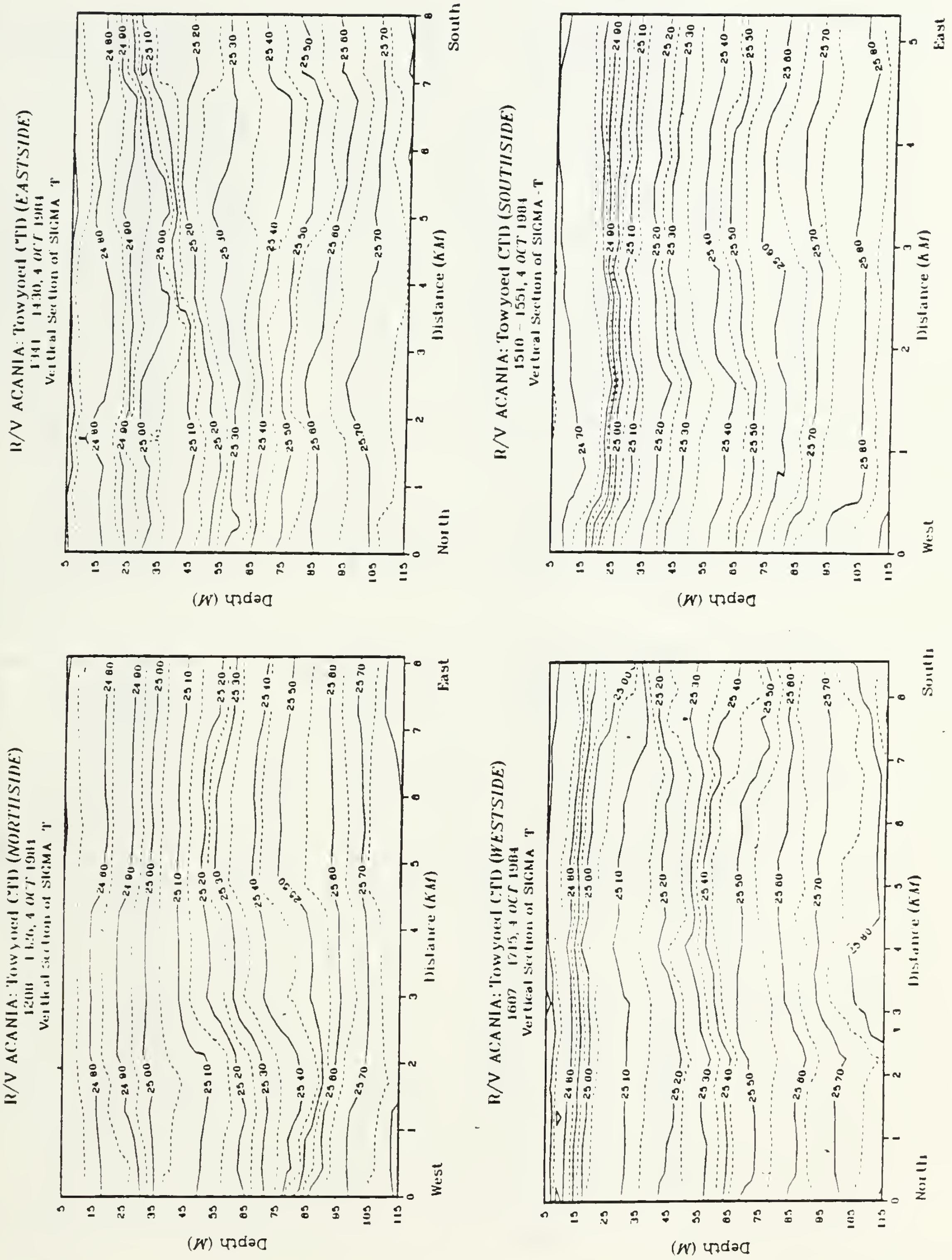

Fig. 4.42 Vertical section of sigma-t for circuit 5.

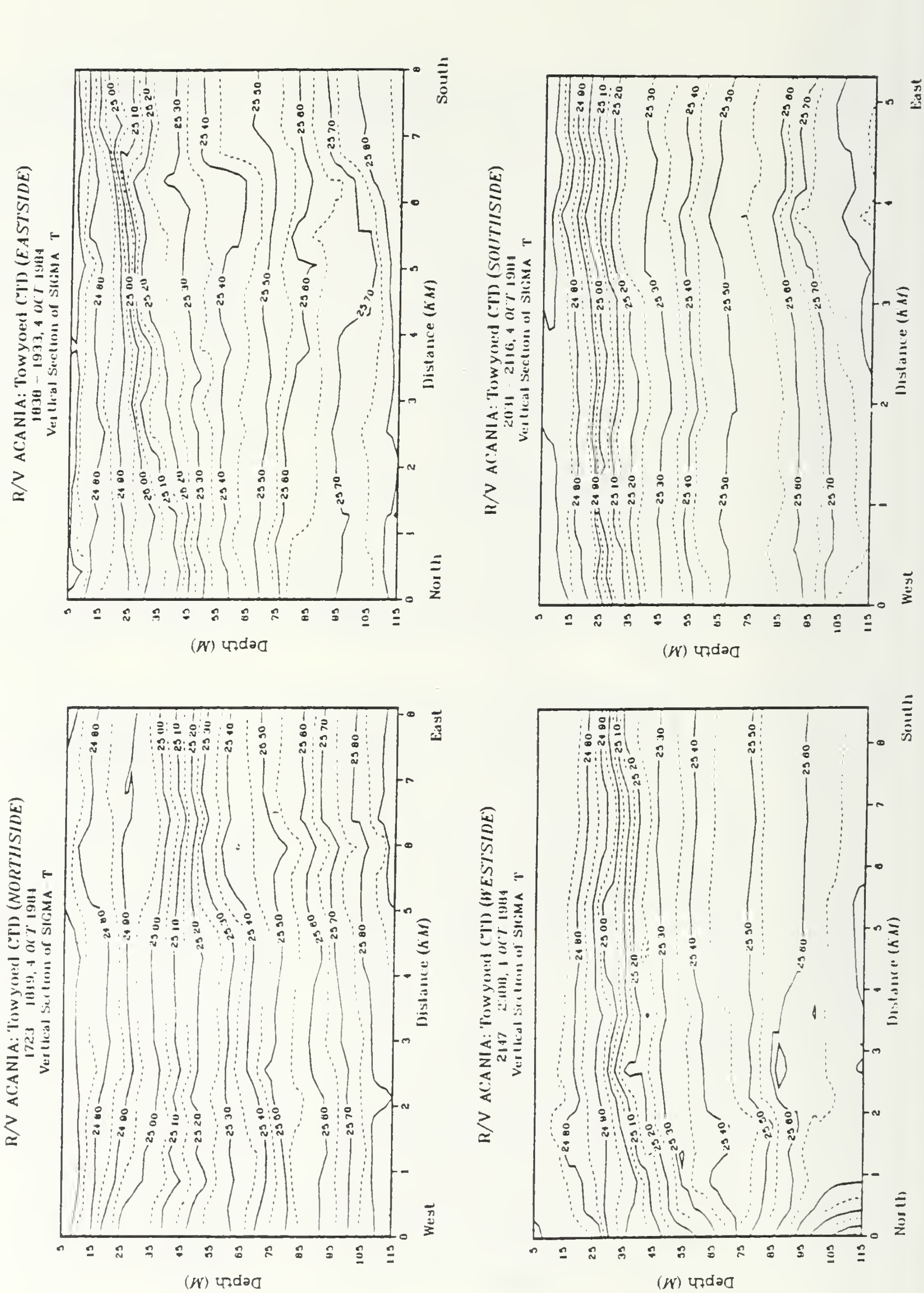

Fig. 4.43 Vertical section of sigma-t for circuit 6.

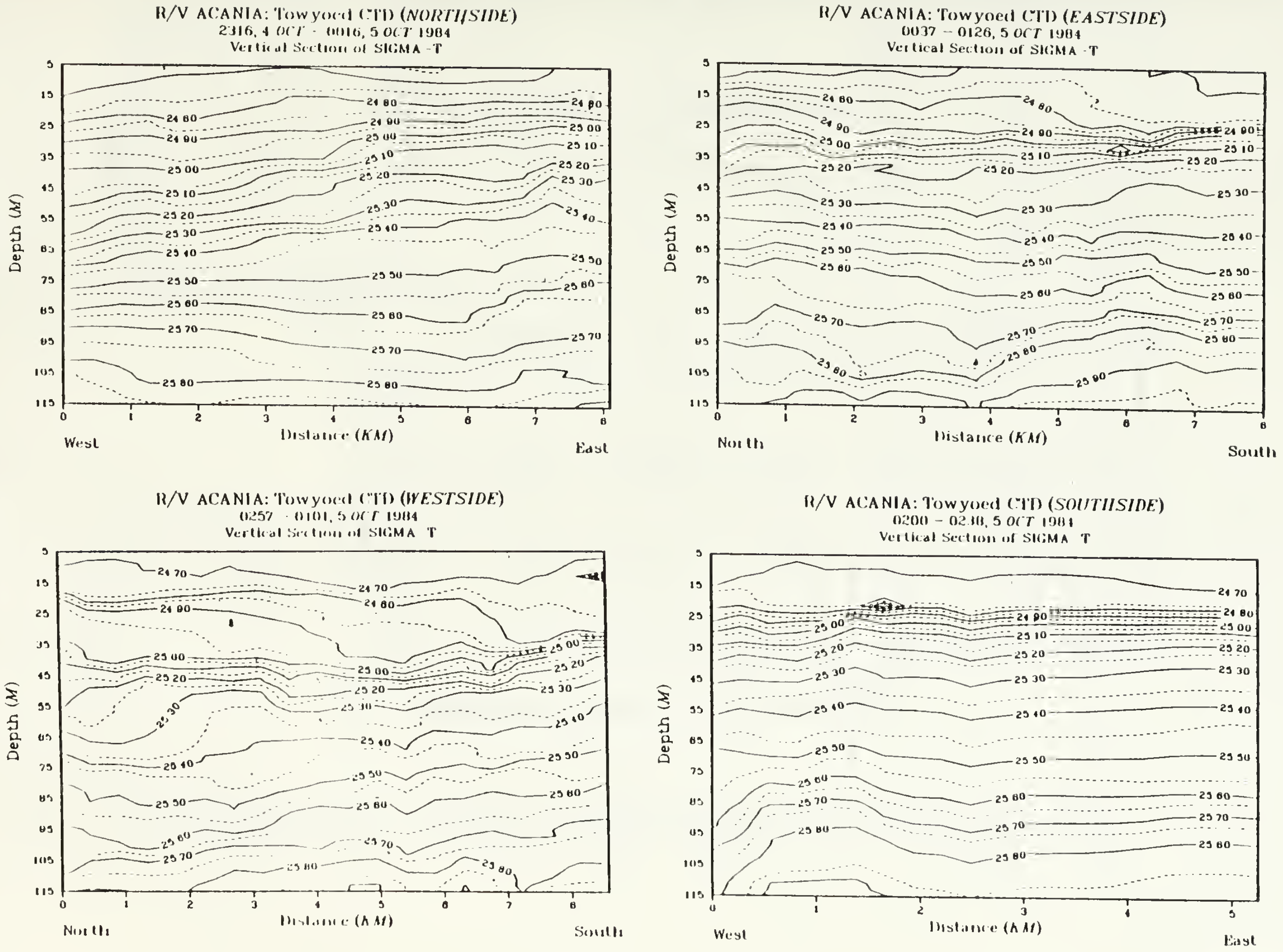

Fig. 4.44 Vertical section of sigma-t for circuit 7.

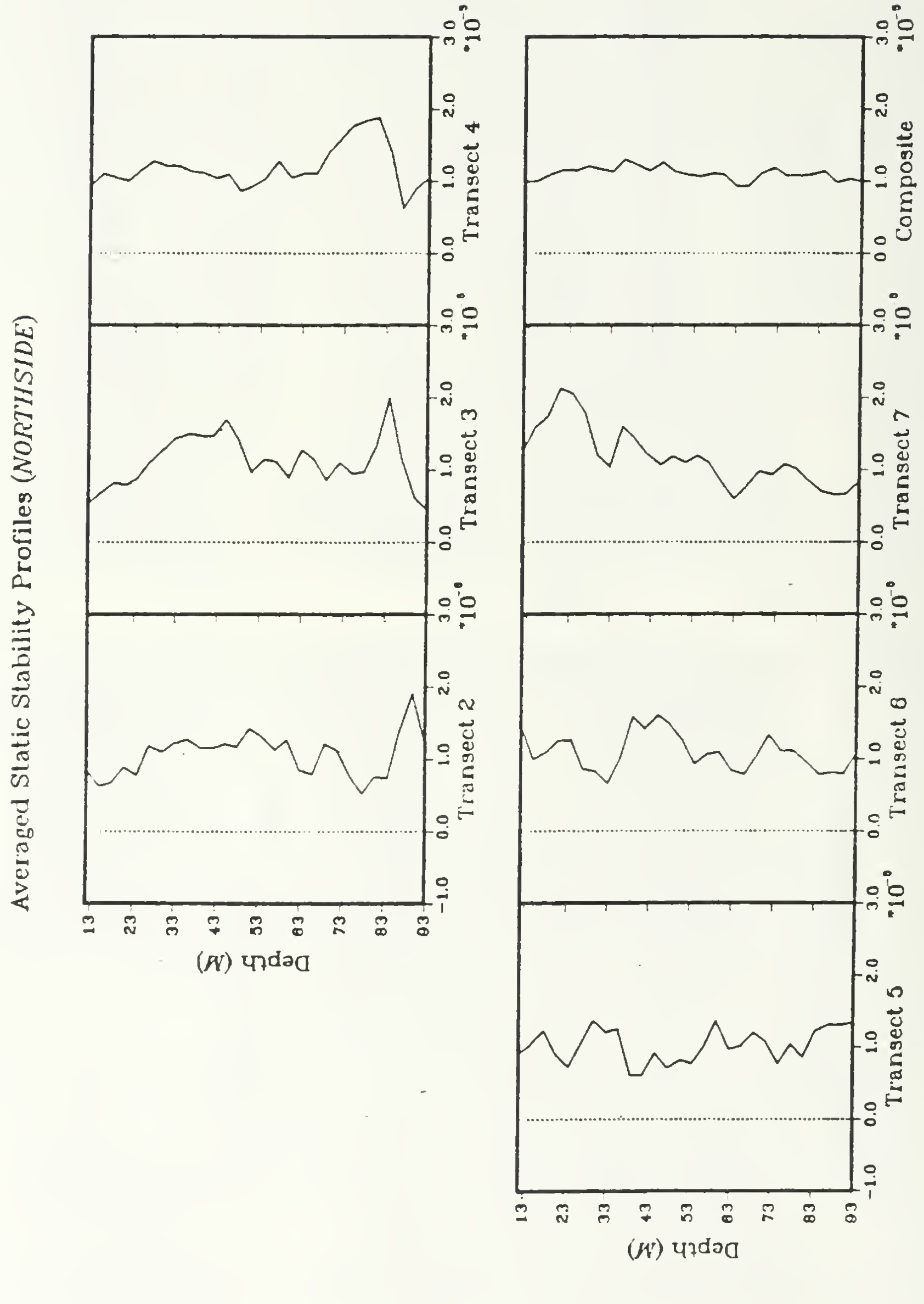

Fig. 4.45 Average profiles of the static stability parameter (E) for the northside.

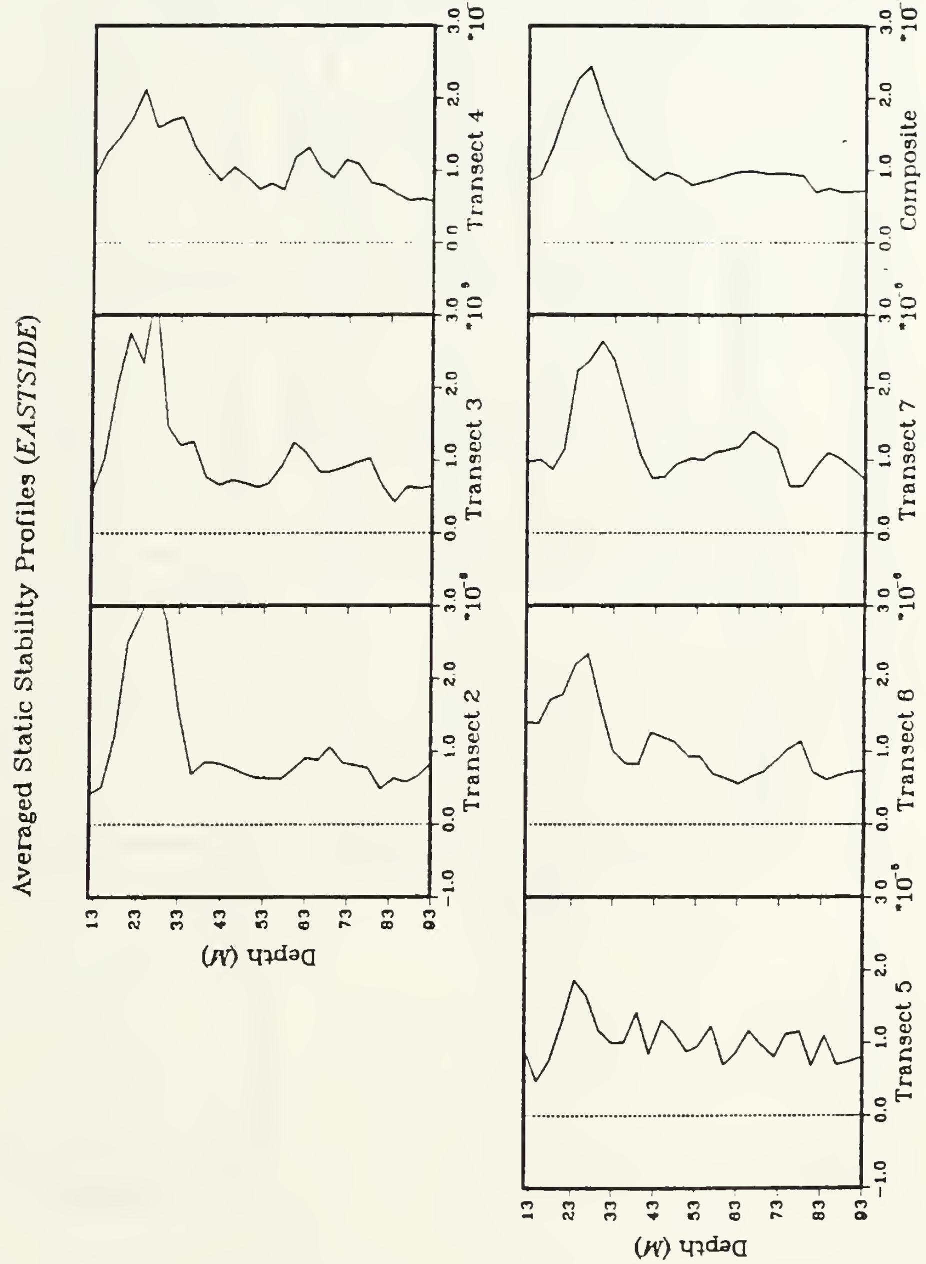

Fig. 4.46 Average profiles of the static stability parameter (E) for the eastside.

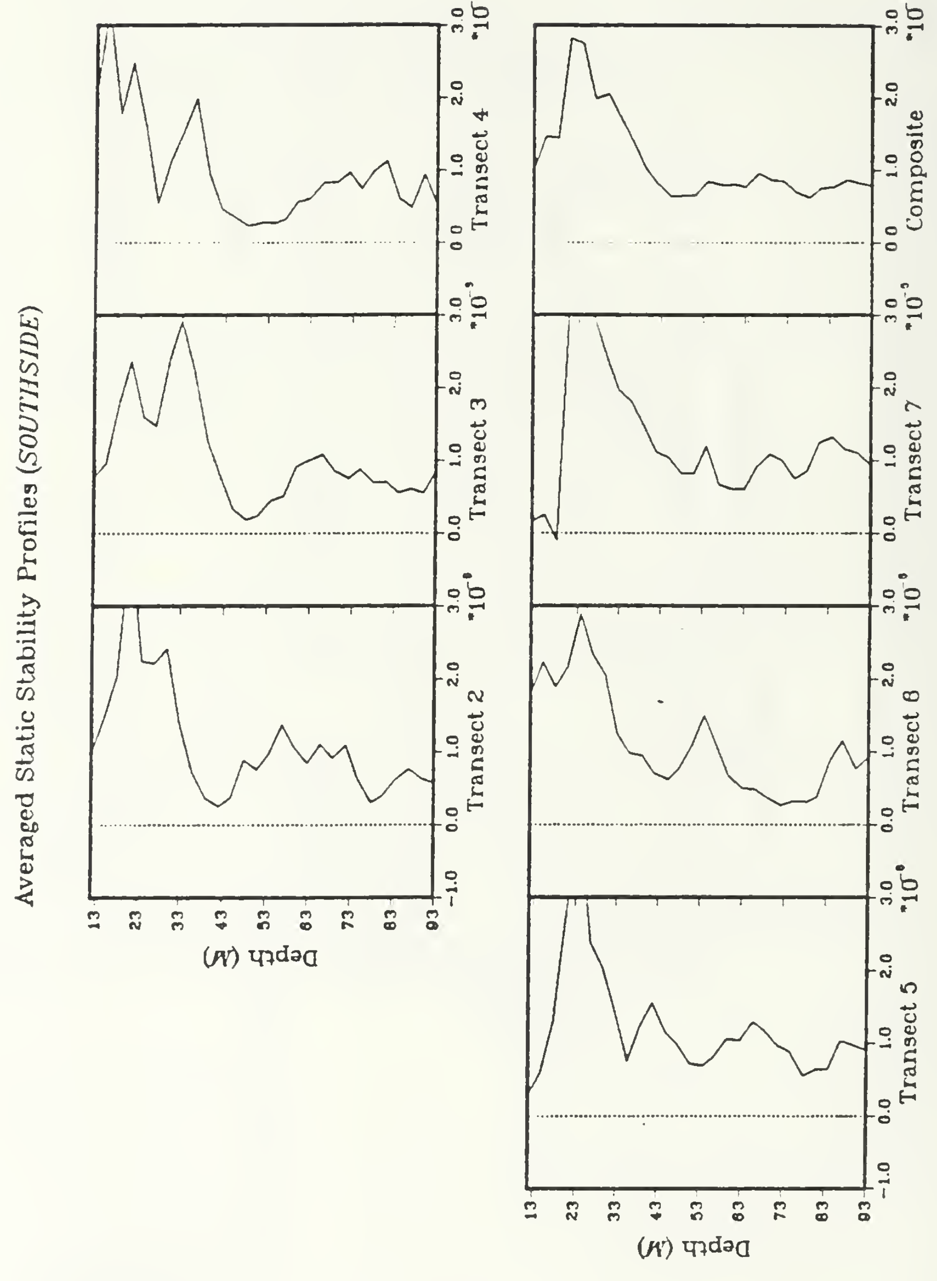

Fig. 4.47 Average profiles of the static stability parameter (E) for the southside.

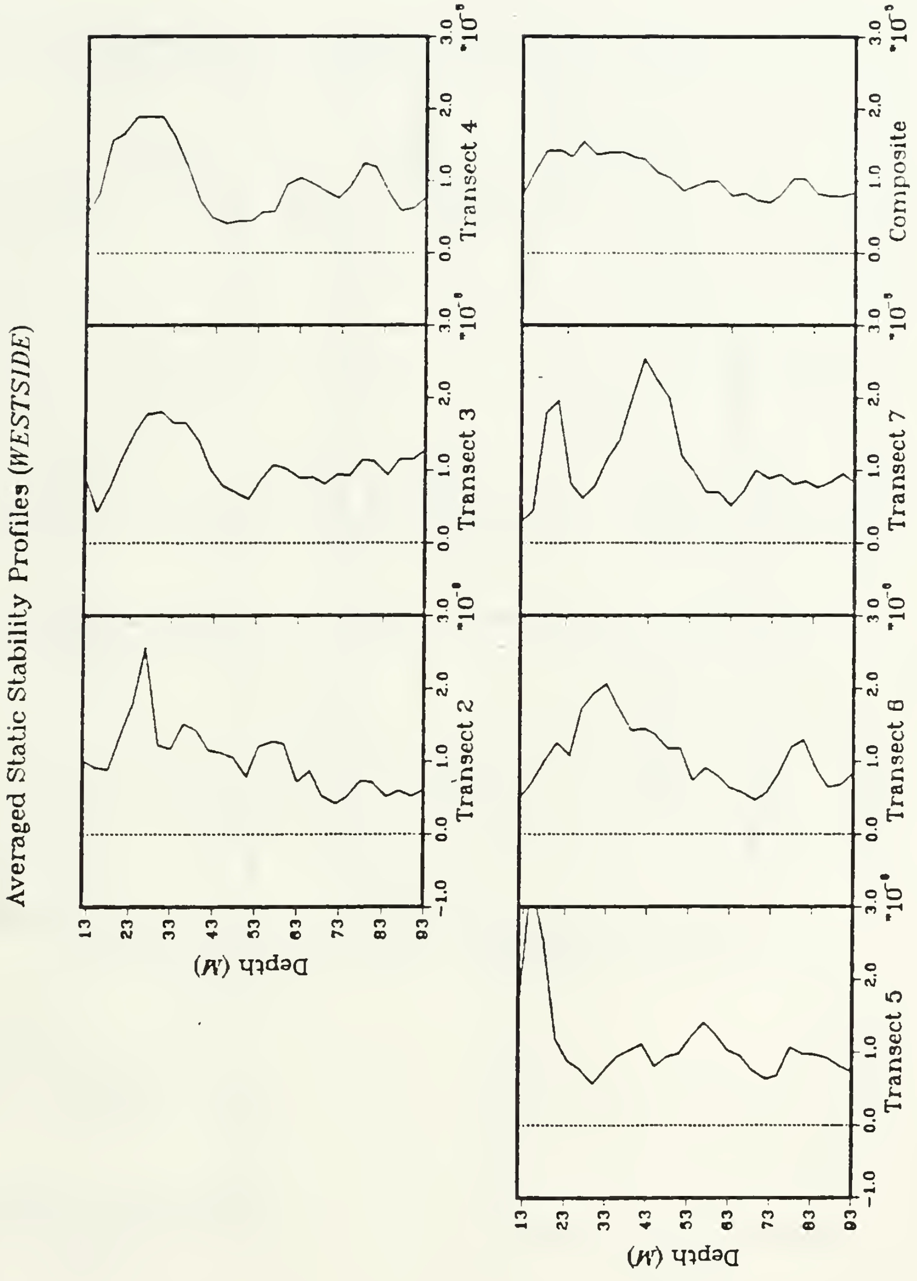

Fig. 4.48 Average profiles of the static stability parameter (E) for the westside.

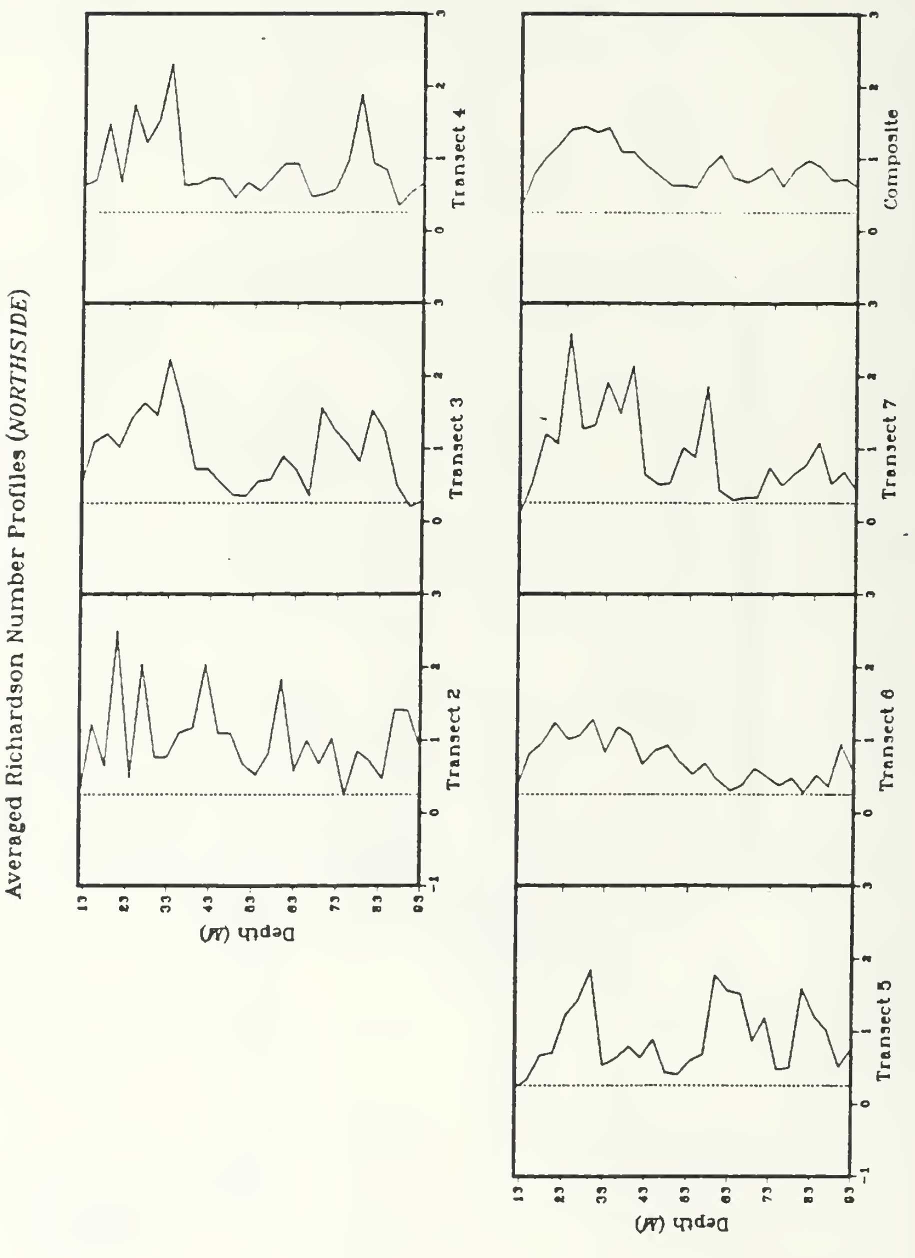

Fig. 4.49 Average profiles of the Richardson number (northside).

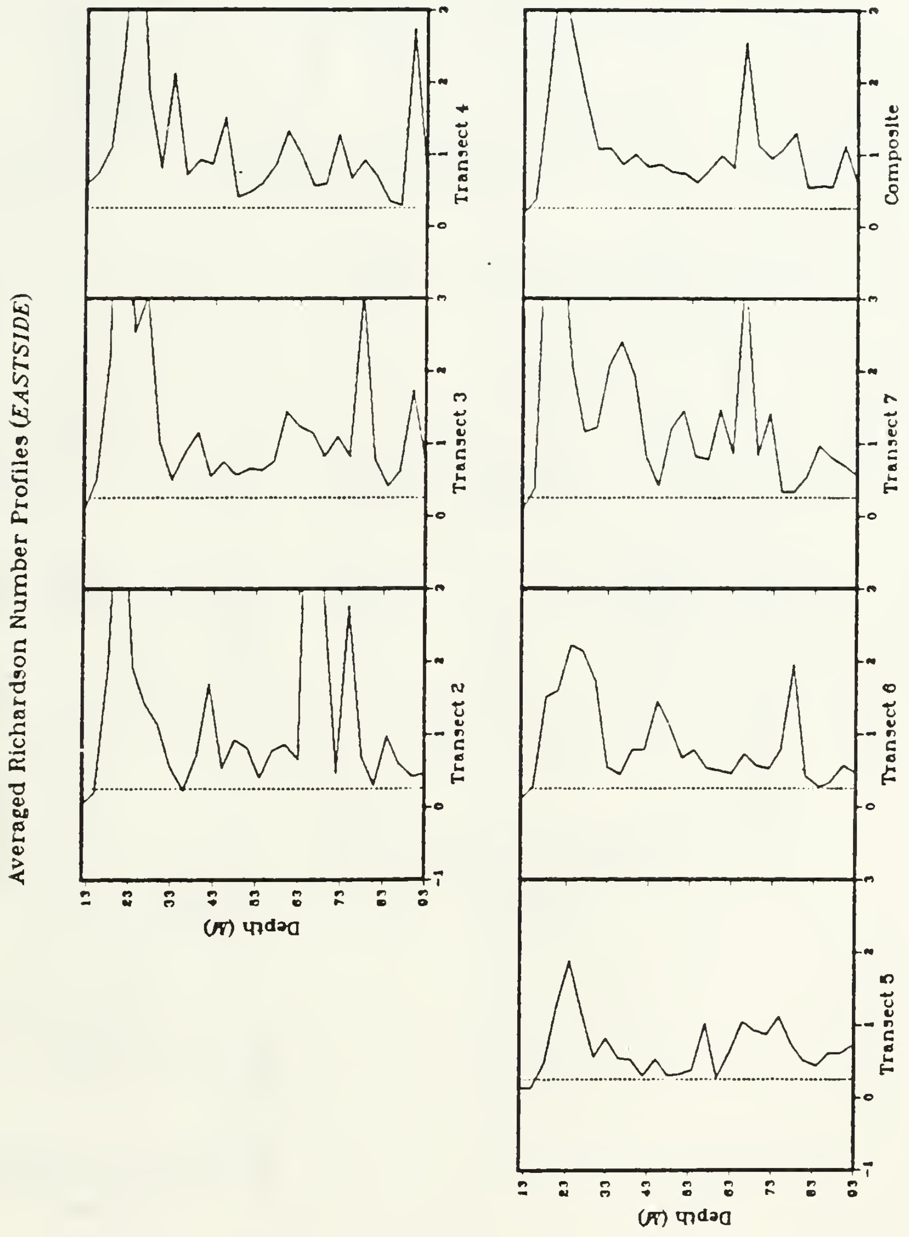

Fig. 4.50 Average profiles of the Richardson number (eastside).

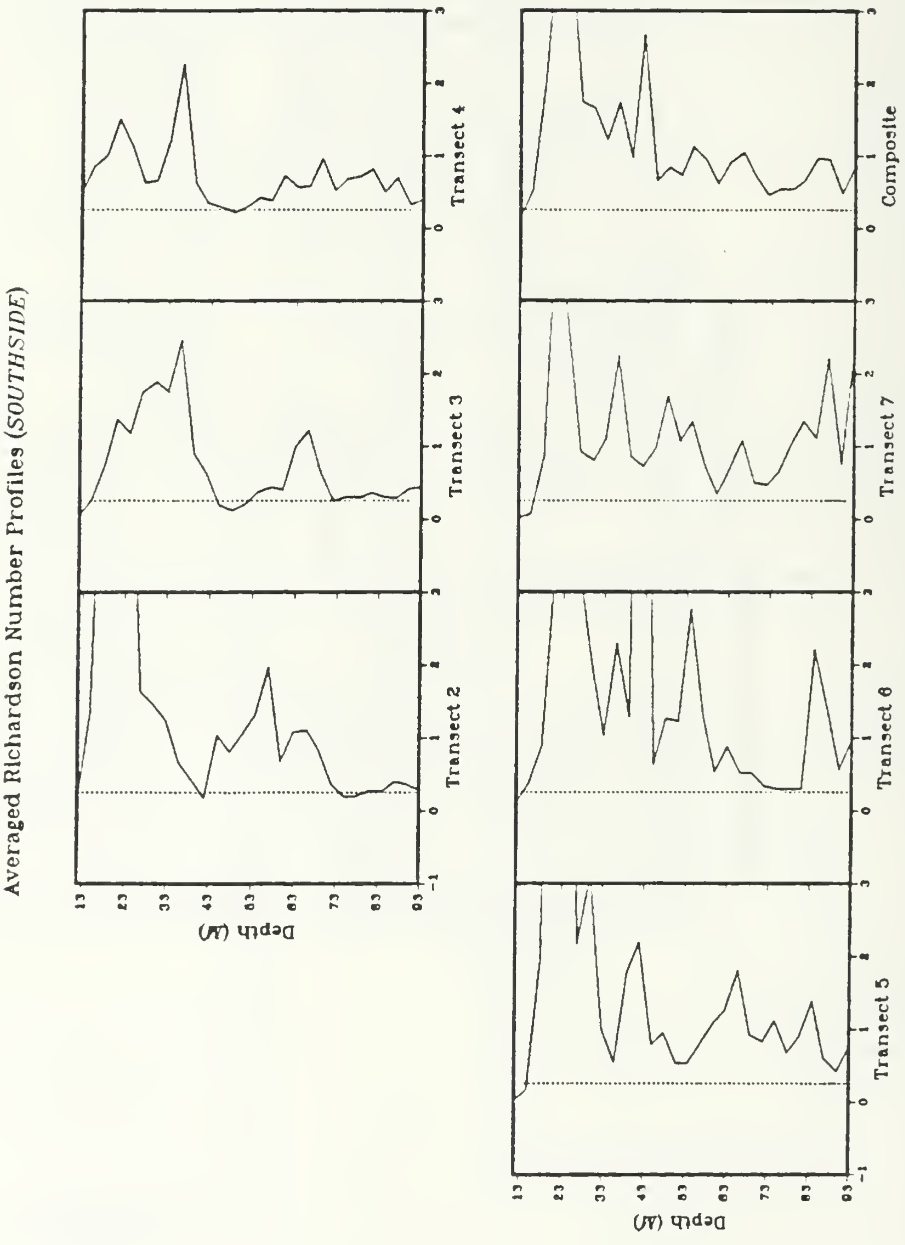

Fig. 4.51 Average profiles of the Richardson number (southside).

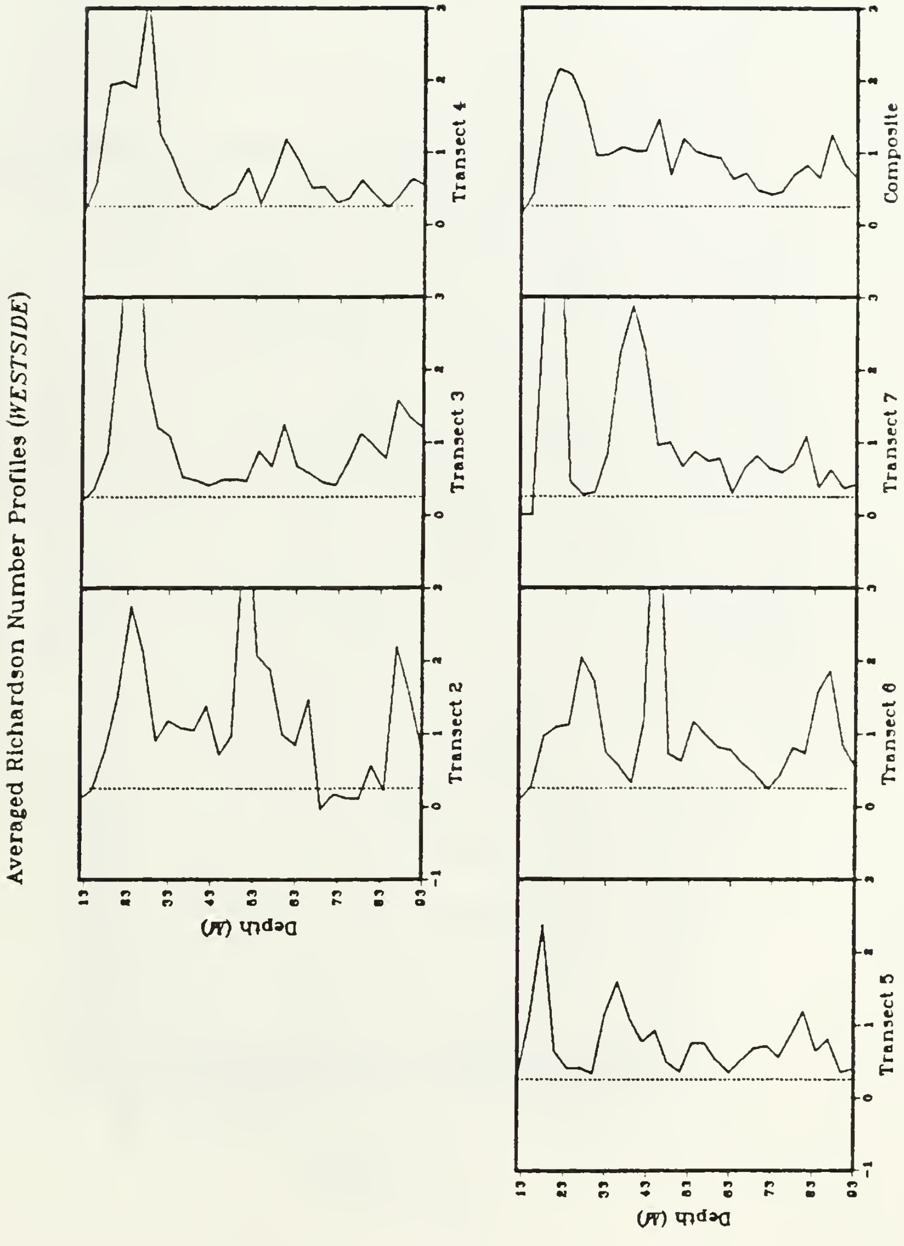

Fig. 4.52 Average profiles of the Richardson number (westside).

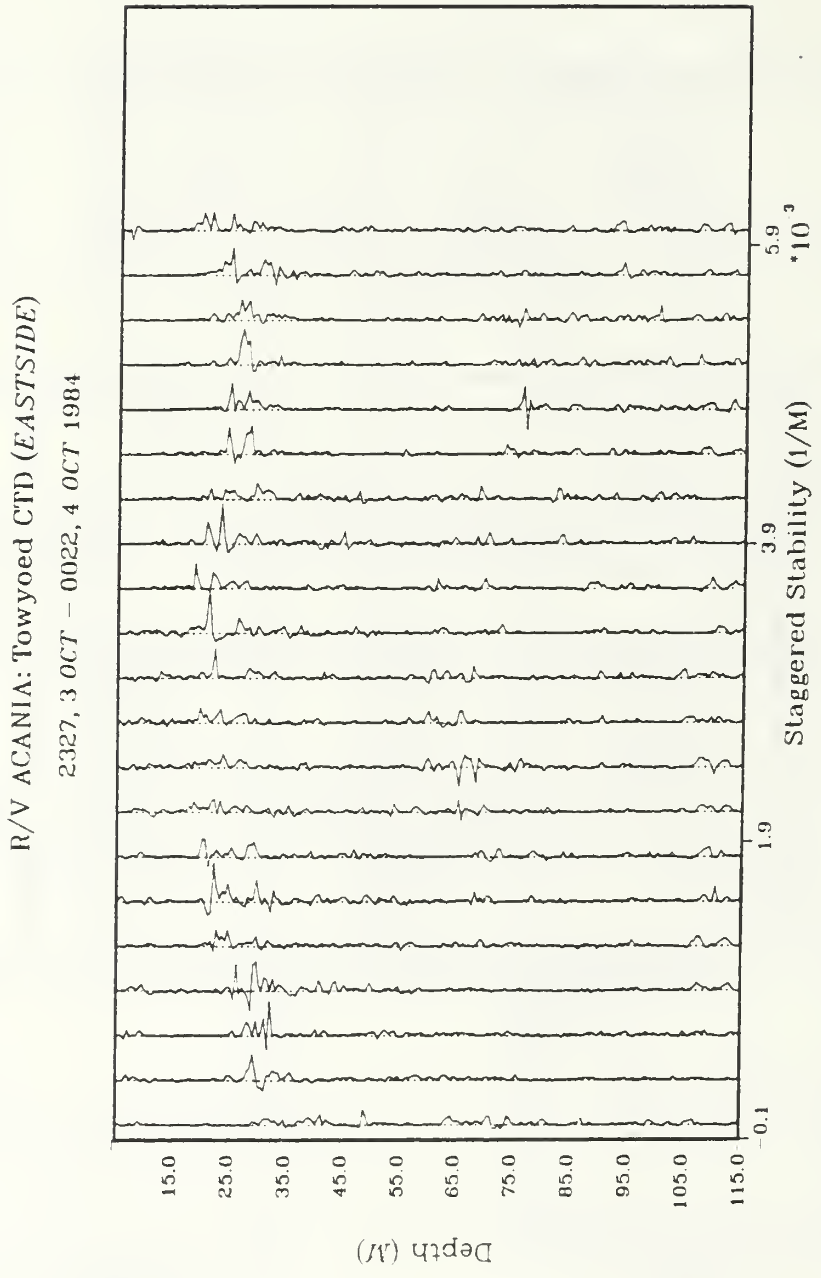

Fig. 4.53 Staggered profiles of the static stability parameter (eastside).

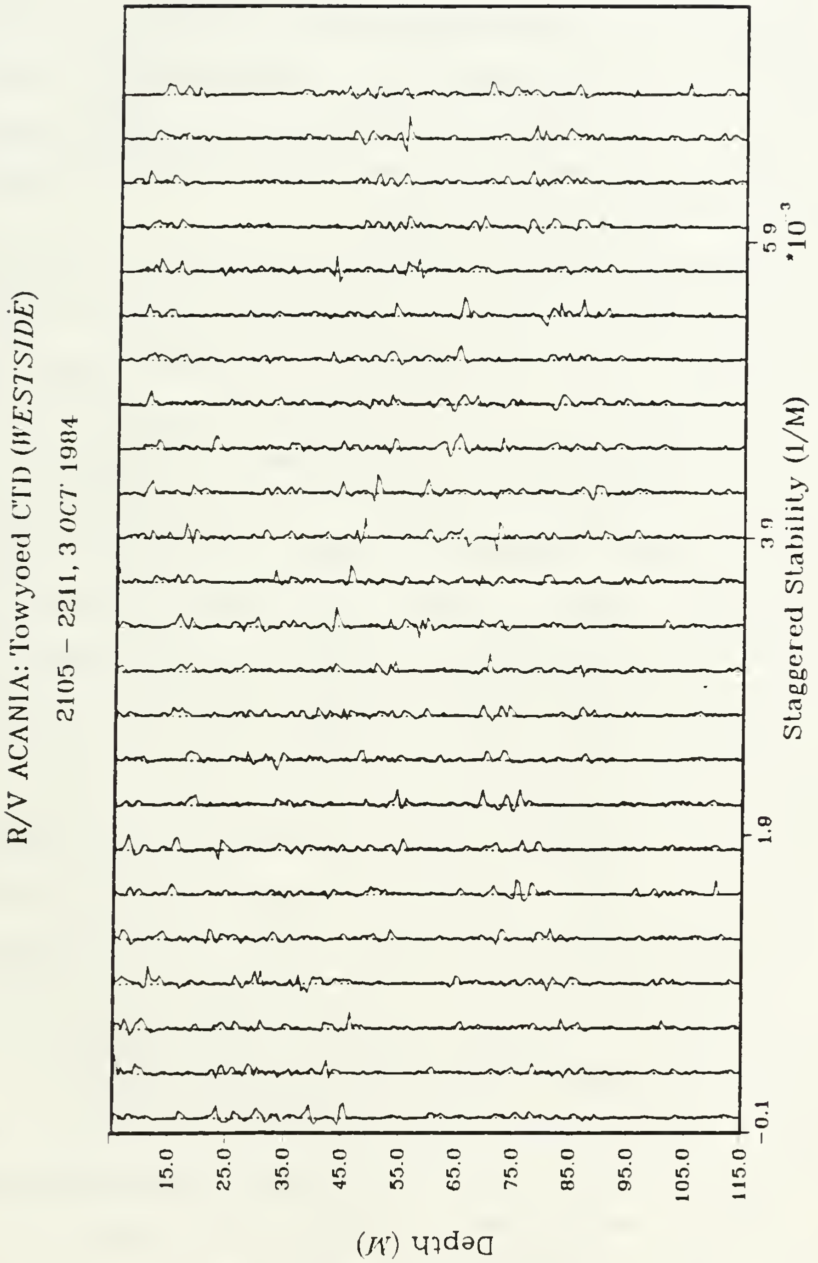

Fig. 4.54 Staggered profiles of the static stability parameter (westside).

V. SUMMARY AND CONCLUSIONS

Water column stability is determined by the interaction of dynamic and static forcing. Examination of the stability and the driving mechanisms in the upper 100m of the measurement area was accomplished by the graphical display of the temperature, salinity, sigma-t, and velocity fields as well as the static stability parameter and the Richardson number. The analysis of these displays indicated a rapidly changing environment and complex horizontal structure.

Several forcing mechanisms and their effect on stability were investigated within the context of the analysis fields and the atmospheric and tidal conditions existing during the study period. These mechanisms were upwelling, currents, tides, bottom topography, and internal waves. All of the mechanisms were found to be a factor in the stability of the water column with the exception of upwelling. The California Current was found to dominate with an apparent absence of the Davidson Current.

The analyzed fields of temperature, salinity, density, and velocity exhibited considerable spatial and temporal variability. This variability took the form of wave-like patterns, migrating parcels, fluctuating isolines, and intensification/weakening of gradients. These disturbances could be attributed to the forcing mechanisms of bottom topography, tidal flow, current systems, and internal gravity waves. The shear, as measured between 25m and 75m was calculated to be at least 5.0 cm/sec. The presence of shear provided for the possibility for dynamic instability. Double diffusive processes were indicated to be a factor in stability by the small reversals in the density field revealed in the staggered static stability profiles. However, despite the large variability evident in the temperature and salinity fields, the sigma-t field did not exhibit comparable variability. This indicates that most of the temperature and salinity disturbances were density compensating and thus maintained stability.

The stability of the water column was found to be both statically and dynamically stable on the average as would be expected considering the episodic nature of instability. However, small patches of instability were identified in the staggered profiles of static stability which were predominantly located in the 25m to 75m region of the water column. This region of the water column is also where the greatest variability in the thermohaline and velocity fields occured. The patches of instability appeared to be primarily due to double diffusive processes initiated by periodic intrusions of warmer, less saline water.

LIST OF REFERENCES

Blumberg, R.E., *Mesoscale spatial and temporal variations of water characteristics in the California Current region off Monterey Bay in 1973-1974.* M.S. Thesis, Naval Postgraduate School, Monterey, California, September, 1975.

Breaker, L.C., *The space-time scales of variability in oceanic thermal structure off the central California coast.* Ph.D. Thesis, Naval Postgraduate School, Monterey, California, December, 1983.

Christiansen, C., *Microstructure profiles.* M.S. Thesis, Naval Postgraduate School, Monterey, California, March, 1980.

Gargett, A.E., T.R. Osborn and P.W. Nasmyth, 1984: Local isotropy and the decay of turbulence in a stratified fluid. *J. Fluid Mech.* **144**, 231-280.

Garrett, C. and W. Munk, 1972: Space-time scales of internal waves. *Geophys. Fluid Dyn.*, **2**, 225-264.

Greer, R.E., *Mesoscale components of the geostrophic flow and its temporal and spatial variability in the California Current region off Monterey Bay in 1973-74.* M.S. Thesis, Naval Postgraduate School, Monterey, California, September, 1975.

Kunze, E. and T.B. Sanford, 1984: Observations of near-inertial waves in a front. *J. Phys. Oceanogr.*, **14**, 566-581.

Munk, W., *Internal waves and small scale processes.* Evolution of Physical Oceanography, B.A. Warren and C. Wunsch, Eds., The MIT Press, 1981.

Osborn, T.R. and R.G. Lueck, 1985: Turbulence measurements with a submarine. *J. Phys. Oceanogr.*, **15**, 1502-1520.

Pollard, R.T., 1979: Properties of near-surface inertial oscillations. *J. Phys. Oceanogr.*, **10**, 385-398.

Pond, S. and G.L. Pickard, *Introductory dynamical oceanography.* 2d ed., Pergamon Press, 1983.

Turner, J.S., 1973: *Buoyancy effects in fluids.* Cambridge Univ. Press, London.

Turner, J.S., *Small-scale mixing processes.* Evolution of Physical Oceanography, B.A. Warren and C. Wunsch, eds. The MIT Press, 1981.

Weller, R.A., 1982: The relation of near-inertial motions observed in the mixed layer during the JASIN (1978) Experiment to the local wind stress and to the quasi-geostrophic flow field. *J. Phys. Oceanogr.*, **12**, 1122-1136.

Wickham, J.B., A.A. Bird, and C.N.K. Mooers, 1986: Mean and variable flow over the Central California continental margin, 1978 to 1980. *Cont. Shelf Res.*, (in press).

INITIAL DISTRIBUTION LIST

		No. Copies
1.	Defense Technical Information Center Cameron Station Alexandria, VA 22304-6145	2
2.	Library, Code 0142 Naval Postgraduate School Monterey, CA 93943-5002	2
3.	Chairman, Department of Oceanography Code 68 Naval Postgraduate School Monterey, CA 93943-5000	1
4.	Office of the Director Naval Oceanography Division (OP-952) Department of the Navy Washington, D.C. 20350	1
5.	Commander Naval Oceanography Command NSTL, MS 39522	1
6.	Commanding Officer Naval Oceanographic Office Bay St. Louis NSTL, MS 39522	1
7.	Commanding Officer Naval Ocean Research and Development Activity Bay St. Louis NSTL, MS 39522	1
8.	Chief of Naval Research 800 N. Quincy Street Arlington, VA 22217	1
9.	Dr. Edward B. Thornton Code 68 Naval Postgraduate School Monterey, CA 93943-5000	3
10.	Dr. Timothy P. Stanton Code 68 Naval Postgraduate School Monterey, CA 93943-5000	3
11.	Mrs. Betty M. Beale P.O. Box 235 Laytonville, CA 95454	5

26
176537
sm

TITLE NUMBER: ______ CUSTOMER NUMBER: ______

LIBRARY: Dudley Knox Library, Naval Postgraduate School
Monterey, California 93953

ROSWELL BOOKBINDING

LIBRARY DIVISION

2614 NORTH 29th AVENUE
PHOENIX, ARIZONA 85009
PHONE (602) 272-9338

Binding in Everything ☒

	F	B	NP
CONTENTS	☐	☐	☐
INDEX	☐	☐	☐
Bind without Index	☐	☐	☐

ISSUE CONTENTS

- Discard ☐
- Bind in Place ☐
- Gather at Front ☐

	IN	OUT
Advertisements	☐	☐
Front Covers	☐	☐
Back Covers	☐	☐
1st only	☐	☐
Accents	☐	☐
Imprints	☐	☐

Special Instructions

EDWARD G. BEALE JR.

B2858

Thesis B2853

Buck Color	596
Print Color	Gold
Trim Height	
Ht Inches	
Over Thick	
For Title	
Extra Lines	
Extra Coll.	
Hand Sew	
Slit	
Rules	
1st Slot No	
Vol Slot No	
Year Slot No	
Call # Slot	
Imp Slot No	
Type Face	
Price	
Mending	
Map Pockets	
2 Vols in 1	

ACTUAL TRIM	DATE
SPINE	JOB
BOARD DIM	LOT
CLOTH DIM	ROUTE
CLOTH BIN	SEQ NO

26

Sm

DUDLEY KNOX LIBRARY
NAVAL POSTGRADUATE SCHOOL
MONTEREY CALIFORNIA 93943-5002

220924

Thesis
B2858 Beale
c.1 Analysis of water column stability using shipboard and submarine density and shear measurments.

220924

Thesis
B2858 Beale
c.1 Analysis of water column stability using shipboard and submarine density and shear measurments.

thesB2858
Analysis of water column stability using
3 2768 000 75782 7
DUDLEY KNOX LIBRARY